JAN 13 1937

VOLUME 84 NUMBER 5

THE ASTROPHYSICAL JOURNAL

AN INTERNATIONAL REVIEW OF SPECTROSCOPY AND ASTRONOMICAL PHYSICS

Founded in 1895 by GEORGE E. HALE *and* JAMES E. KEELER

Edited by

HENRY G. GALE
Ryerson Physical Laboratory of the University of Chicago

FREDERICK H. SEARES
Mount Wilson Observatory of the Carnegie Institution of Washington

OTTO STRUVE
Yerkes Observatory of the University of Chicago

DECEMBER 1936

THE STELLAR TEMPERATURE SCALE - - - - - - - - - - - *A. Pannekoek* 481

A SPECTROSCOPIC EXAMINATION OF METEORITES - - - - - - *Arthur S. King* 507

EFFECTS OF RED SHIFTS ON THE DISTRIBUTION OF NEBULAE - *Edwin Hubble* 517

COMPUTATION OF MEAN PARALLAXES, MEAN ABSOLUTE MAGNITUDES, AND MEAN DISTANCES FOR GROUPS OF STARS FROM COMPONENTS OF THE PROPER MOTIONS - - - - - - - - - - - - - - - - *Gustaf Strömberg* 555

A SPECTROGRAPHIC STUDY OF φ PERSEI - - - - - - - - *Herbert F. Schiefer* 568

THE SPECTRUM OF H_2 FROM λ3612 TO λ4224 - - - - - - - - *Norton A. Kent* 585

PHOTOMETRY OF THE DIFFUSE NEBULA NGC 7023 - - - - - *Philip C. Keenan* 600

ON THE POLARIZATION OF LIGHT IN REFLECTION NEBULAE - - *L. G. Henyey* 609

INDEX - 619

THE UNIVERSITY OF CHICAGO PRESS
CHICAGO, ILLINOIS, U.S.A.

December 1936 Vol. 84, No. 5

THE ASTROPHYSICAL JOURNAL

AN INTERNATIONAL REVIEW OF SPECTROSCOPY AND ASTRONOMICAL PHYSICS

Edited by

HENRY G. GALE
Ryerson Physical Laboratory of the University of Chicago

FREDERICK H. SEARES
Mount Wilson Observatory of the Carnegie Institution of Washington

OTTO STRUVE
Yerkes Observatory of the University of Chicago

WITH THE COLLABORATION OF

WALTER S. ADAMS, Mount Wilson Observatory
JOSEPH S. AMES, Johns Hopkins University
WILLIAM W. CAMPBELL, Lick Observatory
HENRY CREW, Northwestern University
CHARLES FABRY, Université de Paris
ALFRED FOWLER, Imperial College, London
EDWIN HUBBLE, Mount Wilson Observatory
HEINRICH KAYSER, Universität Bonn
ROBERT A. MILLIKAN, Institute of Technology, Pasadena
HUGH F. NEWALL, Cambridge University
FRIEDRICH PASCHEN, Reichsanstalt, Charlottenburg
HENRY N. RUSSELL, Princeton University
FRANK SCHLESINGER, Yale Observatory
HARLOW SHAPLEY, Harvard College Observatory

Former Editors:

GEORGE E. HALE JAMES E. KEELER EDWIN B. FROST

The Astrophysical Journal is published by the University of Chicago at the University of Chicago Press, 5750 Ellis Avenue, Chicago, Illinois, during each month except February and August. ¶The subscription price is $6.00 a year; the price of single copies is 75 cents. Orders for service of less than a half-year will be charged at the single-copy rate. ¶Postage is prepaid by the publishers on all orders from the United States, Mexico, Cuba, Porto Rico, Panama Canal Zone, Republic of Panama, Dominican Republic, Canary Islands, El Salvador, Argentina, Bolivia, Brazil, Colombia, Chile, Costa Rica, Ecuador, Guatemala, Honduras, Nicaragua, Peru, Hayti, Uruguay, Paraguay, Hawaiian Islands, Philippine Islands, Guam, Samoan Islands, Balearic Islands, Spain, and Venezuela. ¶Postage is charged extra as follows: for Canada and Newfoundland, 30 cents on annual subscriptions (total $6.30); on single copies, 3 cents (total 78 cents); for all other countries in the Postal Union, 80 cents on annual subscriptions (total $6.80), on single copies, 8 cents (total 83 cents). ¶Patrons are requested to make all remittances payable to The University of Chicago Press, in postal or express money orders or bank drafts.

The following are authorized agents:

For the British Empire, except North America, India, and Australasia: The Cambridge University Press, Fetter Lane, London, E.C. 4. Prices of yearly subscriptions and of single copies may be had on application.

For Japan: The Maruzen Company, Ltd., Tokyo.

For China: The Commercial Press, Ltd., 211 Honan Road, Shanghai. Yearly subscriptions, $6.00; single copies, 75 cents, or their equivalents in Chinese money. Postage extra, on yearly subscriptions 80 cents, on single copies 8 cents.

Claims for missing numbers should be made within the month following the regular month of publication. The publishers expect to supply missing numbers free only when losses have been sustained in transit, and when the reserve stock will permit.

Business correspondence should be addressed to The University of Chicago Press, Chicago, Illinois.

Communications for the editors and manuscripts should be addressed to: Otto Struve, Editor of THE ASTROPHYSICAL JOURNAL, Yerkes Observatory, Williams Bay, Wisconsin.

The cable address is "Observatory, Williamsbay, Wisconsin."

The articles in this journal are indexed in the *International Index to Periodicals*, New York, N.Y.

Applications for permission to quote from this journal should be addressed to The University of Chicago Press, and will be freely granted.

Entered as second-class matter, January 17, 1895, at the Post-Office, Chicago, Ill., under the act of March 3, 1879.
Acceptance for mailing at special rate of postage provided for in Section 1103, Act of October 3, 1917, authorized on July 15, 1918.

PRINTED IN THE U.S.A.

THE ASTROPHYSICAL JOURNAL

AN INTERNATIONAL REVIEW OF SPECTROSCOPY AND ASTRONOMICAL PHYSICS

VOLUME 84 DECEMBER 1936 NUMBER 5

THE STELLAR TEMPERATURE SCALE[1]

A. PANNEKOEK

ABSTRACT

The methods of determining stellar temperatures from color and energy distribution, from ionization, and from the Boltzmann function are discussed and are shown to depend upon complicated conditions in the atmospheres of the stars which are not sufficiently known at the present time to permit the derivation of reliable temperatures. Direct methods of determining the effective temperatures of stars give 3300° for class cMo and 10,500° for class Ao. These values are regarded as well established, their uncertainty being estimated at no more than 5 per cent. It is suggested that from the degree of accordance between these temperatures and those obtained by other indirect methods information may be obtained concerning the conditions prevailing in the atmosphere of the stars.

1. To find the temperature of a star, the most direct and the most promising method is to make use of the energy distribution in the spectrum. According to Planck's law for black-body radiation, the logarithmic intensity difference for two light sources is a linear function of $1/\lambda$, and the gradient is equal to $0.43 \times 14{,}600/T$, after a correction factor $(1 - e^{-c_2/\lambda T})^{-1}$ has been applied, which is only important for high temperatures and long wave-lengths. Measurements of these gradients—relative to the sun, to a standard star, or to a light source of known temperature—have been made by Wilsing,[2] Rosenberg,[3] H. H. Plaskett,[4] Sampson,[5] Jensen,[6] and by Greaves with his

[1] Part of a symposium on astrophysics, presented at the Harvard Tercentenary Conference on Arts and Sciences, September 3, 1936.

[2] *Publ. Ap. Obs. Potsdam*, **56**, 1909; **74**, 1919.

[3] *Nova Acta K. Leop. Akad.*, **101**, No. 2, 1914.

[4] *Pub. Dom. Ap. Obs. Victoria*, **2**, No. 12, 1923.

[5] *M.N.*, **83**, 174, 1923; **85**, 212, 1925. [6] *A.N.*, **248**, 242, 1933.

fellow-observers at Greenwich.[7] The first results showed serious discrepancies in the temperature scales. Careful comparisons and reductions of these data by A. Brill[8] have shown that their chief cause was a change of the gradient with wave-length. That the logarithmic intensity difference is not a linear function of $1/\lambda$ is confirmed by the measures of Jensen. So it appears that the radiation of a star cannot be black-body radiation.

Of course, there was no other reason to suppose that the stars radiate as black bodies than that in a first coarse approximation they seemed to do so. This hypothesis was introduced for the sound reason that it was the only means of deriving a temperature from the spectral intensity gradient. This temperature was called "color temperature"; it is of great practical importance because the most easily determinable data on color, such as color index and effective wavelength, depend on the same gradient and, therefore, are strongly correlated to this color temperature.

The ionization theory afforded another method of finding stellar temperatures, by making use of the intensities of absorption lines. The state of ionization of an element depends on temperature and pressure. To eliminate the uncertainties of first appearance, of abundance and of absolute values, Fowler and Milne[9] introduced the method of maxima of absorption lines. Observations show the spectral class for which a line has its maximum intensity. By theory the temperature is computed for which the atoms producing this line have a maximum concentration in the state of ionization and excitation required to produce it. Three assumptions are involved in this deduction: the abundance of the element is constant over the spectral sequence; the absorption coefficient is constant for all spectral classes; and the pressure is the same in all these atmospheres. Because this pressure is unknown, an absolute determination is not possible. By the assumption that the Balmer series has its maximum at 10,000° (A0), the pressure was fixed; and it determined the temperature of other maxima. The application of this method for lower temperatures is not easy, because there are few pronounced maxima. For high temperatures, however, just where the gradient ceases to

[7] *Greenwich Obs.*, 1932; *M.N.*, **94**, 488, 1934.

[8] *A.N.*, **218**, 209, 1923; **219**, 27, 356, 1923. [9] *M.N.*, **83**, 403, 1923; **84**, 499, 1924.

give reliable results, it proved most useful. Especially through the work of Mrs. Cecilia H. Payne-Gaposchkin[10] the temperature scale of the B and O stars could be determined by the maxima of *Si*, *C*, *O*, and *N* in different stages of ionization.

These ionization temperatures may be considered as an extrapolation to high temperatures of a scale based on spectral energy distribution. Hence, the assumption of the stars radiating as black bodies —which we know they do not—is underlying the entire temperature scale.

Now it seems that such an assumption cannot be avoided. Even in the case of the sun we make use of it; the effective temperature is the temperature of a black body that emits the same quantity of energy. For this reason the color temperature is sometimes called another kind of effective temperature. There is, however, an important difference: the effective temperature measures the total stream of energy passing through a unit surface area of the star. This stream is determined by the interior conditions; it determines (for given conditions of composition of the atmosphere and of gravitation at the surface) the state of the stellar atmosphere, the temperature and the ionization in each layer, the spectral distribution of the emitted light, and the line intensities. The amount of this energy stream is the independent datum, and all the other quantities are functions of it. The effective temperature is a number indicating this energy stream. Therefore, the effective temperature is not an uncertain value founded on an incorrect assumption, but it is the exact expression of a fundamental datum of the star. When we speak of the temperature of a star, this effective temperature is meant. Color temperature and ionization temperature have the meaning, that they may be considered as more or less correct substitutes for the effective temperature.

Table V in Brill's discussion of the stellar temperatures in the *Handbuch der Astrophysik*[11] shows the large discrepancies between the different determinations. The differences between the temperature scales resulting from different comprehensive discussions, though smaller, still show their uncertainty, as may be seen from a

[10] *Harvard Circ.*, Nos. 252 and 256, 1924.

[11] *Handbuch d. Astrophysik*, **5**, Part I, 150–151, 1932.

comparison of the scale derived by Mrs. Payne-Gaposchkin and quoted by Eddington,[12] the scale given by Russell, Dugan and Stewart,[13] and the scale given by Brill as the result of his discussions.[14] That these figures do not even mark the limits of uncertainty is shown in the result of the careful determination at Greenwich of the

	Bo	Ao	Fo	Go	Ko	Mo
C. H. Payne-Gaposchkin	20,000	10,000	7500	5600	4000	3000
Russell, Dugan, and Stewart	23,000	11,000	7400	5600	4200	(3100, M2)
A. Brill	22,000	13,500	8550	5800	4370	3240

color temperature by comparison with laboratory standards. Such absolute measures are difficult, and the elimination of the instrument introduced the uncertain element of atmospheric coloring. Still, the main result cannot be much in error, and it gave 18,000° for the color temperature of Ao stars.

2. The theoretical determination of the absorption coefficients of atoms under the conditions prevailing in stellar atmospheres, by the work of Kramers,[15] Sugiura,[16] Gaunt,[17] and Menzel and Pekeris,[18] provides a new foundation for the determination of stellar temperatures. It must be possible now, at least in the first approximation, to derive, first, the energy distribution in the stellar spectrum as a function of the temperature and, second, the variation of the line intensities with temperature for the real atmosphere, without the assumptions that were necessary ten years ago. Of course, theoretical discussions on the structure of the atmospheres are needed, which can be given as yet only to a certain degree of approximation. For a wave-length in the continuous spectrum, the intensity is found by solving the equations for the integrated light:

$$\frac{dJ}{d\xi} = 3kH\ ; \qquad \frac{dH}{d\xi} = k(J - E)\ ; \qquad J = 2H \text{ for } \xi = 0\ .$$

[12] *The Internal Constitution of the Stars*, p. 141, 1926. [13] *Astronomy*, **2**, 753, 1927.

[14] *Handbuch d. Astrophysik*, **5**, Part I, 193, 1932.

[15] *Phil. Mag.*, **46**, 836, 1923.

[16] *Scientific Papers, Inst. Phys. Chem. Res.*, Tokyo, **17**, No. 339, 89, 1931.

[17] *Phil. Trans.*, A, **229**, 163, 1930. [18] *M.N.*, **96**, 77, 1935.

where $\xi = -\int \rho dh$ is the homogeneous depth, $4\pi J$ = the total radiation, $4\pi H$ = the net stream, $4\pi E$ = the black-body radiation, k = the absorption coefficient, all holding for a special λ. The solution for the energy stream emitted at the surface is:

$$H = \frac{1}{2+\sqrt{3}} \int_0^\infty E(\xi) e^{-k\xi\sqrt{3}} k\sqrt{3}\, d\xi .$$

Denoting by $\bar{k}$ the mean absorption coefficient (Rosseland mean), we have

$$T^4 = T_0^4 (1 + \tfrac{3}{2}\bar{k}\xi) \qquad (T_0 = \text{the surface temperature}),$$

$$E = \frac{c_1}{\lambda^5} (e^{c_2/\lambda T} - 1)^{-1} = \frac{c_1}{\lambda^5} (e^{c_2/\lambda T_0 (1+\frac{3}{2}\bar{k}\xi)^{-\frac{1}{4}}} - 1)^{-1} .$$

In my former computation, a linear function for E was assumed,[19] namely, the first two terms of a Taylor development of this expression. Since the errors of this approximation may be rather large in some cases, we will use here the exact expression, reducing the integral to the form used by Lindblad[20] and Milne.[21] Putting

$$k\sqrt{3}\, d\xi = dt , \qquad \frac{c_2}{\lambda T_0} = a , \qquad \frac{\sqrt{3}}{2}\frac{\bar{k}}{k} = p ,$$

we have

$$4\pi H = \frac{4\pi}{2+\sqrt{3}} \frac{c_1}{\lambda^5} \int_0^\infty \frac{e^{-t} dt}{e^{a(1+pt)^{-\frac{1}{4}}} - 1} = \frac{4\pi c_1}{2+\sqrt{3}} \left(\frac{T_0}{\lambda}\right)^5 f(a, p) ,$$

$$f(a, p) = \int_0^\infty \frac{a^5 e^{-t} dt}{e^{a(1+pt)^{-\frac{1}{4}}} - 1} .$$

For this function $f(a, p)$ tables are given by Milne (using Lindblad's data); since they, however, extend only from $p = 0$ to $p = 2$, they had to be extended to special large values of p needed here. The results for the net stream $4\pi H$ are compared with the black-body radiation for the effective temperature

$$\pi E(T_1) = \frac{\pi c_1}{\lambda^5} (e^{a_1} - 1)^{-1} ,$$

[19] *Ibid.*, **95**, 529, 1935.

[20] *Upsala U. Årrskrift*, p. 33, 1920.

[21] *Phil. Trans.*, A, **223**, 201, 1922.

where $a_1 = c_2/\lambda T_1 = a\sqrt[4]{1/2}$. In the tabulated values the factor πc_1 has been omitted in $4\pi H$ as well as in πE. The values for $\bar{k}/k$ were taken from the data of *Amsterdam Publications* No. 4 (for log $g = 4.4$).

In Table I the results are given for effective temperatures $T_1 = 5040/0.2$, etc., corresponding to $T_0 = T_1\sqrt[4]{1/2}$. They afford the differences in the gradient $\varphi = c_2/T(1 - e^{-c_2/\lambda T})^{-1}$ between the stellar and the black-body radiation for the intervals 6000–5000 A and 5000–4000 A. The differences from the former computation are not large, and the theoretical color temperatures show the same character. The high color temperature of 18,000° found at Greenwich for the Ao stars, for which usually an effective temperature of about

TABLE I

$\frac{5040}{T}$	log p			log $4H/c_1$			log E/c_1			$\Delta\varphi$		φ	
	6000	5000	4000	6000	5000	4000	6000	5000	4000	5500	4500	5500	4500
0.2	−1.07	−0.88	−0.65	0.837	1.103	1.416	0.910	1.179	1.492	+0.02	0.00	0.90	0.79
0.3	−0.76	− .56	− .31	0.528	0.773	1.062	0.611	0.851	1.118	− .03	− .10	1.05	0.90
0.4	−0.37	− .16	+ .10	0.296	0.539	0.838	0.356	0.564	0.780	− .24	− .38	1.06	0.86
0.5	−0.14	+ .07	+ .34	0.101	0.342	0.637	0.122	0.295	0.458	− .47	− .61	1.07	0.87
0.6	−0.06	+ .17	+ .41	9.900	0.130	0.389	9.899	0.037	0.143	− .63	− .70	1.16	1.05
0.7	+0.08	+ .20	+ .24	9.733	9.904	0.019	9.684	9.783	9.831	− .50	− .31	1.55	1.71
0.8	+0.14	+ .08	− .09	9.559	9.606	9.503	9.472	9.533	9.520	+ .08	+ .41	2.39	2.70
0.9	+0.08	− .05	− .31	9.330	9.290	9.052	9.262	9.284	9.211	+ .43	+ .76	3.01	3.33
1.0	+0.03	−0.15	−0.47	9.103	8.983	8.635	9.054	9.035	8.901	+0.70	+0.98	3.56	3.83

10,000° is assumed, is not only confirmed but is even surpassed by the theoretical values. Computation shows constancy and even temporary decrease of color temperature, in going from Ao to Bo, at variance with observation, which, after allowance has been made for space reddening, indicates a slow but steady increase. Hence it is not possible to derive effective temperatures from the observed gradients in the case of hot stars, so long as the qualitative discrepancy between theory and observation is not removed.

In order to investigate it more closely, the energy distribution over the entire spectrum was derived for the case of an effective temperature of 10,080° ($5040/T = 0.5$). The data for the computation and the results are given in Table II.

The variations in surface radiation depend on $p = 0.87\bar{k}/k$; the mean absorption $\bar{k}$ determines the increase of temperature with

depth, and the special absorption $k(\lambda)$ determines from what depth we find radiation of this λ reaching the surface. For these high-temperature stars where the absorption coefficient is determined by hydrogen, it jumps at each band edge to a higher value on the blue side but then decreases continually with λ^3 down to the next edge. The emitted radiation is strong on the longer wave-length side of each edge and falls there abruptly to a smaller value. (We disregard here the smoothing of the highest intensity peak at each edge in consequence of the line-crowding.) This small emission at the short

TABLE II

λ	p	a	log $4H/c_1$	log E/c_1
12,000	0.33	1.41	9.20−10	9.25−10
9000	0.69	1.88	9.54−10	9.64−10
8206	1.10	2.06	9.80−10	.....
	0.30		9.69−10	
7000	0.49	2.42	9.91−10	9.95−10
4000	2.19	4.22	0.64	0.46
3646	2.90	4.63	0.75	.....
	0.15		0.27	
3000	0.27	5.63	0.35	0.56
2500	0.47	6.76	0.39	0.54
2000	0.91	8.45	0.45	0.41
1500	2.17	11.27	0.62	0.00
1000	7.30	16.90	1.01	8.82−10
911	9.6	18.54	1.09	8.42−10
	0.00		6.9 −10	

wave-length side of each edge is often spoken of as an "absorption band," for which a correction should be applied to get the clear spectrum. Figure 1 shows that this is not a correct statement of the phenomena. The whole spectrum is distorted; and corrections should also be applied, even larger ones, to the bright parts on the long wave-length side of the edges.

The energy-curve of the spectrum emitted by the stellar atmospheres in Figure 1 shows, first, that in the Paschen region (between λ 8206 and λ 3646, where the third hydrogen-level determines the absorption) the gradient is stronger than in the black-body radiation; this is the phenomenon already treated, which appears in the color temperature. In the Balmer region (between λ 3646 and λ 911, where the second hydrogen-level dominates the absorption) the de-

viation is still more striking; here the emitted radiation increases in a steep ascent for the wave-lengths just above the Lyman edge, to dwindle to nothing below 911 A. These regions are, it is true, not observable; but this strong distortion of the spectrum must produce considerable effects in other phenomena. The radiations of wave-lengths 1215 A, 1024 A, 971 A (La, $L\beta$, $L\gamma$), producing the transi-

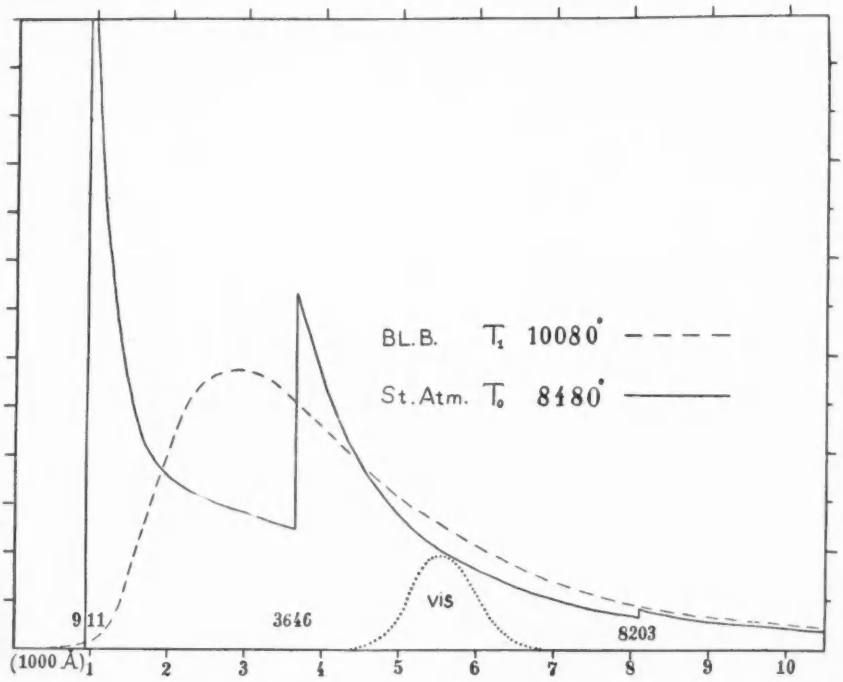

FIG. 1

tions from the lowest to the second, the third, and the fourth level, have here an intensity 22 times, 120 times, and 215 times larger than in the black-body radiation. Hence, in the upper layers of the atmosphere the higher levels must be more strongly occupied than in the case of thermodynamic equilibrium, and the more so the higher the level considered. This must increase the general absorption; moreover, it offers an explanation of the remaining discrepancies in the color temperature of the A stars.

Since the transitions 1–2 and 1–3 chiefly dominate the occupation of these higher levels, we may expect that the number of atoms in the third level is increased 5 to 6 times more than the number of atoms in the second level. Hence, the absorption due to ionizations from the third level is, in the same ratio, stronger than from the second level, relative to the former computations based on the Boltzmann ratios. Since the mean absorption $\bar{k}$ for this temperature[22] is chiefly a combination of second- and third-level absorption, this means that $\bar{k}/k$ and p must be smaller in the Paschen region and larger in the Balmer region. This will produce a smaller difference in intensity gradient between the stellar and the black-body spectrum for the Paschen region than was found in our first computation —a change in the right direction. It will not be easy, however, to determine the exact amount. What we computed here was the spectral-energy distribution in the radiation emitted at the surface of the star. For the deeper layers the composition of the radiation approaches black-body radiation at an increasing rate; and all these deeper layers, with their different occupation of higher levels and their, consequently, different absorption coefficients, determine the real observed spectrum. Accordingly, in a second approximation a more refined treatment will be necessary in which the conditions in each atmospheric layer and its contributions to the total radiation are taken into account.

There is still another point to be considered. We have assumed the surface temperature to be $T_0 = T_1\sqrt[4]{1/2}$ (in this case 8470°), as follows from the Schwarzschild relation for black-body radiation. (The deviation from the linear gradient in the surface layers, giving the exact ratio $T_1/T_0 = 1.23$ as computed by Hopf, does not concern us here, because for us T_0 means only a constant in the linear function we use at greater depth.) For the distorted energy-curve of the real stellar radiation, the same ratio will not hold. Now that it has been found in the first approximation, based on the surface temperature $T_0 = 8470°$, we are able to integrate the radiation over the entire spectrum to find the total amount of emitted energy and to

[22] Cf. Table 8, *Pub. Astro. Inst. Amsterdam*, **4**, 1935.

see to what effective temperature it corresponds. By reading from the curve and by numerical integration, we find

$$\log \int \frac{4Hd\lambda}{c_1} = 0.290 ,$$

whereas

$$\log \int \frac{E}{c_1} d\lambda = \log \frac{\pi^4}{15} \left(\frac{T_1}{c_2}\right)^4 = 0.205$$

when computed with $T_1 = 10{,}080°$. The total amount of energy comes out somewhat larger for the stellar atmosphere and corresponds to an effective temperature somewhat higher, 10,400°. This means that for a star with effective temperature 10,080° the surface temperature is somewhat lower than that computed by the Schwarzschild relation. The difference is not large enough to upset the foregoing results; it has to be taken into account in a second approximation.

3. For the stars of low temperature there are difficulties of another kind. The absorption coefficient is due to the ionization of metal atoms from different levels. Because we do not observe any band edge corresponding to a metal-atom level, we assume that there is some smoothing process at work; and for the absorption coefficient we take the value computed by a smoothed formula:

$$k = \text{Const. } T^{-\frac{3}{2}} \nu^{-3} (e^{h\nu/kT} - 1) .$$

The computations were made for the temperatures 5040° and 3150° ($5040/T = 1.0$ and 1.6). The result is contained in the values of Table III. The absorption coefficient is a minimum for a large infrared wave-length (11,000 A for 5040°, 17,000 A for 3150°), and increases strongly with decreasing wave-length in the visual part of the spectrum (because at low temperatures the lowest levels are strongly occupied relative to the higher levels). The consequence is that the short wave-length part of the spectrum, including the visible region, is much weakened (as is shown in Figure 2 for $T_1 = 3150°$), whereas the maximum in the near infrared is increased and displaced toward the longer wave-length side and the far infrared again

is weakened. The slope in the visible part of the spectrum deviates strongly from the corresponding black-body radiation and indicates

TABLE III

	$T_1 = 5040°$				$T_1 = 3150°$			
	a	p	$\log 4H/c_1$	$\log E/c_1$	a	p	$\log 4H/c_1$	$\log E/c_1$
50,000.....	0.68	0.30	.....	.....	1.08	0.63	6.31	.....
25,000.....	1.35	0.85	7.69	7.68	2.16	1.45	7.36	7.30
20,000.....	1.69	1.12	8.05	8.00	2.70	1.66	7.64	7.55
15,000.....	2.25	1.48	8.43	8.37	3.61	1.74	7.94	7.82
12,000.....	2.82	1.70	8.71	8.62	4.51	1.55	8.08	7.97
9000.....	3.76	1.70	8.99	8.88	6.01	1.02	8.08	8.04
7000.....	4.83	1.45	9.12	9.02	7.73	0.51	7.80	7.95
6000.....	5.63	1.12	9.11	9.05	9.01	0.28	7.48	7.81
5000.....	6.76	0.76	9.00	9.04	10.82	0.10	6.95	7.55
4000.....	8.45	0.36	8.64	8.90	13.52	0.02	6.18	7.05
3000.....	11.27	0.08	7.84	8.49	18.03	0.001	4.85	6.03

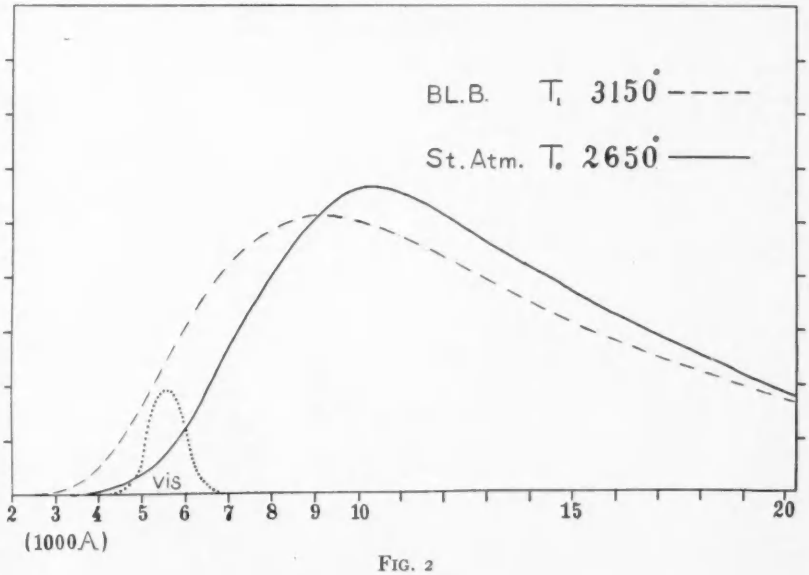

FIG. 2

far too low a temperature. All these deviations are strongest for the lowest temperatures. Integrating the energy values of Table III over the whole spectrum, we find here again a total stream of energy somewhat larger than belongs to the corresponding T_1 (log = 9.032

instead of 9.001 for $T_0 = 4230°$, 8.221 instead of 8.185 for $T_0 = 2650°$) and corresponding to a black-body radiation of 5130° and 3220°, only slightly larger than the values of $T_0 \sqrt[4]{2}$.

We can make use of the measurements of Jensen to derive temperatures from the spectral gradients of low-temperature stars. Jensen measured for a range of wave-lengths the relative intensities of a number of stars relative to α Ursae Minoris. By means of seven stars, which he has in common with the Greenwich observers (η UMa, α Leo, α Lyr, α CrB, α Agl, α UMi, α Aur), we can use the absolute Greenwich gradients to reduce his results for α Orionis to absolute values (i.e., intensities relative to a black body of $T = \infty$) and compare them with H and E multiplied by λ^5. The result of the comparison is shown in Figure 3. (The shorter wave-lengths, from 4000 A downward, are not reliable because here in the class A comparison stars the hydrogen depression makes itself felt.) Compared with the black-body-curve, the slope of the observed intensity-curve indicates a temperature below 3150°. On the contrary, the theoretical curve computed for the stellar atmosphere shows a steeper slope than the star. Hence, T_1 for the star must be above 3150°—or, more exactly, above 3220°—and the theoretical curve belonging to $T_1 = 3600°$ seems to fit better. An exact result is not possible because Jensen's measurements show a variation of the gradient with wave-length which is not present in the theoretical curves.

There are other sources of uncertainty here. It is doubtful whether for these low temperatures we can rely upon the smoothed formula for the absorption coefficient where it is due only to the ionization of a small amount of sodium and potassium atoms. Even if we were able to observe and measure the continuous background of the spectrum, its gradient would give information about the variation of the absorption coefficient rather than about the temperature. But it is well known that, owing to the crowding of absorption lines, chiefly those constituting the molecular absorption bands, the sifting-out of the continuous spectrum is well nigh out of the question. Thus, for such low-temperature stars the gradient of the visible spectrum, observed with present means, cannot give very reliable results for the temperature.

4. The theoretical knowledge of the coefficient of continuous absorption must provide the foundation for the use of line intensities for the derivation of stellar temperature. The intensity of an absorption line depends on the ratio s/k of two quantities: s, the diffusion coefficient in the line (depending on abundance, state of ionization,

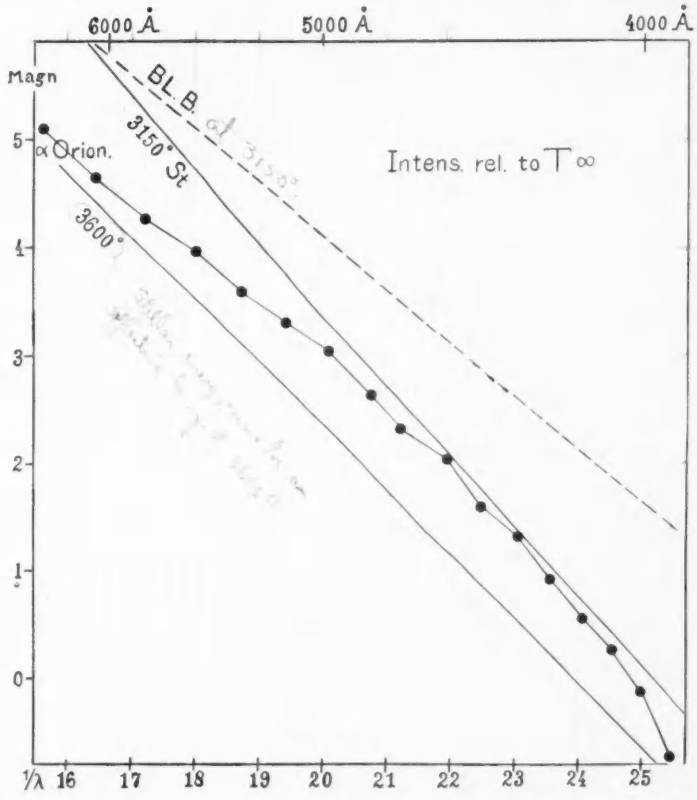

FIG. 3

level, and transition probability of the atoms involved); and k, the continuous absorption coefficient. Because k is variable with temperature in a known way, the maximum intensity of an absorption line is not simply identical with the maximum concentration of the atoms producing it, but one can be derived from the other. Moreover, it is not necessary to assume a pressure; all the layers in an atmosphere with different pressures take part in the formation of the

line, and the theoretical treatment of the atmosphere gives the line intensity, where the intensity of the total stream of energy (i.e., the effective temperature T_1) and the surface gravity g appear as the determining parameters. The only assumption we cannot avoid making use of is that of constancy of abundance over the range of spectral classes.

The most conspicuous of the line maxima used in determining stellar temperatures is the maximum of the Balmer series of hydrogen in class Ao. Fowler and Milne were able to explain it easily because the hydrogen atoms in the second level of energy have a clearly depicted maximum of concentration, for which 10,000° was assumed. If, however, the variation of k is taken into account, we get an extremely flat and ill-defined maximum at a lower temperature (7000° to 8000° for $\log g = 5$ to 2; cf. Figure 6 in *Amsterdam Publications* No. 4). Unsöld has shown[23] that in a pure hydrogen atmosphere the intensity of the Balmer lines must steadily increase for decreasing temperature. The reason is simply that the diffusion coefficient s for these lines depends on the concentration of H in the second level, whereas they are situated in the Paschen region, where the absorption coefficient k depends on the concentration of H in the third level, and that the relative number of the atoms in the second state compared to those in the third state increases with decreasing temperature. Going down below 10,000° the intensity of the Balmer lines must go on increasing because, though N_2 and s are strongly decreasing, N_3 and k are decreasing still more strongly. As soon, however, as k for hydrogen falls below the absorption coefficient due to the metal atoms, the k of the stellar atmosphere begins to increase; and now the intensity of the Balmer lines decreases rapidly. Their maximum, therefore, is not due to themselves but to the transition of the continuous hydrogen to the metal absorption. If the relative abundance of the hydrogen to the metal atoms is assumed to be 50 instead of 1000, the maximum is raised 1000°. It is not likely that in this way we can escape the difficulties. Moreover, the intensity of the Balmer lines is an expression chiefly of their width, which is due to the Stark effect and depends, in the first place, on the surface gravity. Hence, in comparisons with observational data a careful

[23] *Zs. f. Ap.*, **8**, 32, 1934.

arrangement according to the gravity g is first necessary before the variation with T_1 can come out in the right way. We may expect that further approximations in the theoretical treatment of the A stars may clear up the discrepancies; but, for the moment, the maximum of the Balmer lines is not a good indicator of temperature.

This hydrogen case is an example of a more general phenomenon. Between 10,000° and 6000° the continuous absorption coefficient varies irregularly with temperature, because here is the transition from hydrogen to metal absorption. The variations of line intensities in this realm are determined more by these irregularities than by the variations in the element producing the line. The exact course of these irregularities depends on the assumed composition of the atmosphere, especially on the relative abundance of hydrogen and metal atoms. In the maxima of absorption lines within these temperatures, composition and temperature are interrelated.

Below 6000° and above 10,000° the absorption coefficient runs smoothly and slowly with temperature, so that the maxima are related in a simple way to temperature. Lines absorbed by the lowest level of ionized atoms (as H and K of Ca^+) present very flat and uncertain maxima; hence they cannot give exact results for the temperature. The matter is different for lines absorbed by higher levels, where the temperature of the maximum depends chiefly on the excitation potential. Here, however, the crowding and blending of lines make determinations difficult, and exact photometric measures of line intensities are lacking on the whole. Moreover, the variation of k with temperature depends here on the assumed composition of the metal atom mixture.

The case is more favorable for high-temperature stars above 10,000°, where the absorption coefficient depends on hydrogen only and the absorption lines can be separated easily. Thus for the B and O stars the former results of Fowler and Milne and of Mrs. Payne-Gaposchkin from metalloid lines can be put upon better foundations. After the method indicated and used in *Amsterdam Publications* No. 4, the line intensities have been computed for a range of temperature, then plotted, and the temperature of the maximum read. The pressure and the atmospheric parameters s, σ, σ' were taken for two cases of surface gravity, $\log g = 4.4$ (dwarfs)

and log $g = 2.4$ (giants). In Table IV the results for the temperatures of the maxima are given, and in the last columns the spectral classes of these maxima are indicated, first according to old results of H. H. Plaskett and Mrs. Payne-Gaposchkin, and then according to the latest results of E. G. Williams.[24] The resulting scale of temperatures is not very different from the former investigations; for Bo the corresponding temperature is nearly 25,000°.

TABLE IV

	Ion. P.	Exc. P.	log g = 4.4	log g = 2.4	H. H. Pl. and C. H. G.	E. G. W.
Si^+	16.3	9.8	12,900°	11,200°	Ao	.....
C^+	24.3	18.0	21,000	16,800	.....	B3
N^+	29.5	18.4	21,000	18,700	B2	B1–2
Si^{++}	33.3	18.9	22,000	19,400	B1–2	B1–2
He	24.5	20.9	18,000	14,400	B2–3	.....
O^+	34.8	23.3	24,000	21,000	B1	B1
Si^{+++}	44.9	23.9	31,500	27,000	O9	O9
N^{++}	47.4	27.3	35,000	31,500	O7–8	O9
C^{++}	47.7	29.4	30,600	28,000	O9?	O9–Bo
O^{++}	54.9	33.7	37,400	33,600	O9–Bo	O8
N^{+++}	77.3	39.7	39,000	33,600	.....	.....
He^+	54.2	50.8	44,000	39,000	.....	.....
C^{+++}	64.2	55.5	50,000:	44,000	.....	.....

5. Now that the intensity of a line expressed, for example, as the half-width for 50 per cent residual intensity, or as the equivalent width, can be measured as well as computed, it is not necessary to make use of maxima. The intensities themselves may be used, and so a larger quantity of data may be utilized. The number of good intensity measures, it is true, is only small as yet. We can, therefore, make use of a few cases only as instances of the method.

For the line K of Ca^+ the half-width in the solar spectrum is 6.3 A; this corresponds (according to formulas 28 and 46 in *Amsterdam Publications* No. 4) to log abundance = −4.71, that is, the number of *Ca* atoms is 20, if all the metals together are taken as 1000. By means of this abundance we compute log $\Delta\lambda^2$ and the half-width $\Delta\lambda$ itself (in the case of disappearing atoms):

$5040/T$ =	0.4	0.5	0.55	0.6	0.65
log $\Delta\lambda^2$ =	−2.58	−1.04	−0.13	+0.63	+1.28
$\Delta\lambda$ =	0.051	0.30	0.86	2.1	4.4 A

[24] *Ap. J.*, **83**, 319, 1936.

From some slit-spectra of α Lyrae, taken in August 1935, with a two-prism spectrograph attached to the Wyeth reflector at the Harvard College Observatory, I find an equivalent width of 0.97 A. From theoretical profiles, we found for the relation between half-width and equivalent width:

log E.W.....	0.40	0.20	0.00	9.80	9.60	9.40	9.20	9.00	8.80
log H.W.....	9.89	9.69	9.48	9.28	9.06	8.95	8.78	8.68	8.54

Thus, an equivalent width of 0.97 A means a half-width of 0.29 A, corresponding to $5040/T = 0.50$. Hence, assuming for α Lyrae the same abundance of *Ca* atoms as for the sun, we find a temperature of 10,100°.

In the same way we can make use of the results of Mrs. E. T. R. Williams-Vyssotsky[25] for the equivalent width of the line K in a number of class A stars. We find (taking $\log g = 4.4$):

	Sirius	Mean Ao	A2	A3	A5
E. W.....	0.62	1.08	2.94	4.03	4.5
H. W.....	0.19	0.33	0.91	1.25	1.39
$5040/T$.....	0.47	0.50	0.55	0.57	0.58
T.....	10,700°	10,100°	9200°	8800°	8700°

It must be remarked that the assumed relative abundance of hydrogen and metal atoms goes into this result in its full amount, because it determines the relative values of k for A stars and the sun. If hydrogen atoms are 100 times (instead of 1000 times) more abundant than metal atoms, the temperatures deduced are raised 1200°. Moreover, the assumption of equal abundance of calcium in the sun and the A stars is involved, whereas after the results of W. W. Morgan[26] the abundance of different metals must be different in different A stars. The deviations, however, from constant composition do not seem to amount to large factors; since the variation of the concentration of active atoms with temperature is very rapid, the uncertainties of temperature resulting from these differences will not be large.

There may be a way to escape these uncertainties and to eliminate the differences of abundance and of absorption coefficient at the same time, namely, by comparing the line intensities for ionized and

[25] *Harvard Circ.*, No. 348, 1930.

[26] *Pub. Yerkes Obs.*, 7, No. 3, 1935.

neutral atoms of the same element. The line λ 4227 of *Ca* and the K line λ 3933 of Ca^+ both belong to the lowest level; therefore, no other factors are involved than the variations of k with wave-length, which are small for this small distance in λ and are neglected in the following computation. For α Lyrae the equivalent width of *Ca* 4227 was found from the Victoria spectra to be 0.044 A. According to the curve of growth derived by Struve and Elvey for this star,[27] this value is already situated on the wing part of the curve, where the equivalent width increases as the square root of the concentration. Hence, the ratio of the concentrations of *Ca* and Ca^+ atoms is the square of the ratio of the equivalent widths of λ 4227 and λ 3933, i.e. $(0.044:0.97)^2$, of which the logarithm is -2.70. For the sun we have the half-width of λ 4227, taken from the profile derived by Redman,[28] 0.57 A; compared with the half-width 6.3 A of the K line, we find the logarithm of the ratio of the concentrations $\log (0.57:6.3) = -2.08$. Hence, we find (x = rate of ionization):

$$\log \left[\left(\frac{x}{1-x} \right)_{\alpha \text{ Lyr}} : \left(\frac{x}{1-x} \right)_{\odot} \right] = 0.62 .$$

Computing this ratio after the ionization formula $x/(1-x) = K/P$ (taking $\log g = 4.4$), we find:

T	= 10,080°	8400°	7200°	6300°	5800° (⊙)
$\log K/P$	= 4.61	3.89	3.31	2.83	2.46

The observational result would give a temperature for α Lyrae nearly 1000° above the solar temperature. In this A0 star both λ 4227 and K have strongly decreased relative to the sun, but nearly in the same ratio, whereas theory demands that λ 4227 should have decreased much more rapidly. Indeed, for a temperature of 10,000° we should expect λ 4227 to be nearly 7 times fainter, so that it would have entirely disappeared in the spectra of A0 stars. Of course, we could assume that the line seen at that wave-length is not the *Ca* line λ 4227 but has some other origin; indeed, a faint Ti^+ line corresponds in wave-length. We shall see, however, that the same

[27] *Ap. J.*, **79**, 409, 1934.

[28] *M.N.*, **95**, 751, 1935.

phenomenon presents itself for other elements; hence, it is not likely that we can so easily explain away the discrepancy.

6. Adams and Russell derived[29] in 1928 the scale of stellar temperatures by comparing the number of atoms in different levels with the Boltzmann function. The factors of abundance and transition probability for each line were eliminated by using for each star relative values compared with the sun. Then the logarithm of the concentration ratio is a linear function of the excitation potential E:

$$\log Y = \text{Const.} - E\left(\frac{5040}{T'} - \frac{5040}{T}\right).$$

The relative concentrations (or numbers) of active atoms producing the lines were found by comparing the stellar with the solar-line intensities and calibrating the Rowland scale of solar intensities by means of multiplets. The *Fe* spectrum bears nearly 90 per cent of the weight, because here the levels extend continuously from $E = 0$ to 4.5 volts. It appeared that for α Orionis and α Scorpii, log Y was not a linear function of E; for large E the variation in log Y slowed down. So it was necessary to replace E in the formula by a quadratic expression $E - 0.083E^2$. This means that the limiting slope of the curve for $E = 0$ was used to derive the difference in $5040/T$. The same quadratic expression was then used for the other stars. In this way temperatures of 9900° for Sirius and 2900° and 3000° for α Ori and α Sco were found.

Here the line intensity, after calibrating, was directly connected with the number or the concentration of atoms. We now know that line intensity is directly connected with s/k, so that numbers expressing line intensities must be multiplied by factors k to find numbers expressing the concentration of atoms. Hence, corrections = log $(k_{st}/k\odot)$ must be applied to log Y. The values of log k were taken from *Amsterdam Publications* No. 4, using $5040/T = 1.6$, log $g = 1.4$, for α Ori and α Sco; $5040/T = 0.5$, log $g = 4.4$, for Sirius; and $5040/T = 0.88$, log $g = 4.4$, for the sun. The differences Star *minus* Sun vary with wave-length; Dr. Russell kindly provided me with the separate wave-lengths of the lines used, so that for each group the reduction could be computed. In Table V the k correct-

[29] *Ap. J.*, **68**, 9, 1928.

ions and the uncorrected and the corrected values of log Y are given. It appears that by thus taking account of the variations of the absorption coefficient with temperature and wave-length, the constant part of log Y is changed considerably, whereas the slope is

TABLE V

E	α Orionis, α Scorpii						Sirius		
	log Y		log Δk		log Y corr.		log Y	log Δk	log Y corr.
0.06	+2.05	+2.30	−1.30	−1.40	0.75	0.90	−2.66	+2.13	9.47
0.94	+1.28	+1.23	1.54	1.57	9.74	9.66	2.13	2.29	0.16
1.54	+0.54	+0.97	1.33	1.42	9.21	9.55	2.30	2.11	9.81
2.21	+0.30	+0.47	1.44	1.35	8.86	9.12	2.00	2.25	0.25
2.56	−0.06	−0.05	1.67	1.70	8.27	8.25	2.00	2.43	0.43
2.89	−0.19	−0.03	1.40	1.41	8.41	8.56	1.85	2.22	0.37
3.24	−0.33	−0.10	1.41	1.43	8.26	8.47	1.97	2.23	0.26
3.47	−0.54	−0.27	1.52	1.50	7.94	8.23	1.77	2.32	0.55
4.03	−0.76	−0.40	1.57	1.57	7.67	8.03	1.77	2.36	0.59
4.50	−0.87	−0.77	−1.58	−1.60	7.55	7.63	−1.60	+2.38	0.78

changed by only a small amount. Figure 4, where the corrected log Y are represented, shows that the curvature for α Ori and α Sco still exists. Retaining Russell's formula, and hence assuming that in all the stars the occupation of the higher levels follows $E - 0.083\ E^2$, we find the expressions

$$\log Y = 0.88 - 0.82\ (E - 0.083E^2) \text{ for } \alpha \text{ Ori and } \alpha \text{ Sco},$$
$$\log Y = -0.50 + 0.41\ (E - 0.083E^2) \text{ for Sirius}.$$

Assuming that the temperature determining the observed distribution over the levels coincides with the effective temperature, we find the values of $5040/T = 1.70$ and 0.47; hence $T = 2960°$ for α Ori and α Sco and $T = 10{,}700°$ for Sirius. We have to consider here that the quadratic expression is only an interpolation formula which certainly does not hold for higher values of E, so that the limiting slope for $E = 0$, on which depends the temperature found, has the uncertainty of an extrapolated value.

The quadratic deviation from the Boltzmann distribution, the so-called "Adams-Russell phenomenon," has not found an adequate explanation as yet. Dr. Russell, in a letter, suggested the possibility that for these two Mo stars the value of log Y for the lowest E may

be systematically wrong, because the lines belonging to the lowest levels are extremely strong in these stars and so cannot be exactly compared with the solar lines. If the result for $E = 0.06$ is excluded, the remaining values, as Figure 4 shows, may be represented by a

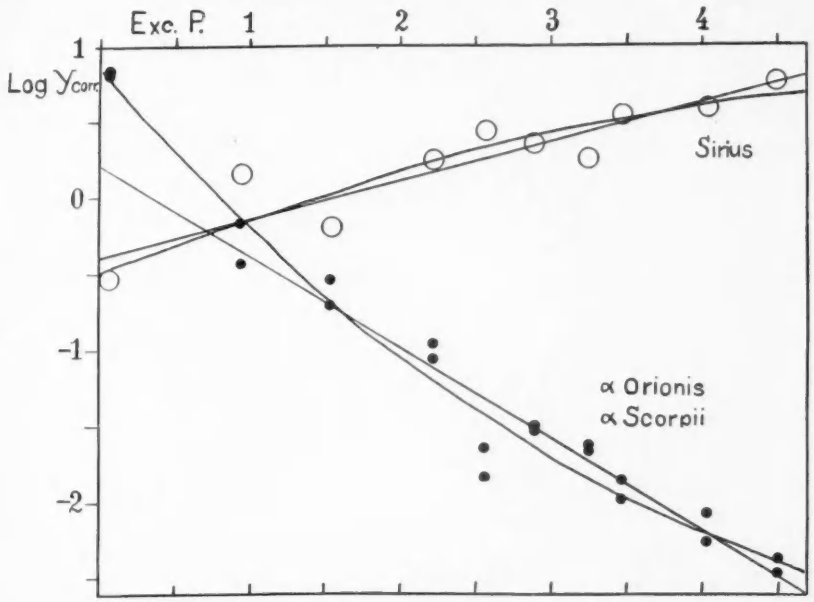

FIG. 4

straight line, which, of course, has a smaller slope. For Sirius, log Y as a function of E is as well represented by a straight line as by the curve of Adams and Russell. The resulting linear expressions are

α ORI, α SCO − SUN		SIRIUS − SUN	
log Y uncorr.	$= +1.60 - 0.57E$	log Y uncorr.	$= -2.55 + 0.21E$
log $k/k\odot$	$= -1.40 - 0.03E$	log $k/k\odot$	$= +2.15 + 0.05E$
log Y corr.	$= +0.20 - 0.60E$	log Y corr.	$= -0.40 + 0.26E$

Then for $5040/T$ we have 1.48 and 0.62; hence $T = 3400°$ for α Ori and α Sco, and $T = 8130°$ for Sirius. Because the mean slope used here is smaller than the limiting slope in the quadratic formula, the scale of temperatures is narrower.

The data of Adams and Russell used here can give still another result. The constant in the foregoing formulas represents the relative number of atoms for the star and the sun for $E = 0$, i.e., for

the lowest level; it depends only on abundance and state of ionization. Comparing these values for *Fe* and Fe^+, the abundance of the element is eliminated in their ratio; and the same holds for the values of k, in so far as we may assume that the average wave-length for the *Fe* and the Fe^+ lines was the same. Hence, in the same way as in the case of *Ca* and Ca^+, this ratio is equal to the ratio of $x/(1-x)$ for the star and sun. The values of log Y in the case of Sirius given by Adams and Russell for Fe^+, *Ti*, and Ti^+ were first corrected for k and then reduced to $E = 0$ by means of the slope derived from *Fe*.

TABLE VI

E	log Y	log Y corr.	$-0.26E$	log Y_0	E	log Y	log Y corr.	$-0.26E$	log Y_0
	Fe^+					*Ti*			
2.83	−0.18	+2.02	−0.73	+1.29	0.03	−2.00	+0.20	−0.01	+0.19
3.56	−0.54	+1.66	−0.95	+0.71	0.83	2.11	0.09	.22	− .13
					1.02	1.07	1.13	.27	+ .86
	Ti^+				1.44	1.13	1.07	.37	+ .80
					1.82	1.82	0.38	.47	− .09
					2.09	1.00	1.20	.54	+ .66
					2.26	−0.90	+1.30	−0.59	+0.71
1.16	−1.05	+1.15	−0.30	+0.85					
1.57	−0.78	1.42	.41	1.01					
2.00	+0.08	2.28	.52	1.76					
2.93	−0.75	+1.45	−0.76	+0.69					

Taking averages for log Y_0, the ratio log Y_0^+ − log Y_0^n = log $[x/(1-x)$ St. : $x/(1-x)\odot]$. We have

log Y_0 for *Fe* −0.40, for Fe^+ +1.00 log $Y_0^+/Y_0^n = +1.40$;

log Y_0 for *Ti* +0.43, for Ti^+ +1.08 log $Y_0^+/Y_0^n = +0.65$.

Computing log $x/(1-x)$ = log K/P for different temperatures (log g = 4.4), we find:

	10,080°	8400°	7200°	6300°	5800°(⊙)
Fe	3.68	2.78	2.03	1.37	0.87
Ti	4.11	3.29	2.63	2.10	1.64

The corresponding temperature for *Fe* is 7500°; for *Ti*, 6600°. Hence we meet with the same phenomenon as in the case of *Ca:* the decrease of the lines of the neutral atoms relative to the enhanced lines from the sun to Sirius is far too small for their large difference in temperature. Assuming a temperature of 10,000° for Sirius, all those arc lines which we see in the Sirius spectrum should be invisible after the ionization formula, provided the right curve of growth has been used. But these faint lines probably are situated on that part of the curve of growth where a large variation of atom concentration corresponds to a small change in line intensity. So it is probable, here as well as in the case of *Ca*, that pecularities of the curve of growth, depending upon turbulence and collisions in the star and upon the Weisskopf-Wigner corrections of the atoms, play a rôle and make the exact determination of temperatures by this method difficult. These computations of Y_0 and of their ratio have also been made with the quadratic formula; they give so nearly the same results that it is unnecessary to give them in detail. For the low temperature Mo stars the ratio $\log Y_0^+/Y_0^n = -0.55$ for *Fe* and -1.32 for *Ti*. It is not well possible to use these results for the derivation of temperatures because, owing to the chromospheric character of their atmospheres, we do not know what pressure to use in the computation of the ionization. On the other hand, in so far as these relations are trustworthy, they may better be used to derive some information about the pressure in the relevant atmospheric layers, once their temperature is known.

7. The effective temperature itself is derived for the sun by measuring the total radiation, the solar constant, and reducing it by means of the angular semi-diameter of the sun to radiation per unit surface. For the stars this method can be applied in a direct way only, where the angular diameter can be determined by interferometer measures, i.e., for red giants and supergiants. The total radiation, the bolometric magnitude, is then derived from the visual magnitude by means of the "reduction to bolometric magnitude," such as is given by Eddington:[30] for 3600°, −0.95 mag.; for 3000°, −1.71 mag.; for 2540° −2.59 mag. Then for α Sco we find from the angular semidiameter of 0".021 and from the visual magnitude 1.2 the

[30] *Op. cit.*, p. 138, 1926.

temperature 2980° (red. to bol. mag. = −1.74; bol. mag. = −0.54). Eddington's table of reduction from visual to bolometric magnitude has, however, been computed for black-body radiation. Hence, this derivation does not materially differ from the computation made in the textbook of Russell, Dugan, and Stewart, where the black-body radiation for λ 5290 is compared with the visual magnitude of the star. A better approximation will be reached if, for the reduction from visual to bolometric magnitude, we make use of the spectral intensity-curve computed here for the stellar radiation. The curve for 3150° in Figure 3 gives a reduction of −2.70 mag., i.e., 1.2 mag. larger than the black-body-curve gives for the same temperature. Making use of the interpolated values: for 3360°, −2.02 mag.; for 3600°, −1.46 mag., we find now from the same data on α Sco the temperature 3310° (red. to bol. mag. = −2.18).

Though in this way the systematic error of former derivations is avoided, the method remains somewhat unsatisfactory because the total radiation is derived from the measurement of a minute part of it at the extreme border of the spectrum. To find the effective temperature directly, bolometric or radiometric measurements of the total radiation are needed. Pettit and Nicholson have measured stellar radiations with vacuum thermocouples,[31] and by means of absolute standardization of their instrument in various ways they could derive stellar temperatures from the interferometer diameters. They found 3270° for α Ori and α Sco.[32] The measures had first to be reduced to "no atmosphere," i.e., corrected for the atmospheric absorption bands in the red and infrared; this correction was derived from measures on solar energy-curves, of course, by supposing the stellar radiation to be black-body radiation of a certain low temperature. This involves the possibility of a certain error; the radiation of the star has a different energy distribution from a black body, and for its derivation even the knowledge of k may not be sufficient because of the strong molecular absorption bands in the stellar spectrum itself. Still, it is not likely that appreciable errors will arise, because the atmospheric bands are well distributed over the most contributing parts of the spectrum. Hence this determination deserves a large weight. We might suppose that a certain limb-darkening of these stars, now theoretically determinable from the knowledge of k, could

[31] *Ap. J.*, **68**, 279, 1928. [32] *Ibid.*, p. 301.

produce an important correction to the angular diameters derived from interferometer measures. The figures of Table III, however, show that p and $\bar{k}/k$ for visual rays is very small; hence there is no appreciable limb-darkening here.

The accordance of the two results based upon interferometer measures is very satisfactory now, so that 3300° may be assumed as the effective temperature of these cMo stars.

8. The same data may be found in an indirect way from eclipsing variables. If all the data about the eclipses, and hence the ratios of the stellar diameters to the orbit, are well known, the radial velocity gives the diameters in kilometers. Then we want the parallax to derive angular diameters, which, when combined with the observed radiation, give the temperatures.

This method has been applied by S. Gaposchkin[33] to a large number of eclipsing variables. Because most of the parallaxes were highly uncertain, only a rough accordance with the scale usually adopted, with many large deviations, could be ascertained. Lately Pilowsky[34] made another statistical application of this method. A number of eclipsing variables with known radial velocities gave stellar diameters, which were plotted as a function of the spectral class. From a number of binaries the Russell diagram was derived, giving absolute magnitude, i.e., total radiations, as a function of spectral class. Combining both curves, we find the temperature as a function of spectral class. The uncertainty here arises from the individual deviations from the statistical curves; in the first-named curve a deviation of 0.3 in log R occurs, which means a factor of 1.4 in T. In order to strengthen the correlation, the statistical relations of radius, absolute magnitude, and spectral class to mass were determined; but here the deviations from the curve are still larger. Though a general concordance with the usual scale of temperatures is arrived at, it is not likely that this statistical treatment will allow great accuracy. The physical correlation between spectral class and temperature is much narrower and more exact than the statistical correlation between either of them and such data as mass, diameter, and absolute magnitude. So it will be better to look for separate stars for which all the data are well known.

We will consider here only spectral class A, as a well-marked

[33] *A.N.*, **248**, 213, 1933. [34] *Zs. f. Ap.*, **11**, 265, 1936.

point in the scale of stellar temperatures. Among them we have only three stars with sufficiently reliable trigonometric parallaxes: β Persei, $0''.031 \pm 4$; β Aurigae, $0''.037 \pm 4$; and α Coronae, $0''.053 \pm 10$. For the first star the partial eclipse leaves the ratio of stellar to orbital radius rather indeterminate. For the first and the third stars the velocity of the companion has not been observed; so the relative orbit can be derived only from uncertain estimates of mass. Only β Aur remains, for which the computation has been given already in Russell, Dugan, and Stewart's textbook. For the two extreme suppositions of uniform disk and of completely darkened limb, Shapley found $r/a = 0.147$ and 0.159. With m for each component, $2.07 + 0.75 = 2.82$, with the reduction to bolometric magnitude -0.24 (for 10,000°, following Eddington), with the radial velocity of 220 km/sec, and with the period of 3.960 days we find for T the values 9630° and 10,130°. From the energy distribution of Table II and of Figure 2, however, the reduction to bolometric magnitude is found to be 0.23 mag. larger than for black-body radiation; taking this difference into account, the values for T are 10,300° and 10,740°. Hence, 10,500° may be assumed as the temperature of this Ao star.

9. Thus, two points in the scale of stellar temperatures may be considered as well established: 10,500° for Ao and 3300° for cMo; we may estimate the limit of uncertainty of these values to be nearly 5 per cent of their value. They have been derived by direct methods of determining the effective temperature itself. The results from other methods which gave the first results for temperatures, from color and energy distribution, from ionization, and from the Boltzmann function are so strongly dependent on complicated conditions in stellar atmospheres that it is, as yet, not possible to derive reliable temperatures from them. On the other hand, the temperatures now established may enable us to make a decision between different assumptions made in the discussion of energy gradients and line intensities. With the progress of the theoretical treatment of stellar atmospheres and their absorption coefficients, an increasing accordance may be expected. But this degree of accordance will serve rather as a test of the theories and as a source of knowledge concerning stellar atmospheric conditions than as a determination of temperature.

A SPECTROSCOPIC EXAMINATION OF METEORITES*

ARTHUR S. KING

ABSTRACT

Spectrograms of the material from thirteen meteorites, belonging to the nickel-iron, stony, and graphite types, were examined, and thirty-two of the constituent elements identified. Over half of these are not usually detected in chemical and mineralogical analyses of meteorites, some being among the rare terrestrial elements. Estimates of the abundance of the elements identified in iron and in stony meteorites, based on the degree of development of the spectra and the types of lines appearing, showed a fair agreement with the corresponding abundances found in chemical analyses by Noddack and Noddack. The distinctive differences in composition of iron and stony meteorites are discussed, also the evidence that elements abundant in the stony type may be disintegration products of those composing iron meteorites. The band spectra of meteoritic and of terrestrial graphites indicated no difference in the relative abundance of the carbon isotopes.

The composition of meteorites has been studied for the most part by the methods of chemical and mineralogical analysis used for terrestrial minerals. As spectroscopic analysis has seldom been employed, the following investigation was carried out to determine its usefulness in supplementing the other methods, as well as to study a collection of meteorites most of which had not been examined spectroscopically.

Earlier studies, involving in each case an examination of the spectra of a number of meteorites, have been made by Lockyer and his co-workers,[1] also by Hartley and Ramage,[2] Jewell,[3] and Crookes.[4] These investigations showed the leading spectral characteristics of iron and stony meteorites (siderites and aerolites) and have been confirmed by my own work on the spectra of thirteen meteorites, including four irons, eight stones, and a graphite nodule. In addition to the identification of elements, I have attempted to indicate their relative abundance as shown by the strength of the more persistent lines and the degree of development of the spectra.

* *Contributions from the Mount Wilson Observatory, Carnegie Institution of Washington*, No. 556.

[1] *The Meteoritic Hypothesis*, 1890.

[2] *Ap. J.*, **9**, 221, 1899.

[3] *Ibid.*, p. 229.

[4] *Phil. Trans. R. Soc.*, A, **217**, 411, 1918.

Specimens of the following meteorites, named after the locality of the fall, have been examined:

Irons: Canyon Diablo, Ariz.
Mount Joy, Pa.
Staunton, Va.
Xiquipilco, Mex.
Stones: Pasamonte, N. Mex.
Sioux County, Neb.
Allegan, Mich.
Ulysses, Kan.
Gruver, Tex.
Richardton, N.D.
Weldona, Colo.
Tryon, Neb.
Graphite nodule: Elden, Ariz.

The arc was regularly used as a light-source, the lower carbon electrode being charged with fragments or powder of the specimen. The spectrum of blank carbons, usually those used afterward with meteorite material, was photographed on the same plate. Since an iron meteorite will conduct sufficiently to be used as an electrode, two pieces of Canyon Diablo iron were employed in this way; and in addition, clean drillings from this meteorite were used in the carbon arc. The Mount Joy iron was also used as electrode, against a carbon cathode. In examining the Elden graphite nodule, the arc was used with fragments as electrodes, and also with silver rods containing the material. Several spectrograms of the carbon-tube furnace containing meteorite material were made for comparison with the arc spectra, the spectrum of the empty tube at the same temperature being taken first. As the lines of interest in this work are strong in all sources of moderate excitation, the arc served well for this survey.

Since the arc spectrum of a meteorite contains thousands of lines in the region easily photographed, the spectrum of the meteorite was accompanied on the same plate by arc spectra of its most abundant constituents. From these spectra a great part of the meteoritic lines, perhaps 99 per cent, could be identified by inspection. For iron meteorites, the arc spectra of iron, nickel, and cobalt were used for this purpose. For stony meteorites, arc spectra of iron, chromium, manganese, calcium, and magnesium were used. The meteoritic lines

not identified at once from these arcs either belonged to elements having relatively few lines, such as sodium, aluminium, and silicon, or were the most persistent lines of elements present in very small quantity. In either case they were readily identified from tables such as Kayser's *Hauptlinien*. A final step was to look for traces of the ultimate and other highly persistent lines of elements suspected to be present but not noted in the first examination. The spectrograms were made in the second order of the 15-foot concave grating, except that for the yellow and red the first order was used. The exposures covered the range from λ 2500 to λ 6750.

RESULTS

Table I gives the elements identified, arranged according to atomic number, with estimates of abundance based on their spectra: "1" indicates that the most persistent lines were visible, and "5," that the spectrum was developed so fully as to indicate a high content of the element. In assembling the data a tabulation of this sort was made for each meteorite, but among meteorites of the same type the variations for most elements were found to be small. The abundance given is that usually prevailing, although the range of differences is noted for some elements in the case of individual irons or stones. Even meteorites quite different in appearance and hardness, such as the Pasamonte and Weldona stones, showed very similar spectra, a fact probably to be explained by the presence in the two varieties of different compounds of the same elements.

As is well known from other analyses, the typical iron meteorite is an iron-nickel alloy, although a number of the stronger lines are due to cobalt, copper, and silicon. The spectra of the irons showed the content of chromium and manganese to be very low as compared with that of such terrestrial irons as have been examined by the writer. The stones gave very intense spectra of magnesium and sodium, the D lines of the latter sometimes spreading over a range of 60 A.[5] Calcium, silicon, chromium, and manganese showed rich spectra; while iron, though evidently much less abundant than in iron meteorites, was uniformly present in large quantity. In general,

[5] Sodium, according to chemical analysis, is much less abundant than magnesium; and this high intensity of sodium lines is probably due to the concentration of spectral energy in a few lines.

the more friable stones gave the stronger spectra of silicon, aluminium, and calcium.

The variation of nickel content in different stones is noteworthy. Two very friable stones, Pasamonte and Sioux County, showed only

TABLE I

ABUNDANCES OF ELEMENTS IN METEORITES

Element	Estimated from Spectra		Chemical Analysis (I. and W. Noddack)	
	Irons	Stones	Irons	Stones
Li	1	2	−	5.0×10^{-6}
C	*	*	3.9×10^{-4}	3.4×10^{-4}
Na	1	5	−	7.18×10^{-3}
Mg	2	5	3.2×10^{-4}	1.59×10^{-1}
Al	2–3	1–4	4.0×10^{-5}	1.61×10^{-2}
Si	3	3–5	8.0×10^{-3}	2.143×10^{-1}
P	1	?	1.47×10^{-3}	5.06×10^{-4}
K	1	3	−	2.63×10^{-3}
Ca	2	4	5.0×10^{-4}	1.92×10^{-2}
Sc	−	1	+	1.1×10^{-4}
Ti	1	2–3	4.0×10^{-5}	2.10×10^{-3}
V	1	1	6.2×10^{-6}	3.0×10^{-4}
Cr	1	4	2.4×10^{-4}	5.0×10^{-3}
Mn	1	4	3.0×10^{-4}	2.05×10^{-3}
Fe	5	4	9.02×10^{-1}	1.276×10^{-1}
Co	3	1–2	5.47×10^{-3}	1.81×10^{-4}
Ni	5	1–3	8.46×10^{-2}	2.01×10^{-3}
Cu	3	2	3.05×10^{-4}	1.55×10^{-6}
Zn	1	1−	1.15×10^{-4}	3.4×10^{-6}
Ga	2	1	1.3×10^{-5}	+
Ge	2	1	2.36×10^{-4}	3.3×10^{-5}
Rb	−	1	0	4.5×10^{-6}
Sr	1	1	+	7.2×10^{-5}
Mo	1−	−	1.66×10^{-5}	2.5×10^{-6}
Ru	1−	−	2.39×10^{-5}	0
Ag	1	1	3.2×10^{-6}	0
Sn	1	−	1.02×10^{-4}	4.0×10^{-6}
Sb	1−	−	2.0×10^{-6}	1.0×10^{-7}
Cs	−	1−	−	1.0×10^{-7}
Ba	1	1	+	2.0×10^{-5}
Au	1−	−	1.4×10^{-6}	0
Pb	1	1−	5.3×10^{-5}	5.0×10^{-6}

* Usually masked, owing to the use of carbon electrodes. Exceptions noted in text.

faint traces of the strongest nickel lines. The other stones, which, excepting Allegan, were of much harder structure, gave nickel lines of considerable strength. The iron spectrum was well developed for all. Crystallographic analysis would probably account for this

difference by the presence of non-nickel iron compounds, such as troilite, daubreelite, or lawrencite in the crumbly stones; while inclusions of some of the numerous nickel-iron compounds occur in the harder ones. If, however, we consider that the friable meteorites represent the most advanced stage of the stone-forming process, a possible connection with the hypothesis of G. N. Lewis[6] is suggested. According to this hypothesis, the composition of stony meteorites results from the atomic disintegration of the constituents of iron meteorites. Silicon, aluminium, calcium, and magnesium, known disintegration products of iron and nickel, are prominent in the stony type. If iron and nickel are equally subject to transmutation, the usual proportion in iron meteorites (about 11 to 1) would leave enough iron to give a strong spectrum after the nickel content had become very low. In fact, as Lewis notes, the splitting-off of an alpha particle from nickel should give iron and increase the disparity between iron and nickel in the stones. An atomic disintegration theory should account also for the large increase of manganese (not considered by Lewis) over that present in the irons. Evidence on this point is supplied through the transmuting, by Fermi and his coworkers,[7] of cobalt into manganese by neutron bombardment. Cobalt, fairly abundant in the irons, is even harder to detect than nickel in the Pasamonte and Sioux County stones, while manganese is plentiful.

However, the Allegan meteorite, a very friable stone, showed nickel and cobalt lines of fair strength, indicating a content of both, in agreement with the chemical analysis of this stone by Merrill and Stokes.[8] The evidence in favor of nuclear changes seems just sufficient to justify keeping the possibility in mind in future work with a large variety of stony meteorites.

The Elden meteorite, found about 35 miles from the Canyon Diablo Meteor Crater in Arizona, is a rare specimen, being composed largely of carbon in the form of graphite (46.5 per cent[9]), and is the largest known of the type. The graphite forms a matrix

[6] *Phys. Rev.*, **46**, 897, 1934.

[7] *Proc. Roy. Soc.*, A, **146**, 483, 1934.

[8] *Proc. Wash. Acad. Sci.*, **2**, 41, 1900.

[9] From analysis by W. A. Sloane, U.S. Bureau of Mines.

crossed by numerous intersecting veins composed chiefly of nickel-iron. The meteorite was described by L. F. Brady,[10] who suggested that it might have been an inclusion in iron belonging to the Canyon Diablo fall, the iron shell having fallen away. Evidence in confirmation of this explanation was given by R. E. S. Heineman,[11] who found a very similar, though smaller, nodule imbedded in a section of Canyon Diablo iron.

The spectrum showed strong *CN* bands in the arc and *C* II lines in the spark. Aside from this evidence of high carbon content, the Elden spectrum was mainly of iron and nickel and very similar to that of the Canyon Diablo iron.[12] Exceptional features, however, were stronger spectra of the alkali metals and earths than is usual with irons and evidence of more barium than in any other of the meteorites examined.

The last two columns of Table I give the abundance found in chemical analyses of iron and stony meteorites by Ida and Walter Noddack.[13] These results are averages for each type, made from mixtures of material from 16 irons and 42 stones. Iron particles were extracted magnetically as far as possible from the pulverized stone mixture, so that the iron content for the stones is low. A plus sign indicates that the element was detected, sometimes by spectroscopic means, but the amount was not measurable.

Table I shows a fairly close agreement between the spectroscopic and chemical abundance for both iron and stony meteorites. Elements found by Noddack and Noddack to be present in their mixtures in amounts greater than a few parts in a million, but not listed in my table, are gases, such as oxygen and chlorine, or metals whose

[10] *Amer. Jour. Sci.*, **21**, 173, 1931.

[11] *Ibid.*, **23**, 417, 1932.

[12] The writer is indebted to Professor F. A. Jenkins of the University of California for a comparison of the relative abundance of the two carbon isotopes, C^{12} and C^{13}, in the Elden meteorite and in terrestrial graphite. The bands at λ 4737 and λ 4744.5, due to $C^{12}C^{12}$ and $C^{12}C^{13}$, respectively, were produced in a discharge tube of the form previously used in the study of isotope bands (Wooldridge and Jenkins, *Phys. Rev.*, **49**, 404, 1936). Microphotometer measures of the bands given by the two graphites showed definitely that there is no difference in the relative intensity greater than the error of measurement. For details of this experiment see Jenkins and King, *Pub. A.S.P.*, **48**, December, 1936.

[13] *Naturwissenschaften*, **18**, 757, 1930.

persistent lines are in an inaccessible spectral region. A fundamental limitation to the detection of very small percentages by the spectroscopic method must be recognized. The most persistent lines are those produced in transitions from the ground level in the atom. If the energy involved in such a transition is concentrated in one line, or at most a very few lines, the spectroscopic sensitivity may be very great. But when this energy is divided among a considerable number of lines, perhaps several multiplets, as is usual in the complex spectra, the possibility of detecting very small amounts becomes correspondingly less. The few elements not detected in my spectra, but for which Noddack and Noddack obtained measurements, are of this kind. Examples are the rare earths cerium, neodymium, and samarium, measured as three to four parts in a million, and the platinum metals, also of very low content. The latter have been the special object of chemical analyses of the Canyon Diablo meteorite,[14] and evidence of the whole platinum group has been found. Ruthenium only was identified in my spectra, by means of a very faint line. Noddack and Noddack give it the highest abundance in the group, by a small margin; but it may be noted that other chemical analyses do not agree on this point. In the case of platinum, the strongest line, λ 3064.71, would be effectively concealed by a strong nickel line.

The conditions of my experiments were unfavorable for the detection of either oxygen or carbon. Oxygen is one of the chief constituents of stony meteorites; but oxide bands in the open arc, as well as the infrared oxygen lines, could as well have come from the air. Carbon, given an abundance of about 4×10^{-4} by Noddack and Noddack in both irons and stones, and found in meteorites as diamond and graphite, would regularly have been masked through the use of carbon electrodes. The Canyon Diablo meteorite, when used as electrodes, showed the *CN* bands faintly. The strength of the carbon spectrum from the Elden nodule has been mentioned. Sulphur, another prominent meteoritic substance, is difficult in arc spectra on account of the high excitation potential of lines in the accessible region.

[14] See summary by J. L. Howe, *Science*, **66**, 220, 1927.

The grounds for identification of some of the elements present in small amounts may now be discussed.

The presence of *lithium* in meteorites has often been left uncertain by analysis, though in stones it would be expected to accompany the large content of sodium. The ultimate line λ 6708 could be seen in the irons and showed considerable strength in the stones, as did λ 6103.6.

Very faint lines of *phosphorus* were measured at λλ 2533.99, 2553.27, and 2554.92 in the Canyon Diablo iron. Spectra of the stones in this region may not have been sufficiently strong.

Scandium was identified in stones by means of faint lines at λ 3911.81 and λ 4023.69.

The strongest lines of *titanium* and *vanadium* could be seen in both irons and stones, while in the stones a large number of titanium lines were identified.

Zinc gave λ 4722 and λ 4810 distinctly in the Canyon Diablo and Xiquipilco irons.

Gallium, found in very small amounts in terrestrial minerals, though rather widely distributed in igneous rocks, showed λ 4033.01 and λ 4172.05. The first, being only 0.06 A from an ultimate line of manganese, was masked in the stones, but was easily detected in the irons on account of the faintness of the manganese line. The second, λ 4172, is 0.08 A from an iron line of medium strength but was usually resolved in both types. Gallium, though seldom detected in meteorites by other methods, was identified in the early spectroscopic investigations; and its presence in meteorites has been taken as evidence of its probable presence in the sun,[15] the gallium lines in the solar spectrum being at that time difficult of detection on account of blends.

Germanium, another rare terrestrial element, showed its ten strongest lines from λ 2592 to λ 4686 distinctly in the irons. They were weaker in the harder stones, such as Tryon and Weldona, and very faint in the soft stones, Pasamonte and Sioux County. Several of these lines are found in the solar spectrum. Goldschmidt[16] questions the extreme scarcity of germanium in terrestrial rocks on the

[15] Hartley and Ramage, *Ap. J.*, **9**, 214, 1899.

[16] *Proc. R. Inst.*, **26**, 73, 1929.

ground that it is very generally associated with aluminium and in chemical reactions is likely to be masked by the latter.

Rubidium gave λ 7800 and λ 7947 faintly in the Pasamonte stone and still weaker in the Elden graphite. These lines did not appear in the Canyon Diablo iron.

Strontium could, as a rule, be detected by λ 4607. A spark spectrum of the Elden graphite, however, gave λ 4077 and λ 4215 of *Sr* II with considerable strength.

Molybdenum and *ruthenium* were identified in the Canyon Diablo iron by λ 3193.98 and λ 3498.95, respectively. The latter was very faint but measured in close agreement with the accepted wavelength.

The ultimate lines of *silver*, λ 3281 and λ 3383, could, as a rule, be seen in both irons and stones. These lines were sometimes strong in Canyon Diablo spectrograms, but varied in strength according to the part of the specimen examined.

Tin lines were very faint and often blended with those of other elements; λλ 3034.12, 3177.05, and 3263.33 were identified.

Antimony was recognized by λ 3232.52 only.

The ultimate line of *caesium*, λ 8521.15, could be seen very faintly in the Pasamonte stone and in the Elden graphite, not in the Canyon Diablo iron. Other speciments were not examined in this region.

The *barium* line λ 5535.53 was of fair strength in both irons and stones. Sometimes other lines appeared, especially in the Elden graphite.

Gold showed λ 3675.95 very faintly on two Canyon Diablo spectrograms.

The *lead* lines λλ 3639.6, 3683.5, and 4057.8 could usually be seen, sometimes also λ 2833.1. They were stronger in the irons and quite variable on different spectrograms.

CONCLUDING REMARKS

Leaving out of account a search for elements present in small quantity as exhaustive as that of Noddack and Noddack, we find that fully half of the elements listed in Table I, as identified by their spectra, are not, as a rule, detected in chemical and mineralogical analyses of meteorites. A quantitative spectrum analysis would have as

its main object the meteoritic content of these less abundant elements. For this purpose a very small amount of the material would be sufficient; and with standardized samples of various elements at hand and a routine established, the analysis could be made in much less time than by the other methods. For the production of certain spectra special experimental arrangements would be necessary. How these would compare in difficulty with the chemical operations required for some groups of elements, the writer is not prepared to say.

Comparisons of abundances of the elements in meteorites with those in terrestrial minerals have frequently been made.[17] Such a comparison by Noddack and Noddack with the results of their analyses of sixteen hundred minerals showed a relatively higher content of magnesium, iron, and nickel in meteorites than in the earth's crust. Apart from these elements, perhaps the most noteworthy difference is a considerably larger amount of gallium and germanium in meteorites.

Meteoritic elements which are really abundant are well within the first third of the atomic-number series, nickel, No. 28, being the last plentiful element. A similar condition holds for elements in the earth's crust, according to the data of Washington and Clarke;[18] but this predominance of the lighter elements is shown in the paper of Noddack and Noddack to be more pronounced for meteorites, owing chiefly to a relatively higher terrestrial abundance of strontium, barium, zirconium, tungsten, and the rare earths. In the case of compounds, the differences are more conspicuous, some constituents of meteorites not being found among terrestrial minerals.

For their co-operation in supplying specimens of meteorites, I am indebted to Professor H. H. Nininger, of Denver; Professor F. C. Leonard, of the University of California at Los Angeles; Dr. C. O. Lampland, of the Lowell Observatory; and Mr. L. H. Brady, of the Museum of Northern Arizona, Flagstaff.

CARNEGIE INSTITUTION OF WASHINGTON
MOUNT WILSON OBSERVATORY
August 1936

[17] See, for example, G. P. Merrill, *Proc. Amer. Phil. Soc.*, **65**, 119, 1926; Farrington, *Meteorites* (Chicago, 1915), p. 215; I. and W. Noddack, *op. cit.*

[18] *U.S. Geol. Surv. Prof. Paper*, No. 127.

EFFECTS OF RED SHIFTS ON THE DISTRIBUTION OF NEBULAE

EDWIN HUBBLE*

ABSTRACT

Two new surveys of nebulae, to $m_{pg}=18.47$ and 21.03, are described which, together with three earlier surveys to $m_{pg}=19$, 19.4, and 20, indicate the apparent distribution in depth. The numbers of nebulae per square degree, N, to limiting magnitudes m, are represented by the relation

$$\log N=0.6\ (m-\Delta m)-9.052\pm0.005\ ,$$

where

$$\log \Delta m=0.2\ (m-\Delta m)-4.239\pm0.008\ .$$

The corrections, Δm, are interpreted as apparent departures from large-scale uniform distribution due to the effect of red shifts on apparent luminosities.

The effects to be expected are calculated on the two assumptions that red shifts are (*a*) velocity shifts and (*b*) not velocity shifts. With an average $T_e=6000°$ assumed for integrated nebular radiation, $\Delta m=4.0\ d\lambda/\lambda$ (velocity shifts) or $3.0\ d\lambda/\lambda$ (not velocity shifts). The empirical expression, derived from the apparent distribution, together with the velocity-magnitude relation, is $\Delta m=2.94\ d\lambda/\lambda$.

If red shifts are not velocity shifts, the apparent distribution agrees with that in an Einstein static model of the universe or an expanding homogeneous model with an inappreciable rate of expansion, provided spatial curvature is negligible.

If red shifts are velocity shifts which measure the rate of expansion, the expanding models are definitely inconsistent with the observations unless a large positive curvature (small, closed universe) is postulated. The maximum value of the present radius of curvature would be of the order of 4.7×10^8 light-years; and the mean density, of the general order of 10^{-26}. The high density suggests that the expanding models are a forced interpretation of the observational results.

Surveys with large reflectors on Mount Wilson and Mount Hamilton show that the distribution of nebulae[1] over the sky down to limiting magnitudes[2] between 19 and 20 is moderately uniform except as affected by local obscuration within the galactic system and by the occasional great clusters. The distribution in depth, as indicated by the rate of increase of the numbers of nebulae to successive limiting magnitudes, also appears to be approximately uni-

* *Contributions from the Mount Wilson Observatory, Carnegie Institution of Washington*, No. 557.

[1] *Mt. W. Contr.*, No. 485; *Ap. J.*, **79**, 9, 1934; *Lick Obs. Bull.*, **16**, 177 (No. 458), 1934.

[2] Unless otherwise stated, the terms "nebula" and "magnitude" in the present discussion refer to extragalactic nebulae and to photographic magnitudes on the international scale, respectively.

form when tentative corrections are applied for the effect of red shifts on apparent luminosity. The second conclusion is less reliable than the first and requires further investigation before it can be used with confidence in cosmological theory. The following contribution is a re-examination of the subject, carried out in greater detail and with the aid of additional material.

The observational data are five homogeneous groups of nebular counts, each giving the number of nebulae per unit area to a particular limiting magnitude. The five pairs of values determine an empirical relation, $\log N_m = f(m)$, which diverges systematically from the theoretical relation representing uniform distribution. The departures from uniformity, expressed as corrections to the observed magnitudes, are then formulated as a relation $\Delta m = f(m)$, which sums up the observational results of the investigation. This relation includes the effect of red shifts, in addition to observational errors, space absorption, and real departures from uniform distribution; hence its interpretation is of critical importance for cosmological theory.

I. OBSERVATIONAL DATA

PREVIOUS SURVEYS

Three groups of nebular counts are available from previous surveys. These represent the 1-hour exposures on Eastman 40 plates with the 100-inch and 60-inch reflectors already discussed by the writer,[3] and the 1-hour exposures on Imperial Eclipse plates with the 36-inch Crossley reflector discussed by Mayall.[4] Since the details for individual plates are already published, they will not be repeated here. The limiting magnitudes were 20.0, 19.4, and 19.0, with uncertainties of the estimated order of 0.1 mag. The mean values of $\log N$ per plate were derived from all available material in the polar caps ($\beta \gtrsim 40°$), reduced to standard exposures of 1 hour by corrections derived from empirical relations between $\log N$ and $\log E$. The results were reduced to mean $\log N$ per square degree with the aid of corrections for coma and for plate area.

For the present investigation the data were used as follows: The 1-hour exposures with the 60-inch and 100-inch reflectors (214 and

[3] *Mt. W. Contr.*, No. 485; *Ap. J.*, **79**, 8, 1934.

[4] *Lick Obs. Bull.*, **16**, 177 (No. 458), 1934.

228 plates, respectively) were extracted from the Mount Wilson surveys and reduced separately. Mayall's values, representing all the 36-inch material, were adopted as published, except that latitude corrections were applied in order to make the data comparable with the Mount Wilson counts. These corrections[5] increased the mean log N by the increment 0.032 without materially affecting the dispersion. The results are included in Table IV.

NEW SURVEYS

The two additional groups of counts represent 2-hour exposures[6] with the 100-inch reflector and 20-minute exposures with the 60-inch, both on Eastman 40 plates. The fields, as before, are restricted to the polar caps; and the counts are reduced to log N per square degree in the same manner as in the earlier surveys. Each plate was examined three times, the last examination being a continuous review of each group as a unit. It seems probable that a more critical standard was attained in the identification of threshold nebulae. This advantage, combined with the appreciably higher sensitivity of recent emulsions, led to relatively fainter limits, and hence larger numbers of nebulae, than would be expected for corresponding exposures in the former surveys. Details for individual plates are listed in Tables I and II.

LIMITING MAGNITUDES

The limiting magnitudes for the earlier surveys were given to the nearest 0.1 mag., and the published values are adopted without change. Since the new surveys represent extreme cases and play important rôles in the correlation of log N_m and m, the limits are given to another decimal place. The limiting magnitude of the counts on the 20-minute exposures was derived from about fifteen plates of six fields in which nebular magnitudes down to $m = 19.0$

[5] Mayall concluded that "some sort of latitude effect is probably involved in the Crossley material" but that "the data are insufficient to establish the nature of the variations." The more extensive material in the Mount Wilson surveys appears to establish a cosecant law.

[6] Thirteen of the exposures with the 100-inch are not precisely 2 hours but range from 100 minutes to 150 minutes. The corrections reducing log N to the standard exposure range from 0.02 to 0.13 and average 0.066. The uncertainties in these small corrections are believed to be negligible.

TABLE I

SURVEY FIELDS

100-Inch Reflector; 2-Hour Exposures

β	λ	E*	Z	Q	N_1	log N†
+73°	276°	135	29°	FG	157	2.33
63	0	150	40	GE	363	2.54
60	280	150	36	GE	250	2.37
53	17	120	19	GE	238	2.47
52	14	110	31	G	121	2.30
51	22	120	28	E	328	2.58
49	39	120	36	G	177	2.44
47	15	120	36	GE	216	2.47
47	159	135	20	FG	146	2.35
47	164	105	19	GE	203	2.50
46	329	110	45	G	142	2.43
45	20	100	34	G	185	2.58
+40	143	120	35	GE	234	2.53
−40	50	130	24	G	200	2.45
40	57	120	34	G	157	2.41
40	70	130	25	E	214	2.38
40	130	120	22	GE	190	2.41
42	31	115	43	FG	160	2.53
43	30	120	38	GE	222	2.51
43	32	120	34	G	116	2.27
43	61	120	28	FG	174	2.51
44	34	120	43	G	154	2.42
45	45	120	32	G	144	2.35
45	160	120	41	G	175	2.46
47	79	120	21	G	150	2.35
47	104	120	30	GE	241	2.51
47	102	120	33	GE	182	2.39
49	38	115	47	G	185	2.52
50	50	120	30	GE	192	2.40
50	70	120	32	FG	198	2.56
50	120	120	31	FG	172	2.50
55	34	110	41	GE	132	2.30
55	100	120	28	GE	223	2.44
55	140	120	37	G	210	2.49
58	82	120	34	E	294	2.54
58	123	135	39	F	145	2.45
59	89	120	37	GE	246	2.49
60	50	120	43	G	171	2.41
60	110	120	35	GE	260	2.52
62	95	120	36	FG	231	2.60
−72	40	135	51	GE	301	2.56

* E = Exposure-time in minutes.

† log N is reduced to the standard exposure, $E = 120$, by the corrections $\Delta \log N = 1.33 \log E$. (*Mt. W. Contr.*, No. 485; *Ap. J.*, **79**, 8, 1934).

TABLE II

SURVEY FIELDS

60-Inch Reflector; 20-Minute Exposures

β	λ	Z	Q	N_1	log N	β	λ	Z	Q	N_1	log N
+75°	320°	32°	E	18	1.30	−43°	61°	41°	GE	30	1.65
74	315	28	GE	10	1.07	43	66	34	E	16	1.31
73	313	25	E	18	1.29	44	41	34	GE	12	1.23
63	323	24	GE	24	1.46	44	55	38	E	19	1.40
63	325	24	E	15	1.22	44	66	40	E	14	1.27
62	338	28	GE	23	1.44	44	80	20	E	46	1.74
62	340	33	E	16	1.25	45	40	39	GE	18	1.41
60	20	31	E	10	1.05	45	55	39	E	8	1.01
60	135	32	G	14	1.30	45	80	24	E	28	1.53
60	136	35	G	17	1.39	45	102	28	E	38	1.66
60	138	42	G	6	0.96	45	109	33	E	17	1.32
60	170	38	G	5	0.87	47	79	29	E	27	1.51
59	24	30	E	21	1.37	47	102	25	GE	14	1.27
59	28	37	E	21	1.38	49	38	38	GE	27	1.57
58	34	42	GE	6	0.91	49	39	35	GE	21	1.45
58	36	31	GE	13	1.21	49	61	31	E	37	1.65
58	40	38	GE	5	0.82	49	99	32	E	52	1.80
55	21	38	E	13	1.19	49	149	39	E	8	1.00
54	110	37	GE	24	1.50	50	60	35	GE	28	1.58
54	111	39	GE	23	1.49	50	75	24	GE	6	0.89
54	193	25	GE	25	1.50	50	81	32	E	8	0.98
53	195	23	GE	40	1.69	50	99	35	E	13	1.20
53	196	21	GE	8	0.99	50	150	39	E	18	1.36
53	225	40	GE	20	1.43	51	75	24	G	16	1.36
53	294	42	GE	17	1.37	51	81	38	GE	19	1.41
51	247	43	GE	10	1.14	51	89	28	E	7	0.91
50	140	31	G	6	0.96	51	160	44	E	15	1.29
50	141	34	G	8	1.09	51	162	45	E	10	1.11
46	133	28	E	23	1.44	52	81	42	E	14	1.25
46	134	30	GE	27	1.56	52	89	32	E	17	1.30
46	136	34	E	26	1.52	52	163	48	E	14	1.28
42	122	42	GE	8	1.07	53	52	32	E	19	1.35
42	123	45	GE	4	0.78	53	100	26	E	19	1.34
41	121	39	GE	7	1.02	53	110	27	E	29	1.52
40	141	30	G	16	1.41	54	36	42	GE	11	1.18
40	142	34	FG	4	0.90	54	51	34	E	13	1.19
+40	143	39	G	26	1.65	54	100	29	E	32	1.56
−41	171	47	E	9	1.11	54	111	28	E	13	1.17
42	62	36	GE	18	1.41	54	129	34	E	16	1.28
−42	172	47	E	7	1.00	−55	35	45	E	13	1.21

TABLE II—*Continued*

β	λ	Z	Q	N_1	log N	β	λ	Z	Q	N_1	log N
−55°	50°	37°	E	26	1.49	−61	70°	42°	GE	10	1.12
55	73	29	GE	21	1.41	61	95	37	E	12	1.14
55	77	33	E	9	1.01	62	95	42	E	41	1.69
55	100	31	E	22	1.40	63	99	36	E	20	1.36
55	111	30	E	27	1.49	63	118	41	E	22	1.42
55	125	32	E	22	1.40	64	100	36	E	33	1.58
55	126	34	E	38	1.65	64	119	41	E	18	1.34
55	130	36	E	17	1.30	65	100	38	E	34	1.60
56	42	39	GE	9	1.07	65	103	42	E	25	1.48
56	73	32	E	55	1.80	65	120	40	E	21	1.39
56	77	31	E	18	1.32	66	85	40	E	16	1.26
56	127	36	E	37	1.64	66	104	39	E	43	1.69
57	40	46	E	17	1.34	67	85	38	E	13	1.17
57	41	42	GE	11	1.17	68	64	43	E	26	1.49
57	60	36	G	9	1.12	69	63	45	E	16	1.28
57	123	33	GE	31	1.59	−70	62	48	E	11	1.14
58	60	39	GE	16	1.32						
58	123	35	E	26	1.49						
59	51	40	E	18	1.33						
59	122	39	E	18	1.33						
59	123	38	E	18	1.33						
59	150	44	GE	13	1.24						
59	152	45	GE	24	1.51						
60	50	44	E	12	1.17						
−60	71	38	GE	26	1.53						

or 19.2 have been measured from schraffierkassette images. The scale was determined from the North Polar Sequence and three Selected Areas in which the scale has been extended by Baade beyond the reliable ranges in the *Mount Wilson Catalogue of Photographic Magnitudes*.[7] The fifteen plates were scattered at intervals throughout the period of time required to complete the survey. Since the total range in the limits of the individual plates is only 0.25 mag., the mean value, 18.47±0.03, is believed to be reliable except for uncertainties in the scale of the comparison stars and in the zero point of the scale of nebular magnitudes.

The estimation of the limiting magnitude for 2-hour exposures necessarily involved considerable extrapolation. A dozen 20-minute exposures with the 100-inch telescope, scattered throughout the

[7] Seares and others, *Carnegie Institution of Washington Publication*, No. 402, 1930.

group, were centered on the same fields as were used in calibrating the 20-minute exposures with the 60-inch. The mean limiting magnitude of these plates, reduced to the zenith and to excellent quality, is 19.11 ± 0.02, very close to the limit of the reliable nebular magnitudes determined with the schraffierkassette. Hence, for 2-hour exposures, the limiting magnitude should be

$$19.11 + 2.5\, p \log \frac{120}{20} = 19.11 + 1.94p\,,$$

where p is the Schwarzschild exponent in the reciprocity law.

The value of p for surface images of equal density on fully developed Eastman 40 plates increases as the density diminishes and approaches unity at the threshold itself. The value unity was used for deriving magnitudes in the previous surveys, and observational data were presented which justified the procedure. A re-examination of the material with special reference to very small surface images suggests values of p ranging from 0.95 to 1.0 for the particular conditions under discussion, and indicates that the mean should give the desired results to a close approximation. The limiting magnitude for the 2-hour exposures is then 21.00 ± 0.04, with uncertainties of much the same order as those for the nebular magnitudes around $m = 19$ in the standard fields.

A second method of calibration, also applied in the previous surveys, depends upon a known relation between diameters and surface brightness of threshold images.[8] Several 2-hour exposures on Selected Areas, in which Baade has extended the scale of stellar magnitudes, were made under conditions of poor seeing. Stars with known magnitudes were thus smeared out into surface images similar to, although considerably larger than, nebular images at the threshold of identification on plates of excellent quality. The same sorts of results are obtained with small extra-focal images, although the shadow of the Newtonian flat introduces uncertainties. The relative diameters of the threshold images of these stars and the threshold images of nebulae on good-seeing plates with equal exposures indicate the relative surface brightness and hence the difference in the integrated magnitudes. For instance, a 2-hour exposure

[8] *Mt. W. Contr.*, No. 453; *Ap. J.*, **76**, 106, 1932.

of S.A. 68, with diameters of faint images about 8″.5, registered stars down to about 19.9. Diameters of threshold nebulae on the sharpest survey plates average about 3″.2. From the relative areas, the nebular images should be 2.12 mag. fainter than the stellar images, but the correction for surface brightness as a function of diameter reduces the increment to 1.15 mag.; hence the threshold magnitude for the nebulae is 21.05.

Four 2-hour exposures are available and, in addition, six 1-hour exposures and five schraffierkassette plates (images 16″×16″) with

TABLE III

LIMITING MAGNITUDE FOR 120-MINUTE EXPOSURES

MEAN EXP.	NO. OF PLATES	MEAN DIAM.	m_e		REMARKS
			Observed	Reduced*	
Min.					
20	12	3″.2	19.11±0.02	21.00±0.02	Good seeing
60	6	6	19.57 .06	21.02 .05	Poor seeing
120	4	7	20.20 .06	21.02 .06	Poor seeing
145	5	16	19.08±0.06	21.08±0.06	Schraffierkassette
Mean				21.03±0.03	

* The reduced values of m_e refer to nebulae with diameters of 3″.2 at the threshold of identification on 120-minute exposures at the zenith, made with the 100-inch reflector on Eastman 40 plates. Exposures with the schraffierkassette range from 110 to 180 minutes, $\overline{E}=145$, $\overline{\log E}=2.164$. Mean diameters are approximate; the reduced limiting magnitudes are the means of those for the individual plates in each group.

exposures ranging from 2 to 3 hours. Results from the latter two groups involve extrapolations in exposure times as well as in diameters. Limiting magnitudes from the three groups, together with the limit from the 20-minute exposures, are listed in Table III. The limiting magnitudes, m_e, refer to nebulae with diameters of 3″.2 at the threshold of identification on 2-hour exposures at the zenith. The simple mean, 21.03±0.03, is adopted as the most probable value. The small probable error, of course, merely indicates the consistency of the data and does not fully eliminate the possibility of systematic errors.

The series of five limiting magnitudes form a consistent system in which the scale appears to approximate closely the conventional scale over the range involved, and the accidental errors are less than

0.1 mag. This conclusion is drawn from examination of the Mount Wilson data alone, but Mayall's data for the Crossley counts are thoroughly consistent and may be included in the general statement.

The zero point of the scale is uncertain by the amount of the errors in the standard nebular magnitudes between 18.5 and 19.0. These arise from two sources. One, the uncertainties in the scale of the standard sequences of stellar magnitudes, is believed to be small since it involves the North Polar Sequence and three independent extensions of that scale from about $m = 17.0$ downward. The other arises from the method of measuring nebular images and involves the question of the relative amount of luminosity contributed by extremely faint but relatively large outer regions of nebulae. A rough rule is that reliable total magnitudes may be derived by smearing the nebulae and comparison stars over areas with diameters three times the diameters of the nebulae, as estimated by simple inspection of focal plates.[9] These conditions were fulfilled in measuring the very faint nebulae in the standard regions, and hence the uncertainties arising from outer regions are believed to be less than 0.1 mag.

For many purposes, including investigations of distribution and associated problems, the zero point is relatively unimportant; the significant feature is the scale. The present series of magnitudes can be represented to the nearest 0.1 mag. by extrapolations from $m =$ 19.0, based on the reciprocity law with an exponent p between 0.95 and 1.0. The reliability of the scale thus depends largely on the value of p. Since it is improbable that p should be greater than unity, any appreciable revision would probably reduce the range in the observed magnitudes and make the faint magnitudes brighter with respect to the bright magnitudes.

SIGNIFICANCE OF LOG N

The mean values, $\overline{\log N}$ and $\log \overline{N}$, for the five surveys are listed in Table IV, together with the dispersions, σ, calculated from the residuals relative to $\overline{\log N}$. The three quantities should satisfy the relation

$$\log \overline{N} = \overline{\log N} + 1.151\sigma^2 ,$$

[9] The rule is based on a comparison of magnitudes from extrafocal and schraffierkassette images with those derived by Stebbins and Whitford from accurate measures with photoelectric cells, made directly at the foci of reflecting telescopes.

provided that the frequency distributions of log N are normal error-curves; the small differences, C − O, show that this condition is very closely approximated.

The surveys represent random sampling with average samples of five different sizes. The significance of the dispersions is somewhat obscured by the fact that the sizes of samples do not correspond to the adopted log N but represent the numbers of nebulae actually identified on the plates before the counts were reduced to standard conditions. The latter data are included in the table and show that the dispersion tends to diminish as the size of the sample increases.

TABLE IV

DATA FROM INDIVIDUAL SURVEYS*

Tel.	E	NP	$\bar{N}_1$	m	$\overline{\log N}$	σ	$\log \bar{N}$	$\log \bar{N}$ (obs)
60-in.	20	121	19	18.47	1.829	0.224	1.887	1.885
36-in.	60	284	35	19.0	2.103	.225	2.161	.....
60-in.	60	214	41	19.4	2.312	.156	2.340	2.342
100-in.	60	228	52	20.0	2.650	.176	2.686	2.685
100-in.	120	41	200	21.03	3.154	0.084	3.162	3.162

* Tel. = telescope; E = exposure time in minutes; NP = number of plates; $\bar{N}_1$ = average number of nebulae actually identified per plate; m = limiting magnitude of survey; $\overline{\log N}$ = mean logarithm of number of nebulae per square degree; σ = dispersion in log N; $\log \bar{N} = \overline{\log N} + 1.151\sigma^2$; $\log \bar{N}$ (obs) = logarithm of the mean number of nebulae per square degree (each plate reduced to standard conditions).

This tendency, together with the close agreement of the results for the two galactic hemispheres and the absence of conspicuous systematic variations in latitude or longitude, emphasizes once more the random character of the large-scale distribution of nebulae throughout the sample of the universe available to inspection.

While the large-scale distribution appears to be essentially uniform, the small-scale distribution is very appreciably influenced by the well-known tendency toward clustering. The phenomena might be roughly represented by an originally uniform distribution from which the nebulae have tended to gather about various points until now they are found in all stages from random scattering, through groups of various sizes, up to the occasional great clusters.[10] The

[10] This representation is purely formal and has no genetic implications. For purposes of speculation, the reverse development seems preferable, namely, that nebulae were formed in great clusters whose gradual evaporation has populated the general field.

tendency appears to operate on a relatively modest scale—at least no clusters are known with more than a few hundred members; hence irregularities tend to average out among samples that are large compared to a single cluster.[11] In small samples irregularities are conspicuous, and, as an empirical fact, they lead to a random distribution of log N rather than of N. Accidental errors of observation and reduction also tend to introduce random scattering of percentage deviations (since they are generally equivalent to variations in limiting magnitude), but the effects are relatively small and are presumably constant for all the surveys.

The significant quantity, for the present purpose, is the arithmetical mean, $\overline{N}$, related to the geometrical mean by the expression already given, in which σ represents the combined effects of irregularities and accidental errors. If the errors are small compared to the irregularities, as in the surveys using small samples, the relation may be used as it stands, or $\overline{N}$ may be calculated directly from the data. On the other hand, if the samples are so large that the dispersion is dominated by errors rather than by irregularities, the term including σ may be ignored, and $\overline{N}$ derived from the simple relation

$$\log \overline{N} \text{ (distribution)} = \overline{\log N} \text{ (observed)} .$$

The dispersion arising from accidental errors alone is probably of the order of 0.06 in log N (0.1 mag) and about equal to that arising from irregularities in the survey using the largest samples. Appropriate corrections for accidental errors would consist of a constant term, $1.151\ (0.06)^2 = 0.004$, to be subtracted from each log $\overline{N}$ in Table IV. However, the term is much smaller than the various probable errors, and it may be neglected or thrown in with the uncertainties of the zero point of the magnitude scale. It appears, therefore, that the tabulated log $\overline{N}$ may be used directly for comparing the numbers of nebulae to the successive limits of the various surveys.

[11] Samples in the regions of great clusters were rejected in the present surveys; and, for this reason, irregularities tend to average out for samples that are large compared to single groups of nebulae.

COMPLETENESS OF THE COUNTS

Completeness of the counts was investigated by comparing plates of the same regions made with different apertures and exposures, the 2-hour exposures with the 100-inch being taken as standards. In this way it was possible to count all the nebulae actually recorded, regardless of whether or not they were identified in the course of the survey, on plates of 20-minute and 1-hour exposures with the 60-inch and of 1-hour exposures with the 100-inch. The numbers actually recorded, N_2, were then compared with the numbers previously identified, N_1, reduced to quality E, corrected by the coma factor, and then designated as N_c. Since the investigations were restricted to the central regions of the plates, the two corrections (for quality and coma) concern the identification, and not the registration, of nebular images. The differences, $N_2 - N_c$, represent the numbers of nebulae recorded below the threshold of identification. This threshold is above the threshold of registration by the amount

$$\Delta m_n = \frac{\log N_2 - \log N_c}{0.6} .$$

Additional evidence is furnished by similar comparisons of 20-minute and 1-hour exposures with the 60-inch, the 1-hour exposures with the 100-inch being used as standards; and also by comparisons of the 20-minute exposures with the 1-hour exposures with the 60-inch as standards.

The available material, much of which is listed in the surveys, includes about fifteen comparisons of 20-minute exposures, about ten of the 1-hour exposures with the 60-inch, and six of the 1-hour exposures with the 100-inch, and leads to values for Δm_n of 0.60 ± 0.04, 0.55 ± 0.04, and 0.57 ± 0.06, respectively. The last value, representing 1-hour exposures with the 100-inch, is necessarily the least reliable. These direct tests of the completeness of the counts are consistent with the conclusion derived from measures of nebular magnitudes, namely, that the value of Δm_n is of the general order of half a magnitude.

The results for the three surveys indicate a satisfactory degree of homogeneity and suggest no conspicuous systematic variation de-

pending upon limiting magnitude. For these reasons it is assumed that the Crossley counts and the 2-hour survey with the 100-inch behave consistently, although no direct controls are available. Corrections for incompleteness would probably make the limiting magnitudes in Table IV slightly brighter, but the amounts would be very small and approximately constant throughout the series. Therefore, they may be included among the uncertainties of the zero point of the magnitude scale.

Finally, the effect of systematic variations in plate densities arising from the different exposure times has been investigated. It seemed possible that an optimal density for the identification of faint nebular images might exist, which would affect the counts systematically. Fortunately, the extensive material in the 1-hour exposures with the Mount Wilson reflectors exhibits a range in plate densities sufficient to test this possibility. The results indicated that no appreciable systematic effects would be expected except in a few of the densest 2-hour exposures. On these latter plates the counts may be slightly smaller than normal, but the effect on log $\overline{N}$ for the survey would probably be negligible.

The examination of possible sources of systematic errors strongly suggests that the data in Table IV exhibit a maximum range in m and a minimum range in log $\overline{N}$. The conclusion has an important bearing on the interpretation of the data.

RELATION BETWEEN LOG N, m, AND Δm

In Figure 1, values of log $\overline{N}$, hereafter designated as "log N," are plotted against the corresponding limiting magnitude m. The five points determine the linear relation

$$\log N = 0.501m - 7.371 ,$$

probably within the uncertainties of the data. Since uniform distribution is expressed by

$$\log N = 0.6(m - \Delta m) + C ,$$

where Δm is a correction to the observed magnitude required by red shifts, etc., the deviation from uniformity, expressed by Δm, is

$$\Delta m = 0.165\, m + \frac{7.371 + C}{0.6} .$$

This relation represents the differential corrections over the observed range but is not suitable for extrapolation much beyond that range. The constant C is known to be of the order of -9; hence the correction is zero in the vicinity of $m = 16.5$ and negative for brighter

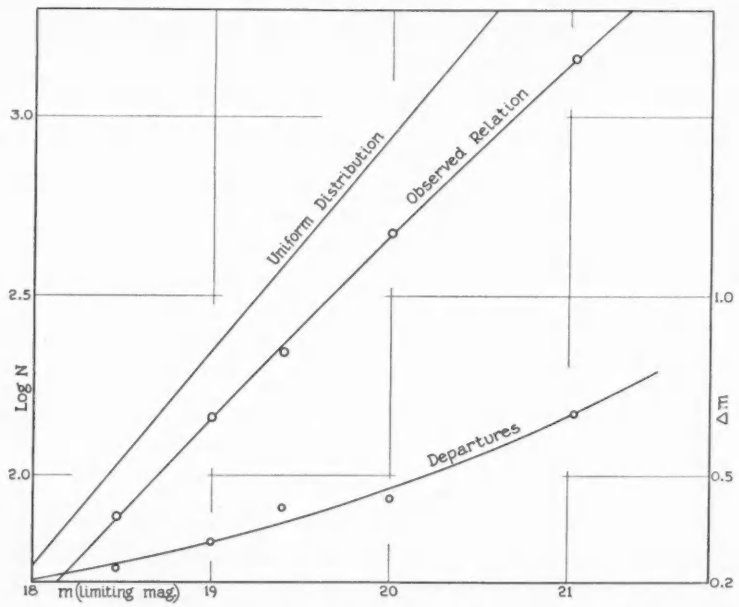

FIG. 1.—Apparent distribution of nebulae in depth. The straight line marked "Uniform Distribution" is the relation log N (per square degree) $= 0.6m - 9.052$, which represents uniform distribution with the density equal to that observed in the vicinity of the galactic system. The curve marked "Observed Relation" is a least-squares solution representing the mean results of the five surveys, on the assumption that apparent departures from uniformity, when expressed as corrections to the observed limiting magnitudes, are linear functions of the distance. The solution is log $N = 0.6\ (m - \Delta m) - 9.052$, where log $\Delta m = 0.2\ (m - \Delta m) - 4.239$. The curve marked "Departures" exhibits the corrections, Δm, as a function of the observed limiting magnitudes, m.

limits. For the Harvard survey of bright nebulae ($m = 12.9$) the correction would be about -0.6 mag., which seems to be definitely inconsistent.

A more significant representation is derived as follows: the correction to the observed magnitudes introduced by uniform space absorption would be a linear function of the distance. Corrections

due to red shifts will also approximately follow a linear function, because red shift itself is a linear function of distance; and the corrections, expressed in terms of magnitudes, approximate linear functions of red shifts. Finally, any systematic deviations from uniform distribution would be partially compensated by corrections to the magnitudes, which were linear functions of distance. Hence, as a first approximation, we may assume that Δm is a linear function of distance.[12] Then

$$\log \Delta m = 0.2(m - \Delta m) + b\,,$$

and the corresponding expression for uniform distribution is

$$\log N = 0.6(m - 10^{0.2(m - \Delta m) + b}) + C\,.$$

The values of b and C are readily found by successive approximations when the equation is written in a form suitable for least-squares solutions. As a first approximation, Δm in the exponent may be ignored. As a second step, the values of Δm derived in the first step are introduced in the exponent. The third approximation, with values of Δm derived in the second, appears to be sufficient; further approximations do not change the significant figures in the results. The solution, expressed as the mean of the regression-curves, is[13]

$$C = -9.052 \pm 0.005\,,$$

$$b = -4.239 \pm 0.008\,.$$

[12] The term "assume" in the statement should be stressed because the empirical data are insufficient to distinguish definitely a linear relation between Δm and distance, from a linear relation between Δm and m. As usual, curves of many different forms would satisfactorily represent the observed points in Fig. 1, and the selection is guided by information from other sources. The apparent distribution must evidently be corrected for known effects on apparent luminosities. The chief, if not the only, effects known at the moment are those due to red shifts, whose calculated values closely approximate the selected relation $\Delta m = \text{Constant} \times \text{Distance}$, over the range of the surveys. Later it will be shown that these effects alone account for apparent departures. If other effects are postulated, they must be arbitrarily adjusted to compensate one another. This evidence justifies the selection of the particular expression for departures, although the expression does not emerge directly from the observational data of the five surveys.

[13] Values of C previously derived were -9.12, by the writer, and -9.2, by Mayall. The present revision is influenced by the method of analysis rather than by the addition of new data.

The solution adjusts C and b to fit a particular set of data; errors in one constant are compensated by adjustment of the other. Independent confirmation of either constant not only would be important in itself but would inspire greater confidence in the other. A check on C would be afforded by counts of bright nebulae, for which the corrections Δm are negligible. Surveys to $m = 14$ to 15 are under way with this end in view, but the only significant data available at the moment are those in the Harvard survey.[14]

These counts are believed to be complete over the entire sky to the tabulated magnitude, 12.9. Accurate photoelectric-cell measures by Stebbins and Whitford[15] indicate that the limiting magnitude should be corrected by -0.1 mag. and that the dispersion is not more than 0.2 mag. The polar caps offer two samples, but one (the northern) is dominated by the great Virgo cluster and the group south-following, which Shapley has called the "Extension to the Coma-Virgo cluster." The influence of the aggregation may be avoided by omitting the regions, R.A. $= 12^h$ to 13^h, Dec. $= 0°$ to $+20°$, and R.A. $= 12^h.5$ to $13^h.5$, Dec. $= 0°$ to $-15°$. The two samples combined then contain 592 nebulae ($m = 12.8$) scattered over 14,270 square degrees. Therefore, $\log N = -1.38$ and $C = -9.06$.

The uncertainties are difficult to estimate because the data are rather meager. The mean latitude correction, which would reduce the numerical value of $\log N$ by about 0.03, is probably compensated by clustering outside the omitted regions. The evidence for such clustering is fairly strong. The polar caps furnish two samples of the general order of those in the 2-hour survey, in which $\sigma = 0.084$. Therefore, the probable error for the mean of the two caps might be estimated as of the order of 0.04 or slightly less.

Another way of presenting the data is to say that the solution from the five surveys indicates a limiting magnitude of 12.78 for the Harvard counts, which agrees with that actually observed, well within the uncertainties of the data. It follows that the inclusion

[14] Shapley and Ames, "A Survey of the External Galaxies Brighter than the Thirteenth Magnitude," *Harvard Ann.*, **88**, No. 2, 1932.

[15] *Annual Report of the Mount Wilson Observatory, 1935–1936.*

of the Harvard survey in the general solution would not materially alter the values of C and b as derived from the five surveys alone.[16]

RELATION BETWEEN Δm AND RED SHIFTS

The corrections Δm represent observed departures from apparent uniformity arising from all sources. Nevertheless, they are so small that, for a preliminary discussion, space absorption and real departures from uniformity may be ignored and the corrections referred to effect of red shifts alone. Since red shifts, $d\lambda/\lambda$, and the corrections, Δm, are both approximately linear functions of distance (over the observed range), one can be expressed as a linear function of the other. The velocity-magnitude relation[17] is

$$\log v = 0.2(m - \Delta m) + 0.77 ,$$

or

$$\log \frac{d\lambda}{\lambda} = 0.2(m - \Delta m) - 4.707 ,$$

and

$$\log \Delta m = 0.2(m - \Delta m) - 4.239 .$$

Hence

$$\Delta m = 2.94 \frac{d\lambda}{\lambda} .$$

The probable error of the coefficient in the last relation is relatively small; but, in view of the possibility of systematic errors, a rough estimate of the uncertainties is more significant. The uncertainty of the constant in the first two equations has been previously estimated as not more than 0.02; and, if the same reliability is assigned to the constant b, the uncertainty in the coefficient will be not more than 10 per cent (about three times the probable error).

The most questionable datum is probably the zero point of the magnitude scale; but, fortunately, errors in this quantity do not seriously affect the coefficient. For instance, arbitrary revisions by

[16] With $\log N = -1.38$ and $m = 12.8$ for the Harvard counts, a least-squares solution for the six groups leads to $C = -9.053$, $b = -4.241$.

[17] *Mt. W. Contr.*, No. 549; *Ap. J.*, **84**, 270, 1936.

as much as 0.3 mag. in either direction change the coefficient by less than 15 per cent. In the past, revisions of nebular magnitudes have rather consistently reduced the numerical values. A similar revision of the present data would increase the coefficient; but the change, it is believed, could not be very great.

Other factors involved in the calculations have already been mentioned. The observed range in limiting magnitudes is probably a maximum, and any revision would be expected to reduce the coefficient. The completeness of the nebular counts appears to be comparable in the various surveys. The linear velocity-distance relation has been extrapolated well beyond the observed range; but three of the surveys fall within the observed range, and these alone furnish a value of the coefficient which is comparable with that derived from all five surveys as a group.

The relations

$$\log N = 0.6(m - \Delta m) - 9.052 ,$$

$$\log \Delta m = 0.2(m - \Delta m) - 4.239 ,$$

$$\Delta m = 2.94 \frac{d\lambda}{\lambda}$$

summarize the observational results. They are formally consistent with the assumption that apparent departures from large-scale uniformity, Δm, are linear functions of distance and represent effects of red shifts on apparent luminosity. Therefore a comparison of the observed value of B in the relation $\Delta m = B\, d\lambda/\lambda$ with values calculated on various possible interpretations of red shifts may be expected to indicate which interpretation is the most probable.

II. EFFECTS OF RED SHIFTS ON APPARENT LUMINOSITY

The apparent luminosity of a nebula is measured by the rate at which its light-quanta reach the observer and by the energy in the quanta. Each of these quantities may be influenced by red shifts, and the results are known as the "number effect" and "energy effect," respectively.

Number effect.—If red shifts are velocity shifts, the recession of the nebulae reduces the rates at which the quanta reach the observer, and hence the apparent luminosities, by the factor $1+v/c$. This fac-

tor, the number effect, operates *only* in the case of actual motion. It is constant throughout a given spectrum because it merely reduces the vertical, or intensity, scale of the energy distribution-curves. Since it is non-selective, the number effect increases apparent magnitudes on any system—bolometric, visual, photographic, etc.—by the same amount, namely,

$$\Delta m_N = 2.5 \log \left(1 + \frac{v}{c}\right).$$

In expanding models of the universe obeying the relativistic law of gravitation, the ratio v/c is replaced by $d\lambda/\lambda$.

Energy effect.—The energy effect follows from the familiar relation $E\lambda = \text{constant}$. Red shifts, regardless of their interpretation, evidently reduce the energy of individual quanta and, consequently, the energy of the sum total of all the quanta that reach the earth's atmosphere, by the factor $1+d\lambda/\lambda$. The energy effect is selective, for it changes the horizontal or wave-length scale of the energy-distribution curves. Bolometric magnitudes are increased by the increment $\Delta m_E = 2.5 \log (1+d\lambda/\lambda)$, but the effect must be traced through the atmosphere (selective absorption) and the telescope (selective reflection) to the photographic plate (selective sensitivity) in order to be evaluated in terms of photographic magnitudes. For convenience, the reduction factor, expressed as a magnitude increment, may be termed K. Then, the total effect of red shift on apparent photographic magnitude is to increase the magnitude by the increment

$$\Delta m = 5 \log \left(1 + \frac{d\lambda}{\lambda}\right) + K$$

or by

$$\Delta m = 2.5 \log \left(1 + \frac{d\lambda}{\lambda}\right) + K,$$

depending upon whether or not red shifts are velocity shifts.

EVALUATION OF K

The evaluation of K depends upon the distribution of intensity in nebular spectra. The precise forms of the curves are not well known, but throughout the photographic region they resemble that

of the solar spectrum. The agreement suggests that nebular radiation may be discussed in terms of black-body radiation with about the same degree of confidence that is inspired by similar treatments of solar and stellar radiation. Red shifts distort an original black-body curve for temperature T_0 into new black-body curves corresponding to $T = T_0/(1 + d\lambda/\lambda)$. The lower temperatures introduce increments to the effects of atmospheric absorption, to the heat index, and to the color index corresponding to the original radiation at T_0; and the sums of the increments are the desired values of K. Thus,

$$K = \Delta(\Delta m_r) + \Delta HI + \Delta CI \, .$$

The increments are readily evaluated from curves representing Δm_r (reduction to no atmosphere, including reflection in the telescope), HI, and CI, for stars, as functions of effective temperature.[18]

The values of Δm_r vary less than 0.1 mag. over a range in black-body temperatures from 6000° to 4000°; hence uncertainties in T_0 will introduce only small uncertainties in the increments $\Delta(\Delta m_r)$. The temperature scale for color indices differs widely from the scales derived from heat indices and from water-cell absorptions; but the spectral type is a common denominator by means of which T_0, the zero point for the present purpose, may be transferred from one scale to another. The increments, ΔHI and ΔCI, are then relatively insensitive to the particular scale employed. Actually the scale derived from water-cell absorptions was used for deriving ΔHI; and another, the familiar black-body scale,[19] was used for deriving ΔCI in order that the results for K might, with some justification, be regarded as minimum values. Table V lists values of K determined in this manner for various values of T_0 and of the red shift.

Another, and more purely computational, method of evaluating K may also be employed.[20] A black-body curve for temperature T_0

[18] The data for Δm_r and HI are given in Tables IV and V of "Stellar Radiation Measurements," by Pettit and Nicholson, *Mt. W. Contr.*, No. 369; *Ap. J.*, **67**, 279, 1928. Color indices are conveniently listed on p. 734 of *Astronomy* (1927) by Russell, Dugan, and Stewart. The values of Δm_r, reduction to no atmosphere, include the reflections in the telescope—two silver surfaces.

[19] Russell, Dugan, and Stewart, *op. cit.*, Table XXX.

[20] The method is described by de Sitter, *B.A.N.*, **7**, 205 (No. 261), 1934, and by Hubble and Tolman, *Mt. W. Contr.*, No. 527; *Ap. J.*, **82**, 302, 1935.

is distorted by factors representing atmospheric absorption, reflections in the telescope, and plate sensitivity. The area under the distorted curve represents the intensity actually recorded on the plate. The original curve is then displaced by red shifts and later distorted

TABLE V

K AS A FUNCTION OF T_0 AND $d\lambda/\lambda$

$d\lambda/\lambda$	T_0			
	6500°	6000°	6000°*	5500°
0.05	0.08	0.09	0.09	0.12
.075	.11	.13	.14	.18
.10	.15	.18	.20	.25
.125	.19	.23	.25	.31
.15	.24	.28	.31	.38
.175	.28	.34	.36	.44
.20	.33	.40	.42	.52
.225	.38	.47	.48	.60
0.25	0.44	0.53	0.55	0.68

* De Sitter, *B.A.N.*, **7**, 205 (No. 261), par. 4, 1934.

by the factors previously applied. The ratios of the various recorded intensities to the intensity for zero red shift indicate the energy effects,

$$\Delta m_E = 2.5 \log \left(1 + \frac{d\lambda}{\lambda}\right) + K ,$$

from which the values of K are readily derived.

This method was used by de Sitter[21] in computing Δm_E in terms of pg, pv, and vis magnitudes for $T_0 = 6000°$ and 5000°. The results were expressed in the form of power series, those for photographic magnitudes being

$$(T_0 = 6000°) \qquad \Delta m = 2.90 \frac{d\lambda}{\lambda} + \left(\frac{d\lambda}{\lambda}\right)^2 + \cdots ,$$

$$(T_0 = 5000°) \qquad \Delta m = 4.05 \frac{d\lambda}{\lambda} + 0.8 \left(\frac{d\lambda}{\lambda}\right)^2 + \cdots .$$

[21] *B.A.N.*, **7**, 205 (No. 261), 1934. De Sitter assumed one reflection from silver and one from aluminum, but the difference from the two silver reflections used in the surveys is negligible.

The two methods of determining K lead to results which are in substantial agreement. The greatest uncertainties are those introduced by the assumption of black-body radiation and the neglect of line absorption. Appropriate revisions will be suggested after the characteristics of integrated nebular radiation have been discussed.

The data in Table V could be expressed as power series, following de Sitter's example; but for the present purpose, only the first terms are required. Out to the limits of the surveys, say to $d\lambda/\lambda = 0.22\pm$, the three quantities, K, Δm_E, and Δm_N are all nearly linear functions of $d\lambda/\lambda$. Approximate values of the coefficient B in the relation

TABLE VI

B* AS A FUNCTION OF T_0

T_0	B	
	$K+\Delta m_E$†	$K+\Delta m_E+\Delta m_N$‡
7500°	2.0	3.0
7000	2.4	3.4
6500	2.65	3.65
6000	3.0	4.0
5500	3.6	4.6
5000	4.45	5.45

* B is the coefficient in the relation $\Delta m = B\, d\lambda/\lambda$.

† If red shifts are not velocity shifts, $\Delta m = K+\Delta m_E = K+2.5 \log (1+d\lambda/\lambda)$.

‡ If red shifts are velocity shifts, $\Delta m = K+\Delta m_E+\Delta m_N = K+5 \log (1+d\lambda/\lambda)$.

$\Delta m = B\, d\lambda/\lambda$ are readily obtained from the values of Δm for a given red shift; at $d\lambda/\lambda = 0.2$, for instance, $B = 5\, \Delta m$. These values are listed in Table VI for red shifts interpreted both as velocity shifts and not as velocity shifts and for various effective temperatures.

EFFECTIVE TEMPERATURE OF NEBULAR RADIATION

The choice of an effective temperature for integrated nebular radiation is rather arbitrary. Spectra, in general, are recorded on small scales and are confined to the nuclear regions. Spectral types vary systematically with nebular types; but the range is small, the large majority lying between F5 and G5. Dwarf characteristics are conspicuous in the two spectra (M 31 and M 32) which have been

recorded on considerable scales, and are presumed to be normal features.[22]

Colors of nebulae also vary systematically with the nebular types, and, except for the later spirals, indicate pronounced color excesses, only a fraction of which can be attributed to selective absorption within the galactic system.[23] The measures, by Stebbins and Whitford, were, in general, confined to the central regions of the nebulae and did not include the outer portions.

Mean spectral types (nuclear regions), mean color classes (central regions), and relative frequencies for different nebular types are

TABLE VII

SPECTRAL TYPES AND COLOR CLASSES OF NEBULAE

Nebular Type	Relative Frequency*	Spectral Type†	T_e‡	Color Class¶	T_e
E0–E7	17	G3.6	5710°	g6	4580°
Sa, SBa	19	G3.4	5730	g5	4700
Sb, SBb	26	G1.6	5870	g4	4860
Sc, SBc	38	F8.8	6120	f7	5800
Mean		G1.2	5910	g1.9	5140

* The frequencies are derived from types estimated on large reflector plates of about 650 objects in the Harvard survey of bright nebulae. The rare Irr nebulae are omitted.

† The spectral types are presumably dwarfs. Data by Humason, *Mt. W. Contr.*, No. 531; *Ap. J.*, **83**, 10, 1936.

‡ T_e in the fourth column indicates the effective temperature corresponding to the spectral type, while T_e in the last column indicates the temperature corresponding to the color class.

¶ The color classes are on the scale of giant stars. Data by Stebbins and Whitford, *Annual Rept. of the Mt. Wilson Obs., 1935–1936.*

listed in Table VII, together with the corresponding effective temperatures. The average nebula in the general field is about Sb, spectral type dG1.2, and color class g1.9 (on the scale of giants). The mean effective temperatures, on the particular scale employed, are 5910° from the spectral types and 5140° from the color classes. These data permit a second approximation to the equivalent black-

[22] Exceptions are found in the rare nebulae whose nuclei appear stellar or highly condensed and give emission or early-type spectra.

[23] Investigations of the colors of globular clusters by Stebbins and Whitford (*Mt. W. Contr.*, No. 547; *Ap. J.*, **84**, 132, 1936) suggest a cosecant relation between color excess and galactic latitude, but the selective effect would be a small fraction of the total obscuration. It is not impossible that the correlation may be with position within clouds rather than with latitude.

body temperature that should be used in calculating effects of red shifts.

The data in Tables V and VI indicate the qualitative behavior of Δm as a function of T_0, but purely empirical revisions may be made in order to adapt the results to the actual conditions of the surveys. The revisions involve variations in reflectivity of silver surfaces, departures from black-body radiation, and color excess.

The tabulated values of Δm were based upon reflectivity of freshly burnished silver surfaces, while the surveys were made with mirrors which were resilvered about every six months and burnished about every month. Reflectivity in the violet falls rapidly for a short time and then approaches a fairly steady state. Precise information on variations of the Mount Wilson mirrors (during the era of silver surfaces) is not available, but measures of laboratory mirrors by Strong[24] indicate the order of the deterioration. Curves for reflectivity as a function of λ for silver surfaces 13 and 19 days after burnishing are closely parallel, and the curve for the longer period is believed to approximate the actual conditions of the surveys.[25]

Departures from black-body radiation have been determined in detail only in the case of the sun. Measures of the spectral region in question—from about 6000 A to 3000 A—by Abbot, Pettit, and others furnish an empirical curve for the intensity distribution, which is the curve for the continuous radiation as depressed by line absorption.[26] In the nebulae, the line absorption is presumably comparable with that in the sun, but the distribution of continuous radiation is altered by the observed color excess—of the order of

[24] *Ap. J.*, **83**, 40, 1936, supplemented by unpublished data very generously furnished to the writer.

[25] It makes little difference whether the 13- or the 19-day curve is used, because the significant feature, for the present purpose, is the form of the curve rather than the precise values of the ordinates. Some evidence in favor of the longer interval was derived from a silvered mirror on which Humason selected a region that, in his opinion, appeared to resemble the average state of the large mirrors on Mount Wilson. Strong very kindly measured this selected region and found a curiously close agreement with the 19-day curve.

[26] Abbot, Fowle, and Aldrich, *Smithsonian Misc. Coll.*, **74**, No. 7, 1923. Pettit, *Mt. W. Contr.*, No. 445; *Ap. J.*, **75**, 185, 1932. See also a discussion of these and other data by Mulders, *Zs. f. Ap.*, **11**, 132, 1935.

0.15 mag. (see Table VII). The source of the excess[27] is unknown, but the effect will clearly reduce the equivalent black-body radiation for the nebulae. The effect may be approximated, following a suggestion by Baade, by using observed intensity-curves near the limb of the sun instead of the curve for the integrated light.

The graphical analysis, based on Pettit's measures for integrated sunlight and Abbot's reduction factors for a distance from the center of 0.95 times the radius (which approximates the desired color excess), together with Strong's reflectivity-curve and a table of sensitivities of Eastman 40 plates furnished by the Eastman Kodak Laboratory, gives a relation between the energy effect, Δm_E, and $d\lambda/\lambda$, which is not precisely linear but which fairly approximates the relation for black-body radiation at $T_\circ = 5750°$, over the range in $d\lambda/\lambda$ represented in the surveys. The value of B_E is of the order of 3.25.

Abbot's measures of intensities lead to a slightly larger value of B_E, while Mulders' data give a considerably smaller value—less than 3.0. For these reasons it is concluded that the correct value lies between 3.0 and 3.25, and, in view of the prevalence of early-type giant stars in the outer region of open spirals, is probably nearer the lower limit than the upper. Therefore, the round number 3.0 is adopted, corresponding to an equivalent black-body temperature of 6000°, with a recognized uncertainty of the order of 200°.

Thus, for provisional discussions, the data in Tables V and VI may be used directly with some assurance that the errors are within the uncertainties of the investigation. The uncertainties refer mainly to the unknown origin of the color excess and to the possibility that the

[27] The natural assumption of scattering by finely divided material in the nebulae leads to difficulties in interpreting the appearance of the systems as seen from a distance. Whipple's ingenious attempt to account for the color excess as an effect of a mixture of stellar types in nebulae (*Harvard Circ.*, No. 404, 1935) is not confirmed when the method of calculation is applied to globular clusters. Whipple concluded that the data for the one cluster then available were not inconsistent; but several clusters have been observed by Humason, using the standard nebular spectrograph, and these data, together with colors by Stebbins and his associates, are inconsistent. Moreover, Smith (*Annual Report of the Mount Wilson Observatory, 1935–1936*) reports that the distribution of intensities over the wide range of 8000 A to 3100 A, in elliptical nebulae (where the color excess is most pronounced), show no appreciable indications of mixtures of types.

effect of early giants in the outer regions of spirals has been underestimated—that abnormal intensities exist in the ultraviolet which, when shifted into the photographic region, would materially reduce the tabulated values of K. The former source of uncertainty is probably not important, because different assumptions lead to comparable results. The latter source has been investigated in two ways: First, an ultraviolet spectrum (by Smith) of a nearby, intermediate spiral, extending far out from the nucleus, showed no evidence of conspicuous excess intensities. Second, the relative colors of elliptical nebulae and spirals, in clusters as distant as $d\lambda/\lambda = 0.13$, were found to be appreciably the same as those of similar nebulae in the neighborhood of the galactic system. Since the elliptical nebulae are known to be homogeneous and their spectra have been recorded in the distant clusters, it follows that the spirals also behave normally —that the excess intensities in the ultraviolet are not sufficient to affect seriously the integrated radiation. The observations do not eliminate the possibility of small effects at the limit of the deepest survey; they merely indicate that such effects, if present, are probably not greater than a fraction of 0.1 mag.

III. COMPARISON OF OBSERVATION AND THEORY

It is evident that the observed result, $B = 2.94$, is accounted for if red shifts are not velocity shifts. The comparison is based on an effective temperature, T_0, of 6000°, but the uncertainties cover the range down to about $T_0 = 5750°$. The interpretation is consistent with the data whether the nebulae are pictured as scattered through an old-fashioned, infinite universe or whether a homogeneous model obeying relativistic laws of gravitation is adopted, in which the expansion and spatial curvature are either negligible or zero. The conclusion assumes (*a*) that the large-scale distribution is uniform, (*b*) that nebulae maintain fairly constant luminosities over the time interval involved in the observations, and (*c*) that red shifts are an approximately linear function of distance over the range of the surveys.

The argument for real uniformity follows from the small values of the observed departures from apparent uniformity. They are no greater than the effects of the red shifts calculated under minimum conditions. These calculated corrections, when applied to the obser-

vations, lead to uniformity; further corrections would indicate that the real distribution density increased outward, steadily and symmetrically, in all directions. The latter picture is unwelcome because it implies a curiously unique position for the observer.[28] For this reason uniform distribution is postulated and space absorption is assumed to be negligible. The whole of the observed departures is then referred to effects of red shifts alone.

As for the constancy of nebular luminosities, the question is whether or not luminosities of spirals change materially (say 10 per cent, or 0.1 mag.) during the time required for light to travel from the limit of the deepest survey to the limit of the shallowest survey—an interval of the order of 250 million years. No definite information is available, of course; and probabilities depend upon speculative arguments. Nevertheless, very few students will hesitate to adopt the assumption that systematic variation in so short an interval will be inappreciable. Nebulae are enormous systems, and it is reasonable to suppose that their evolution is correspondingly slow. Theories of stellar radiation, especially of stars with spectral types comparable with those of nebulae, suggest relatively little loss of mass or luminosity over such intervals. Moreover, the sequence of nebular classification may be an evolutional sequence; and it can be stated with some confidence, from the study of nearby nebulae, that the range in mean photographic luminosities, from one end of the sequence to the other, is not more than 0.2 mag. Finally, the velocity-distance relation is sensibly linear over an observed range comparable with the interval in question.

[28] If the nebulae are assumed to be receding with constant velocities in Euclidean space (as a cloud expands in a vacuum), those counted in a given survey would be scattered through a volume V_0 when the light left the limit of the survey, but would be scattered through a larger volume, $V_n = V_0(1+v/c)^3$, when the light reached the observer. Appropriate corrections to the various surveys would then be necessary in order to derive the momentary distribution at a given epoch. The momentary distribution could be uniform at one, and only one, instant. The fact that the data indicate moderate uniformity near the epoch of the surveys—thus formally accounting for an outwardly increasing apparent density—is a remarkable coincidence that immediately suggests the operation of some principle of relativity. This circumstance encourages the recourse to models obeying the relativistic laws of gravitation, the justification for which is discussed in the preliminary contributions on principles and methods by Tolman and the writer, *Mt. W. Contr.*, No. 527; *Ap. J.*, **82**, 302, 1935.

The most impressive evidence for the linearity of the velocity-distance relation is that offered by the great clusters at distances ranging out to about 250 million light-years, or approximately two-thirds of the distance to the limit of the deepest survey. The expression

$$\log \frac{d\lambda}{\lambda} = 0.2(m - \Delta m) - 4.457 ,$$

where m is the observed magnitude of the fifth brightest nebula and $\Delta m = 3\, d\lambda/\lambda$, very closely represents the data for the ten clusters

TABLE VIII

DEPARTURES FROM LINEARITY IN THE VELOCITY-DISTANCE RELATION WHEN RED SHIFTS ARE INTERPRETED AS DOPPLER EFFECTS*

Cluster	$d\lambda/\lambda$	$m_0 - \Delta m_\beta$	$\log d\lambda/\lambda - 0.2 m_c$
Virgo	0.0041	10.50	−4.483
Pegasus	.0127	12.92	.470
Perseus	.0174	13.53	.452
Coma	.0245	14.30	.451
U Ma I	.0517	16.27	.498
Leo	.0653	16.53	.439
Cor. Bor.	.0707	16.75	.445
Boötes	.1307	18.28	.436
U Ma II	0.1403	18.15	−4.371

* The data are extracted from Table I, *Mt. W. Contr.*, No. 549; *Ap. J.*, **84**, 270, 1936, where full details are given. The Gemini cluster ($\lambda = 150°$, $\beta = +20°$) has been omitted because the latitude correction, Δm_β, is known to be very uncertain. Magnitudes refer to the fifth brightest nebulae in the clusters. The corrected magnitudes, m_c, include the effects of red shifts interpreted as velocity shifts: $m_c = m_0 - \Delta m_\beta - 4 d\lambda/\lambda$. The two Ursa Major clusters have minimum weight because they are each represented by a single spectrogram of a single nebula.

that have been investigated. The only residuals as large as 0.1 mag. involve recognized uncertainties, and there are no indications of any systematic trend away from the linear relation. Therefore, a linear extrapolation to distances 50 per cent greater than the observed range will probably serve as a fair approximation. Otherwise, a rather sharp departure from linearity must be postulated, immediately beyond the limits of the observations.[29]

If the corrections $\Delta m = 3 d\lambda/\lambda$ led to a precisely linear relation,

[29] The most recent discussion of the relation, in the form $\log v = 0.2\ (m - \Delta m) + c$, is found in *Mt. W. Contr.*, No. 549; *Ap. J.*, **84**, 270, 1936.

the larger corrections, $4d\lambda/\lambda$, which should be used if red shifts are assumed a priori to be velocity shifts, would evidently introduce departures from linearity. The data are now sufficient to demonstrate the existence of such departures, although the numerical values are

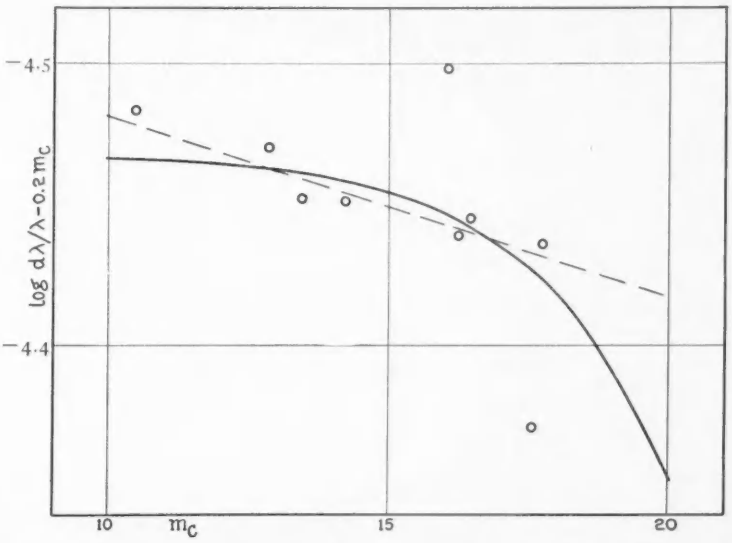

FIG. 2.—Departures from linearity in the velocity-distance relation when red shifts are interpreted as velocity shifts. The points represent mean red shifts, $d\lambda/\lambda$, and corrected magnitudes of the fifth brightest nebula in nine clusters (Table VIII). The observed magnitudes have been reduced to the galactic poles and corrected for red shifts interpreted as velocity shifts, $m_c = m_o - \Delta m_\beta - 4d\lambda/\lambda$. If the velocity-distance relation were linear (as it is when red shifts are referred to some effect other than recession, and the appropriate corrections are $3d\lambda/\lambda$), the differences, $\log d\lambda/\lambda - 0.2m_c$, would be constant, and the points in the diagram would determine a horizontal line. The systematic variation of the differences with m_c indicates the departure from linearity. The straight line corresponds to a linear velocity-*magnitude* relation, $\log d\lambda/\lambda = 0.2064m_c - 4.545$, adjusted to the data, and the curved line to the power series, $d\lambda/\lambda = 1.75 \times 10^{-9}r + 2.7 \times 10^{-18}r^2$, where the distance, r, is expressed in parsecs. The two outstanding residuals refer to the two Ursa Major clusters, which have minimum weight because they are each represented by a single spectrogram of a single nebula.

still uncertain. Mean red shifts and observed magnitudes (reduced to the galactic poles) of the fifth brightest nebulae in nine clusters are listed in Table VIII. The significant correlation is between $d\lambda/\lambda$ and the corrected magnitudes, $m_c = (m_o - \Delta m_\beta) - 4d\lambda/\lambda$.

Departures from the linear velocity-distance relation, $\log d\lambda/\lambda - 0.2\, m_c = C$, are shown in Figure 2, where C is plotted against m_c. The straight line corresponds to a linear velocity-*magnitude* relation,

$$\log \frac{d\lambda}{\lambda} = 0.2064 m_c - 4.545 .$$

The curved line represents the expression of red shifts as a power series of the distance,

$$\frac{d\lambda}{\lambda} = 1.75 \times 10^{-9} r + 2.7 \times 10^{-18} r^2 ,$$

where r is expressed in parsecs.[30] The two outstanding residuals refer to the two Ursa Major clusters which have minimum weight.

The power series will be adopted in the following discussions because it conforms with the notation in theoretical investigations of expanding models of the universe. Since the second-order term is definitely positive, the possible models are restricted to those in which the rate of expansion has been diminishing during the past several hundred million years. The numerical value of the coefficient is rather narrowly limited (probably between 2.4 and 3.4×10^{-18}) over the range of the observed clusters, and extrapolations to the limit of the deepest survey (about $m_c = 18.8$ in Fig. 2) should not introduce serious errors. Further extrapolations rapidly become very uncertain. In view of the importance of the second-order term for theoretical investigations, it may be emphasized that the empirical value is rather precisely the effect of recession which has been introduced as an additional assumption not necessarily demanded by the observations themselves.

HOMOGENEOUS UNIVERSE OF GENERAL RELATIVITY

A detailed comparison may now be made between observational results and world-pictures for homogeneous models of the universe obeying the relativistic laws of gravitation. The principles and

[30] Since the mean absolute magnitude of the fifth nebula in clusters is about $\overline{M}_{pg} = -16.45$, the distances of the clusters in Table VIII are $\log r = 0.2\, m_c + 4.29$. For isolated nebulae, where $\overline{M} = -15.15$, $\log r = 0.2\, m_c + 4.03$. The first term in the power series is essentially that derived in the earlier investigation from resolved nebulae in the general field.

methods have been discussed in a preliminary contribution[31] by Tolman and the writer, where the theoretical formulae derived by Tolman[32] were adapted for application to observational data. It was found that the number of nebulae, N, to the observed limiting magnitude, m_0, would be given by the relation

$$\log N = 0.6(m_0 - \Delta m) + F + C ,$$

where

$$\Delta m = 5 \log \left(1 + \frac{d\lambda}{\lambda}\right) + K$$

or

$$\Delta m = 2.5 \log \left(1 + \frac{d\lambda}{\lambda}\right) + K ,$$

depending upon whether or not red shifts are velocity shifts measuring the rate of expansion of the model. Further,

$$F = \log \left[\frac{3}{2x^3} (\sin^{-1} x - x\sqrt{1-x^2})\right] ,$$

where $x = r/R_0$ represents the distance, r, expressed as a fraction of a constant, R_0, commonly identified as the radius of curvature of space. In expanding models, R_0 refers to a particular epoch.

TABLE IX

EFFECTS OF SPATIAL CURVATURE EXPRESSED AS MAGNITUDE INCREMENTS

r/R_0	$F/0.6$	r/R_0	$F/0.6$
0.05	0.001	0.55	0.075
.1	.002	.6	.092
.15	.005	.65	.112
.2	.010	.7	.135
.25	.014	.75	.162
.3	.020	.8	.196
.35	.028	.85	.238
.4	.037	.9	.292
.45	.048	0.95	.373
0.5	0.061	1.0	0.620

[31] *Mt. W. Contr.*, No. 527; *Ap. J.*, **82**, 302, 1935. The discussion includes a preliminary statement of the observational findings, which are now presented in detail.

[32] *Relativity, Thermodynamics and Cosmology*, Clarendon Press, 1934.

The term F is equivalent to a magnitude increment, $F/0.6$, the values of which are listed in Table IX for successive values of $x = r/R_0$. An inspection of the table indicates that the effects of curvature may be neglected for values of x less than about one-third and that they do not become important until x is greater than one half. Moreover, for $x = 0.9$ and greater, the effects dominate the apparent distribution. These features suggest caution in resorting to curvature to account for observed residuals. No significant contributions can be expected unless R_0 is of the same general order as the penetrating power of existing telescopes.

TABLE X

RED SHIFTS NOT VELOCITY SHIFTS

$\log N - 0.6\,(m_0 - 3d\lambda/\lambda) = \text{Constant}$

m_0	$d\lambda/\lambda$*	$0.6\times(m_0-3d\lambda/\lambda)$	$\log N$	CONSTANT		
				Cal.	Obs.	C−O
21.03.....	0.230	12.204	3.162	−9.042	−9.050	+0.008
20.....	.158	11.728	2.686	.042	.033	−0.009
19.4.....	.125	11.414	2.342	.072	.077	+0.005
19.0.....	.107	11.207	2.161	.046	.051	+0.005
18.47.....	0.086	10.927	1.886	−9.041	−9.044	+0.003

* Calculated from the velocity-magnitude relation, $\log v = 0.2\,(m-\Delta m)+0.77$, from which $5\log d\lambda/\lambda + 3d\lambda/\lambda = m_0 - 23.535$.

Case I. Red shifts not velocity shifts.—The model employed is Einstein's static universe which, for the purpose, is equivalent to an expanding model whose rate of expansion is inappreciable. The data in Table X show that the model is thoroughly consistent with the observations ($B = 3.0$, as compared with 2.94), provided curvature is negligible. The comparison is based on $T_0 = 6000°$; but, as previously mentioned, the uncertainties permit a considerable range in T_0.

Case II. Red shifts are velocity shifts and measure the rate of expansion of the universe.—If curvature is negligible, these models are definitely inconsistent with the observations. The values of B are 4.0 (calculated) and 2.94 (observed). The residuals, $C-O = d\lambda/\lambda$ (approximately), range up to 0.25 mag. and are equivalent to the

number effects introduced by the assumption that red shifts measure actual motion.

If the discrepancies are due to curvature,[33] the effects must be just sufficient to balance the number effects. The curvature must be real and positive, and very great—the model must be closed and small. The calculation of R_0 starts from the value, $C = -9.05$, derived from the direct, least-squares solution of the empirical data, supported by the Harvard survey of bright nebulae and consistent with the static model with negligible curvature. The empirical corrections, Δm_0, are then compared with the corrections for red shifts, calculated from the relations

$$\Delta m_c = \frac{4d\lambda}{\lambda},$$

$$\frac{d\lambda}{\lambda} = 1.75 \times 10^{-9} r + 2.7 \times 10^{-18} r^2,$$

$$\log r = 0.2(m - \Delta m_c) + 4.03.$$

The differences, $\Delta m_c - \Delta m_0$, which are included in Table XI, are the residuals which must be compensated by curvature.

The next step is to plot the curvature increments, $F/0.6$ (Table IX), as a function of $\log r/R_0$. The curve is shown in Figure 3. The range in $\log r$ for the limits of the various surveys (Table XI) is about 0.40. Therefore, the curve in Figure 3 may be searched for some range of the order of 0.40 in $\log r/R_0$ which will furnish the desired series of corrections, $F/0.6$.

No segment of the curve will fit the tabulated residuals exactly. Nevertheless, a segment does exist, $\log r/R_0 = -0.11$ for the deepest survey, which furnishes increments about equal to the residuals *minus* a constant, 0.075 mag. This fit (Table XI), which is rather narrowly limited, may be accepted as a possible solution on the assumption that the small constant, 0.075 mag., reflects a considerable

[33] Since the formulae for the world-pictures were derived by means of co-moving space-like co-ordinates, with respect to which the nebulae have no relative systematic motion, the differences in time required for light to reach the observer from the limits of the various surveys is already taken into account (*Mt. W. Contr.*, No. 527; *Ap. J.*, **82**, 302, 1935).

error in the zero point of the magnitude scale (true magnitudes brighter than observed magnitudes).

TABLE XI

OBSERVATIONS CORRECTED FOR SPATIAL CURVATURE IN AN EXPANDING UNIVERSE

m_c	$d\lambda/\lambda$	Δm_c*	Δm_o	$D=\Delta m_c-\Delta m_o$	log r†	$F/0.6$‡	$D-F/0.6$
21.03....	0.231	0.924	0.676	0.248	8.051	0.180	0.068
20.....	.158	.630	.468	.162	7.904	.077	.085
19.4.....	.124	.500	.368	.132	7.810	.047	.085
19.....	.106	.423	.314	.109	7.746	.034	.075
18.47....	0.085	0.338	0.253	0.085	7.656	0.022	0.063
Mean..	.....	.....	.....	.....	.....	.....	0.075

* $\Delta m_c = 4\ d\lambda/\lambda$.

† log r (in parsecs) refers to the observed limiting magnitude of the surveys.

‡ Corrections for curvature are taken from Table VIII on the assumption that log $r/R_o = -0.11$ for the limit of the deepest survey ($m_o = 21.03$).

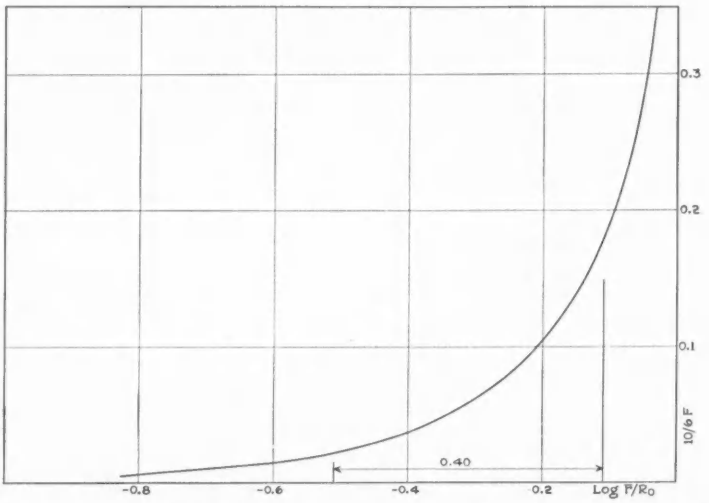

FIG. 3.—Corrections for spatial curvature. The curve shows the corrections to nebular counts, expressed as increments to the limiting magnitudes, required by spatial curvature whose radius is R_o, in a homogeneous universe obeying the relativistic laws of gravitation. The magnitude increments (Table IX) are exhibited as functions of log r/R_o. The section from log $r/R_o = -0.11$ to -0.51 has been selected as furnishing the best fit with the observational results when red shifts are interpreted as velocity shifts measuring the rate of expansion of the universe. The corresponding value of R_o (at the present epoch) is 4.7×10^8 light-years.

The positive curvature, as previously mentioned, indicates a closed, finite universe. The radius, R_0, would be of the order of 1.45×10^8 parsecs or 4.7×10^8 light-years—just less than the estimated mean distance of the faintest nebulae recorded with the 100-inch reflector under optimal conditions. If the radius of curvature were of this order, it would follow that we now observe a large fraction of the universe.[34]

The mean density of the model would be of the general order of 10^{-26} gm/cm^3. Any significant revision of the empirical data would probably reduce R_0 and, consequently, increase the density. Thus the validity of the solution, as a representation of the actual uni-

[34] The spatial curvature and the two terms in the power series for red shifts determine a particular model of the universe among the many homogeneous expanding models which obey the relativistic laws of gravitation. Tolman's calculations of the possible ranges within which the various constants must lie (*Relativity, Thermodynamics and Cosmology*, pp. 472–474) can now be pushed to a much closer approximation. In his notation, the unit of distance is the light-year and

$$\frac{d\lambda}{\lambda} = k\bar{r} - l\bar{r}^2 + \left(\frac{k}{6R^2} + \frac{kl}{3} + m\right)\bar{r}^3 + \cdots\cdots .$$

The co-moving co-ordinate, $\bar{r}$, is equivalent to the co-ordinate r used in the present discussion, namely, the distance derived from apparent magnitudes when the latter are corrected for red shifts. The new data give the following values of the constants:

$$k = 5.37 \times 10^{-10} \text{ (lt. yr.)}^{-1},$$

$$l = -\,2.54 \times 10^{-19} \text{ (lt. yr.)}^{-2}$$

$$\frac{1}{R_0^2} = 4.52 \times 10^{-18} \text{ (lt. yr.)}^{-2},$$

$$\Lambda = (4.4 \text{ to } 6.9) \times 10^{-18} \text{ (lt. yr.)}^{-2}.$$

The cosmological constant, Λ, is determined between upper and lower limits by the assumptions: (*a*) that pressure cannot be less than zero, and (*b*) that the density of matter is greater than zero. The constant m is undetermined; but if it counteracts, rather than adds to, the second-order term in the power series, it will be negative, and the numerical value will be not much greater than

$$2.7 \times 10^{-28} \text{ (lt. yr.)}^{-3}.$$

Since the model is closed and the value of Λ is evidently greater than that for a possible Einstein universe, the model is probably of the type known as a "monotonic universe of the first kind, type M_I." It "would be an ever-expanding type which proceeds from some singular state at $R_s \geq 0$ to the final state of an empty de Sitter universe as $R \to \infty$" (*loc. cit.*, p. 399), in other words, the type that will always be associated with the name of Lemaître.

verse, may depend rather nicely on the question of density. In the neighborhood of the sun the mean density is believed to be of the order of $10^{-23.5}$, and is probably abnormally high because of the local cluster. Since the galactic system, by analogy with other spirals, fades outward to undefined boundaries, it is reasonable to suppose that the mean density of matter in internebular space is thousands of times less than the local density. The smoothed-out density of material concentrated in nebulae is believed to lie between 10^{-28} and 10^{-30}; evidence from various sources[35] is fairly consistent within this range. There is evidently no reason for assuming a mean density of 10^{-26} unless the nebulae are imbedded in a relatively dense, pervading medium which escapes detection.

Photometric evidence is summarized by the statement that space absorption over a light-path of 3.5×10^{26} cm (limit of the deepest survey) is less than 0.1 mag., and probably less than 0.05 mag.[36] A density of 10^{-26} corresponds to an absorption of less than 1 mag. by about 35 (or 70) grams of matter per square centimeter cross-section. This condition immediately rules out many forms of matter (for instance, dust, meteoritic material, and highly ionized gas), but certain forms (for instance, large chunks and non-ionized gas similar to the earth's atmosphere) would still be possible. The permissible forms, however, are probably not those which would be a priori postulated for the contents of internebular space.

CONCLUSION

The observations may be fitted into either of two quite different types of universes. If red shifts are velocity shifts, the model is closed, small, and dense. It is rapidly expanding, but over a long

[35] The limits are set by Smith's value, Mass of the Virgo cluster ÷ Number of nebulae in cluster $= 2\times10^{11}$ suns per nebula (*Mt. W. Contr.*, No. 532; *Ap. J.*, **83**, 23, 1936), and the writer's value, 2×10^{9} suns, derived from spectrographic rotations (*The Realm of the Nebulae*, Yale University Press, 1936). Since the present investigation leads to a density of about one nebula per 1.4×10^{17} cubic parsecs, the smoothed-out densities are 10^{-28} and 10^{-30}, respectively.

[36] This conclusion is necessary in order to avoid a density distribution for the nebulae which increases systematically with distance. The smaller limit is probably permissible because any appreciable absorption would increase the curvature, and hence the density, required to compensate the residuals in Table XI.

period the rate of expansion has been steadily diminishing. Existing instruments range through a large fraction of the entire volume and, perhaps, through a considerable fraction of past time since the expansion began.

On the other hand, if red shifts are not primarily due to velocity shifts, the observable region loses much of its significance. The velocity-distance relation is linear; the distribution of nebulae is uniform; there is no evidence of expansion, no trace of curvature, no restriction of the time scale. The sample, it seems, is too small to indicate the particular type of universe we inhabit.

Thus the surveys to about the practical limits of existing instruments present as alternatives a curiously small-scale universe or a hitherto unrecognized principle of nature. A definitive choice, based upon observational criteria that are well above the threshold of uncertainty, may not be possible until results with the 200-inch reflector become available.

Meanwhile, certain features of the two solutions may be emphasized. The one outstanding objection to the assumption that red shifts are not velocity shifts is, of course, the fact that no other satisfactory interpretation has yet been formulated. Nevertheless, the large-scale characteristics of nature are known only from the kind of data whose interpretation is now in question. The assumption that red shifts measure the rate of expansion of the universe is a long extrapolation from the familiar small-scale Doppler effects. Clearly, the data should be analyzed with the aid of as few assumptions as possible. The observations must be corrected for energy effects, regardless of the origin of red shifts. The interpretation of the corrected data is then direct, economical, and very simple. The observable region is homogeneous and is evidently an insignificant fraction of the universe.

The unexpected and truly remarkable features are introduced by the additional assumption that red shifts measure recession. The velocity-distance relation deviates from linearity by the exact amount of the postulated recession. The distribution departs from uniformity by the exact amount of the recession. The departures are compensated by curvature which is the exact equivalent of the

recession. Unless the coincidences are evidence of an underlying, necessary relation between the various factors, they detract materially from the plausibility of the interpretation.

The high density required by the curvature is another disturbing feature. Although certain specific forms of matter are not ruled out by the photometric data now available, it may be emphasized that the observations merely set upper limits to possible densities and otherwise have no bearing on the actual amount of matter. Dynamical arguments may eventually be developed which will be valid regardless of the form of material. Finally, the small scale of the expanding model, both in space and in time, is a novelty, and as such will require rather decisive evidence for its acceptance.

CARNEGIE INSTITUTION OF WASHINGTON
MOUNT WILSON OBSERVATORY
August 1936

COMPUTATION OF MEAN PARALLAXES, MEAN ABSOLUTE MAGNITUDES, AND MEAN DISTANCES FOR GROUPS OF STARS FROM COMPONENTS OF THE PROPER MOTIONS*

GUSTAF STRÖMBERG

ABSTRACT

Formulae are derived for the computation of mean parallaxes, mean absolute magnitudes, and mean distances from the proper motions of stars, projected on the right ascension and declination axes, on the antapex direction and the perpendicular axes, and on the axis of galactic longitude. Formulae for both the parallactic and the peculiar motions are derived for all the co-ordinate systems mentioned above. The general formulae are given for the derivation of the mean errors in mean parallaxes.

Formulae for computing the dispersion in parallax, distance, and absolute magnitude are also derived.

Mean parallaxes are in general computed from v- and τ-components of the proper motions, combined with values of the velocity of the group of stars relative to the sun and with the velocity dispersion. The usual derivation of v- and τ-components involves, in succession, the determination of total proper motion and its position angle, the angular distance from the star to the apex, the position angle at the star of the great circle through the antapex, and the projection of the proper motion on this great circle and on the perpendicular direction. Although usually facilitated by graphs or tables, the computation is, nevertheless, rather laborious. The writer suggested to the Commission for Stellar Statistics reporting at the Paris meeting of the International Astronomical Union in 1935 that tables be prepared for the derivation of mean parallaxes directly from the proper-motion components in right ascension and declination.[1] Apart from the simplicity of the computation, this method has the advantage that we can give proper weights to the equations of condition and easily correct the mean parallaxes for the effect of systematic errors in proper motion and of galactic rotation. The proposal was adopted by the Commission, and the tables will be constructed at the Lund Observatory.

* *Contributions from the Mount Wilson Observatory, Carnegie Institution of Washington*, No. 558.

[1] *Trans. I.A.U.*, **5**, 230, 1935.

The following pages give a general derivation of the formulae needed in the computation of mean parallaxes, mean absolute magnitudes, mean distances, and the dispersions in these quantities.

GENERAL FORMULAE

The equatorial rectilinear co-ordinates relative to the sun for a star of right ascension α, declination δ, and distance R are

$$\left.\begin{aligned} \xi &= R \cos \alpha \cos \delta , \\ \eta &= R \sin \alpha \cos \delta , \\ \zeta &= R \sin \delta . \end{aligned}\right\} \tag{1}$$

Differentiating with regard to the time and introducing the radial velocity, V, expressed in kilometers per second, the parallax π, and the components μ_1 and μ_2 of the proper motion, expressed in seconds of arc per year, we obtain

$$\left.\begin{aligned} x &= V \cos \alpha \cos \delta - \frac{k}{\pi} (\mu_1 \sin \alpha + \mu_2 \cos \alpha \sin \delta) , \\ y &= V \sin \alpha \cos \delta + \frac{k}{\pi} (\mu_1 \cos \alpha - \mu_2 \sin \alpha \sin \delta) , \\ z &= V \sin \delta + \frac{k}{\pi} \mu_2 \cos \delta , \\ k &= 4.738 \text{ km year/sec} , \\ \mu_1 &= \frac{d\alpha}{dt} \cos \delta , \\ \mu_2 &= \frac{d\delta}{dt} . \end{aligned}\right\} \tag{2}$$

From (2) we find

$$\left.\begin{aligned} V &= x \cos \alpha \cos \delta + y \sin \alpha \cos \delta + z \sin \delta , \\ \frac{k\mu_1}{\pi} &= -x \sin \alpha + y \cos \alpha , \\ \frac{k\mu_2}{\pi} &= -x \cos \alpha \sin \delta - y \sin \alpha \sin \delta + z \cos \delta . \end{aligned}\right\} \tag{3}$$

The observed quantities are V, μ_1, and μ_2. From the first of equations (3) we can determine mean values of x, y, and z, that is, the components of the group motion; and also the residuals in the radial velocities, that is, the peculiar radial velocities V'.

The sun's motion relative to the stars was formerly thought to be a fundamental constant and was early introduced in statistical astronomy; and we shall use this velocity instead of the opposite vector, the group motion, realizing, however, that the sun's motion depends upon the group of objects to which it is referred. Using a standard solar velocity V_0, with the components x_0, y_0, and z_0, and putting

$$x = -px_0 + \eta_x , \qquad y = -py_0 + \eta_y , \qquad z = -pz_0 + \eta_z , \quad (4)$$

we obtain from equations (3)

$$\left.\begin{aligned} V + p\Delta V &= \eta_r = V' , \\ \frac{\mu_1}{\pi} &= pA + \frac{\eta_\alpha}{k} , \\ \frac{\mu_2}{\pi} &= pB + \frac{\eta_\delta}{k} , \end{aligned}\right\} \quad (5)$$

where

$$\left.\begin{aligned} \Delta V &= x_0 \cos \alpha \cos \delta + y_0 \sin \alpha \cos \delta + z_0 \sin \delta = V_0 \cos \lambda , \\ kA &= x_0 \sin \alpha - y_0 \cos \alpha , \\ kB &= x_0 \cos \alpha \sin \delta + y_0 \sin \alpha \sin \delta - z_0 \cos \delta . \end{aligned}\right\} \quad (6)$$

The quantity p is determined by a least-squares solution of the equations of condition $p\Delta V + V = 0$. It is equal to unity if the group motion projected on an axis toward the standard antapex is numerically equal to the standard solar velocity. The quantities η in equations (4) and (5) are the velocity components along the axes indicated by the subscripts, which remain after the effect of the standard solar velocity, multiplied by the factor p, has been subtracted. λ is the angular distance of the star from the standard apex.

In the tables to be published, ΔV, A, and B will be given as func-

tions of α and δ and referred to the standard solar apex, $\alpha_0 = 270°$, $\delta_0 = +30°$, with $V_0 = 20$ km/sec. In other words,

$$x_0 = 0.00\,, \qquad y_0 = -17.32\,, \qquad z_0 = +10.00 \text{ km/sec.} \tag{7}$$

Equations (5) can be written

$$\left.\begin{aligned} pA\pi &= \mu_1 - \frac{\pi\eta_\alpha}{k} = \mu_1 - \epsilon_\alpha\,, \\ pB\pi &= \mu_2 - \frac{\pi\eta_\delta}{k} = \mu_2 - \epsilon_\delta\,. \end{aligned}\right\} \tag{8}$$

If the stars are well distributed over the sky, the condition $\Sigma V'^2 =$ minimum, used in deriving p, implies that $\Sigma\eta_\alpha^2$ and $\Sigma\eta_\delta^2$ also have minimum values. This justifies the use of the conditions $\Sigma\epsilon_\alpha^2$ and $\Sigma\epsilon_\delta^2$ equal to minima, even if the true apex of the solar motion for the group should differ appreciably from the standard apex.

If the number of stars in the group is small, there is danger that an isolated large peculiar radial velocity may greatly influence the value of p. In some cases we know the value of p for the class of stars studied. In other cases we may determine p from the equation

$$p\Sigma|\Delta V| = -\Sigma V|\,, \tag{9}$$

where $V|$ is equal to the radial velocity if ΔV is positive, but has its sign changed when ΔV is negative. The condition used is then equivalent to $\Sigma\Delta V' = 0$. Double vertical bars here and in what follows mean that the inclosed quantities are regarded as positive.

Projecting the proper motions on the great circle through the antapex and on another great circle perpendicular to the former, we obtain expressions for the v- and the τ-components and for λ, the angular distance to the apex:

$$\left.\begin{aligned} v &= \frac{A\mu_1 + B\mu_2}{\sqrt{A^2 + B^2}} = \frac{\pi}{k}\,(pV_0 \sin\lambda + \eta_v)\,, \\ \tau &= \frac{A\mu_2 - B\mu_1}{\sqrt{A^2 + B^2}} = \frac{\pi\eta_\tau}{k}\,, \\ \sin\lambda &= \frac{k\sqrt{A^2 + B^2}}{V_0} = \sqrt{1 - \left(\frac{\Delta V}{V_0}\right)^2}\,. \end{aligned}\right\} \tag{10}$$

These formulae give uncertain values of v and τ when $A^2 + B^2$ is small, that is, for stars near the apex or the antapex. But in this case μ_1 and μ_2 can be regarded as peculiar motions equivalent to τ and can be used directly for computing mean parallaxes, as will be explained later.

MEAN PARALLAXES

The equations of condition for determining mean parallax by the use of the tables here referred to are

$$\left.\begin{aligned} pA\pi - \mu_1 &= \eta_1 - \frac{\pi T_1}{k} = \epsilon_1 , \\ pB\pi - \mu_2 &= \eta_2 - \frac{\pi T_2}{k} = \epsilon_2 . \end{aligned}\right\} \qquad (11)$$

These equations, apart from a change in notation, are identical with equations (8). We have here introduced η_1 and η_2, the true errors in the measurements of μ_1 and μ_2, respectively. T_1 and T_2 are the "peculiar," linear tangential-velocity components remaining after the effects of the standard solar motion have been subtracted from μ_1 and μ_2, respectively. Equations (11) can be used when only one of the proper-motion components is known. If μ_1 and μ_2 are determined with different accuracy, proper weights can be introduced. To simplify the following equations, we will write them as if we used only the proper motion in right ascension, although, of course, similar equations hold for the proper motion in declination, and, in general, the results should be combined.

In the general case we regard the parallax as differing from one star to another in the group studied, and wish to determine the mean parallax, $\bar{\pi}$.

1. *Parallactic motions.*—We assume $\Sigma\epsilon_1^2 = \min$. We have then

$$\Sigma\epsilon_1^2 = p^2\Sigma A^2\pi^2 + \Sigma\mu_1^2 - 2p\Sigma A\pi\mu_1 = \min.$$

If π is nearly constant or if there is no correlation between A and π, we can write

$$p^2\bar{\pi}^2\Sigma A^2 + \Sigma\mu_1^2 - 2p\Sigma A\pi\mu_1 = \min.$$

There is always a correlation between A and μ_1, and also between π and μ_1, and hence between $A\mu_1$ and π. Denoting the coefficient of correlation between $A\mu_1$ and π by r, and the number of stars by n, we have

$$\Sigma A\pi\mu_1 = \Sigma(A\mu_1 - \overline{A\mu_1})(\pi - \overline{\pi}) + \overline{\pi}\Sigma A\mu_1 = \overline{\pi}\Sigma A\mu_1 + nr\sigma_1\sigma_2 ,$$

$$\sigma_1^2 = \frac{\Sigma(\pi - \overline{\pi})^2}{n} , \qquad \sigma_2^2 = \frac{\Sigma(A\mu_1 - \overline{A\mu_1})^2}{n} .$$

Further,

$$\overline{\pi^2} = \overline{\pi}^2 + \sigma_1^2 .$$

Hence

$$\Sigma\epsilon_1^2 = p^2(\overline{\pi}^2 + \sigma_1^2)\Sigma A^2 + \Sigma\mu_1^2 - 2p\overline{\pi}\Sigma A\mu_1 - 2pnr\sigma_1\sigma_2 = \min.$$

By varying $\overline{\pi}$, we find

$$\overline{\pi}p\Sigma A^2 = \Sigma A\mu_1 . \tag{12}$$

If both μ_1 and μ_2 are given for all the stars and if they have the same mean errors, we obtain from equations (10) and (12),

$$\overline{\pi} = \frac{\Sigma(A\mu_1 + B\mu_2)}{p\Sigma(A^2 + B^2)} = \frac{k\Sigma v \sin\lambda}{pV_0\Sigma \sin^2\lambda} . \tag{13}$$

This is a convenient form of the formula generally used, which is ordinarily derived on the assumptions that π is practically constant, that V_0 is the actual group motion, and that the standard apex is identical with the true apex for the group motion.

2. *Parallactic motions.*—We assume $\Sigma\epsilon_1 = 0$. Since we can rearrange the signs of ϵ_1 in any unbiased way we please, we get from equation (11), provided that there is no correlation between π and A,

$$\overline{\pi}p\Sigma|A| = \Sigma\mu_1| , \tag{14}$$

where the bar after μ_1 indicates that the sign of μ_1 is reversed if A is negative. If the v-components are derived for each star separately, the same condition gives

$$\overline{\pi} = \frac{k\Sigma v}{pV_0\Sigma \sin\lambda} = \frac{\Sigma v}{p\Sigma\sqrt{A^2 + B^2}} . \tag{15}$$

3. *Peculiar motions.*—We assume $|\overline{T_1}| = |\overline{V'}| = \theta$, the average peculiar radial velocity. From (11) we obtain

$$|\overline{\epsilon_1}| = \left|\overline{\eta_1 + \frac{\pi T_1}{k}}\right| = |\overline{\mu_1 - pA\pi}| .$$

To solve this equation for $\overline{\pi}$ we must know an approximate value of this quantity, which we will denote by π'. We can now write the approximate equality

$$|\overline{\eta_1}|^2 + \left(\frac{\overline{\pi}\theta}{k}\right)^2 = |\overline{\mu_1 - pA\pi'}|^2 .$$

Hence,

$$\overline{\pi} = \frac{k}{\theta}\sqrt{|\overline{\mu_1 - pA\pi'}|^2 - |\overline{\eta_1}|^2} . \tag{16}$$

As a second approximation, we replace π' by $\overline{\pi}$ and recompute $\overline{\pi}$. For stars near the apex or the antapex, A and B are small and errors in π' have little effect, and we might even neglect the term $pA\pi'$ in the first approximation. For v- and τ-components, respectively, equation (16) becomes:

$$\left.\begin{aligned} \overline{\pi} &= \frac{k}{\theta}\sqrt{\left|\overline{v - \frac{\pi' p V_0}{k}\sin\lambda}\right|^2 - |\overline{\eta_1}|^2} , \\ \overline{\pi} &= \frac{k}{\theta}\sqrt{|\overline{\tau}|^2 - |\overline{\eta_1}|^2} . \end{aligned}\right\} \tag{17}$$

In the last equation we recognize the usual form for deriving $\overline{\pi}$ from τ-components, obtained by neglecting the effect of errors of observation.

4. *Peculiar motions.*—We assume $\overline{T_1^2} = \overline{V'^2}$ and obtain

$$\overline{\epsilon_1^2} = \overline{\eta_1^2} + \frac{\overline{\pi^2}\,\overline{V'^2}}{k^2} = \overline{(\mu_1 - pA\pi)^2} .$$

This equation can be solved by approximations. We find

$$\overline{\pi^2} = \frac{k^2}{\overline{V'^2}}\left[\overline{(\mu_1 - pA\pi')^2} - \overline{\eta_1^2}\right] = \overline{\pi}^2 + \sigma_1^2 . \tag{18}$$

The last equation gives us, after combination with $\overline{\pi}$ from other determinations, a value of σ_1, the dispersion in π.

The equation for the τ-components equivalent to (18) is

$$\overline{\pi^2} = \frac{k^2}{V'^2}(\overline{\tau^2} - \overline{\eta_1^2}) = \overline{\pi}^2 + \sigma_1^2 . \tag{19}$$

If we express all linear motions in astronomical units per year, instead of in kilometers per econd, we can omit the factor k in all the preceding formulae.

The advantages of the foregoing formulae lie in the many different values for $\overline{\pi}$ which we can obtain by different assumptions about the errors. Further, the peculiar motions are here utilized in a much more general way than is possible when they are measured by τ-components alone.

MEAN ABSOLUTE MAGNITUDES

In many cases the mean parallax of a group of stars is in itself of little physical significance. Often we want to determine the mean absolute magnitude of a class of stars and obtain an estimate of the spread of intrinsic brightness. To reduce the spread in parallax due to inequality of the apparent magnitudes of the stars in the group, we must first reduce the proper motion and parallaxes to a common apparent magnitude.

The absolute magnitude M, as defined by the International Astronomical Union, the apparent magnitude m, and the parallax are related by the equation

$$M = m + 5 + 5 \log \pi . \tag{20}$$

We introduce a parallax π_0 reduced to zero apparent magnitude and defined by the equation

$$\pi_0 = \pi \, 10^{0.2m} . \tag{21}$$

We have then

$$\left.\begin{aligned} M &= 5 + 5 \log \pi_0 , \\ \text{or} \qquad \pi_0 &= 0.1 \cdot 10^{0.2M} . \end{aligned}\right\} \tag{22}$$

From equations (11) and (21) we find

$$pA\pi_0 - \mu_1' = \eta_1' - \frac{\pi_0 T_1}{k} = \epsilon_1 \, 10^{0.2m} = \epsilon_1' , \tag{23}$$

where μ_1' and ϵ_1' are the proper-motion component and its residual, respectively, both multiplied by the factor $10^{0.2m}$, that is, reduced to zero apparent magnitude.

We can now determine $\overline{\pi_0}$ in the same way as we determined $\overline{\pi}$ by use of the equations (12) to (17). From equation (18) or (19) we can also obtain a value of $\overline{\pi_0^2}$, which is needed in order to find the dispersion in absolute magnitude, which we will denote by q. We will assume that the absolute magnitudes are distributed according to a normal error-curve about a mean value $\overline{M}$. We have then

$$\left.\begin{aligned} M &= \overline{M} + \Delta\,, \\ \overline{10^{0.2M}} &= 10^{0.2\overline{M}} \cdot \overline{10^{0.2\Delta}}\,, \\ \overline{10^{0.4M}} &= 10^{0.4\overline{M}} \cdot \overline{10^{0.4\Delta}}\,, \\ \overline{10^{0.2\Delta}} &= \frac{1}{\sqrt{2\pi}q}\int_{-\infty}^{+\infty} e^{-\frac{\Delta^2}{2q^2}}\, 10^{0.2\Delta} d\Delta = e^{\frac{0.02q^2}{\mathrm{Mod}^2}} = C\,, \\ \overline{10^{0.4\Delta}} &= \frac{1}{\sqrt{2\pi}q}\int_{-\infty}^{+\infty} e^{-\frac{\Delta^2}{2q^2}}\, 10^{0.4\Delta} d\Delta = e^{\frac{0.08q^2}{\mathrm{Mod}^2}} = C^4\,. \end{aligned}\right\} \tag{23}$$

Thus

$$\begin{aligned} \overline{\pi_0} &= 0.1 \cdot \overline{10^{0.2M}} = 0.1 \cdot 10^{0.2\overline{M}}\, C\,, \\ \overline{\pi_0^2} &= 0.01 \cdot \overline{10^{0.4M}} = 0.01 \cdot 10^{0.4\overline{M}}\, C^4\,. \end{aligned}$$

The final formulae now become

$$\left.\begin{aligned} C^2 &= \frac{\overline{\pi_0^2}}{\overline{\pi_0}^2}\,, \\ q^2 &= \overline{(M - \overline{M})^2} = 50\ \mathrm{Mod} \log C = 21.71 \log C\,, \\ \overline{M} &= 5 + 5 \log \overline{\pi_0} - 5 \log C\,. \end{aligned}\right\} \tag{24}$$

All the logarithms used here are to the base 10.

Some of the formulae given here were published in *Mount Wilson Communications*, No. 103; *Proceedings of the National Academy of Science*, **14**, 834, 1928, where references to and comparisons with earlier formulae by Gyllenberg are given.

MEAN DISTANCES

The distance R to a star expressed in parsecs is the inverse value of the parallax. Since the parallaxes of the stars in a group in general are different, the mean value of R is always greater than the inverse of the mean parallax. If the dispersion in π is σ_1, we obtain by expansion in terms of σ_1/π,

$$\overline{R}\overline{\pi} = 1 + \frac{\sigma_1^2}{\overline{\pi}^2}, \tag{25}$$

where σ_1 can be found from equations (18) or (19).

If the stars in the group have the same apparent magnitude, the spread in distance is due solely to a spread in absolute magnitude. We have then

$$\overline{R} = R(m, \overline{M}) \cdot \overline{10^{-0.2\Delta}} = \frac{C}{\pi(m, \overline{M})},$$

$$\overline{\pi} = \pi(m, \overline{M}) \cdot \overline{10^{0.2\Delta}} = \pi(m, \overline{M})C.$$

Here $R(m, \overline{M})$ and $\pi(m, \overline{M})$ denote distances and parallaxes, respectively, computed from m and $\overline{M}$. We thus obtain, using one of the equations (23),

$$\overline{R}\overline{\pi} = C^2 = e^{\frac{0.04q^2}{\mathrm{Mod}^2}}. \tag{26}$$

This formula was first given by Oort.[2]

If there is a small variation in m, we can write

$$\overline{R} = 10 \cdot 10^{-0.2\overline{M}}\,\overline{10^{0.2m}}C = \frac{1}{\overline{\pi_0}}\,\overline{10^{0.2m}}C = \overline{R(m, \overline{M})}C, \tag{27}$$

where C is given by equation (23).

In the general case we can only use equ. (25).

MEAN ERRORS OF PARALLAXES

In the preceding study we have regarded π and M as quantities differing from star to star. The means of π and of M are derived from a limited set of data, however, and hence are affected by errors

[2] *B.A.N.*, **4**, 81, 1927.

due to the use of relatively small samples. Such errors would be present even if π or M were constant. These statistical errors can be computed in the same way as when π and M were constant for the group.

Equations (12) and (13) are based on a least-squares condition. Denoting by the symbol $E(\pi)$ the mean error in $\overline{\pi}$ and by n the number of stars, we therefore have

$$\left.\begin{aligned} E^2(p\pi) &= \frac{\Sigma\epsilon_1^2}{(n-1)\Sigma A^2} = \frac{\Sigma(A\overline{\pi}-\mu_1)^2}{(n-1)\Sigma A^2}, \\ E^2(\pi) &= \frac{E^2(p\pi)}{p^2} + \frac{(\overline{\pi}^2+\sigma_1^2)E^2(p)}{p^2}. \end{aligned}\right\} \tag{28}$$

Some estimates of the mean error in p, which enters in equations (28), can in general be made.

In the case of equation (14) we might use the same mean error as given by the least-squares condition. We may also use the equation

$$E(p\pi) = \frac{1.25\Sigma|\mu_1 - \rho\overline{\pi}|A||}{\sqrt{n(n-1)}\,\Sigma|A|}, \tag{29}$$

which is analogous to Peters' formula and has the advantage that no squared values occur.

Equation (15) gives the similar equation

$$E(p\pi) = \frac{1.25\Sigma|v - p\overline{\pi}\sqrt{A^2+B^2}|}{\sqrt{n(n-1)}\,\Sigma\sqrt{A^2+B^2}} = \frac{1.25k\Sigma|v - \frac{V_0}{k}\overline{\pi}\sin\lambda|}{V_0\sqrt{n(n-1)}\,\Sigma\sin\lambda}. \tag{30}$$

When we are dealing with means taken regardless of signs, as in equations (16) and (17), we can use the equation[3]

$$E(|\overline{\tau}|) = \frac{0.756|\overline{\tau}|}{\sqrt{n}} \tag{31}$$

for determining the mean error in an arithmetic mean.

Similar equations hold for $|\overline{V^7}| = \theta$, and for $|\mu_1 - pA\overline{\pi}|$.

[3] Cf. Russell, on the accuracy of mean parallaxes, *Mt. W. Contr.*, No. 215; *Ap. J.*, **54**, 140, 1921.

The mean error in $\bar{\pi}$ determined from equation (16) can then be found from the equation

$$\frac{E^2(\pi)}{\bar{\pi}^2} = \frac{E^2(\theta)}{\theta^2} + \frac{k^2}{\theta^2\bar{\pi}^2} E^2(|\overline{\mu_1 - pA\bar{\pi}}|) . \tag{32}$$

From equation (17) we get the analogous equation

$$\frac{E^2(\pi)}{\bar{\pi}^2} = \frac{E^2(\theta)}{\theta^2} + \frac{k^2}{\theta^2\bar{\pi}^2} E^2(|\bar{\tau}|) . \tag{33}$$

In those formulae which depend on a comparison between peculiar angular and linear motions, some improvements can be made by correcting the spread in these quantities for the effect of an ellipsoidal velocity distribution. If the stars are well distributed over the whole sky, no correction is needed. In other cases a knowledge of the ratio of the three axes is needed to apply such a correction.

GALACTIC STARS

If the stars are distributed along the galactic circle, only the proper-motion components along this circle should be used, since in general we have insufficient knowledge of the linear motions perpendicular to the galactic plane. A and B, as well as μ_1 and μ_2, should then be projected on the galactic circle with the aid of the galactic parallactic angle φ, which is given in Ohlson's tables.[4] We have

$$\left.\begin{aligned} \mu_l &= \mu_1 \cos\varphi + \mu_2 \sin\varphi = \mu \sin(\varphi + \psi), \\ A_l &= A \cos\varphi + B \sin\varphi , \\ A_l p\pi - \mu_l &= \epsilon_l . \end{aligned}\right\} \tag{34}$$

In the first of these equations μ and ψ are the total proper motion and its position angle, respectively.

A study of the errors in the mean parallaxes shows immediately that the relative accuracy of the results from parallactic and peculiar motion depends upon the size of the linear group motion relative to the linear peculiar velocities. The quantitative formulation of this fact was first given by Russell.[3] Except for extreme cases, it is ad-

[4] *Annals Obs. Lund*, No. 3, 1932.

visable to use *all* the methods here given for determining mean parallaxes and then weight them properly according to their mean errors when forming the final means.

CORRECTIONS FOR GALACTIC ROTATION

The formulae for computing mean parallaxes are based on the assumption that the velocity distribution is the same everywhere within the region in which the stars studied are situated. If the stars are very distant, this assumption is known to be invalid. The effects of differential galactic rotation can be allowed for by applying corrections to both the proper motions and the radial velocities. In this case we need consider only stars near the galactic plane and use only the proper-motion component parallel to the plane. The corrections to be applied to the proper motion in galactic longitude and to the radial velocities are then

$$\left.\begin{aligned} \Delta\mu_l &= -\left[\frac{A'}{k}\cos 2(l-l_0)\cos b + \frac{B'}{k}\cos b\right], \\ \Delta V &= -RA'\sin 2(l-l_0)\cos^2 b\,. \end{aligned}\right\} \qquad (35)$$

In these formulae l is the galactic longitude of the star, l_0 that of the center of the galaxy; b is the galactic latitude, R the distance in parsecs; and A' and B' are Oort's constants for galactic rotation. There are many determinations of these constants, and I give here only the latest determinations of Plaskett and Pearce from the motions of O and B stars and the calcium clouds:

$$A' = +0.0155 \pm 0.0009 \text{ km/sec parsec},$$

$$B' = -0.0120 \pm 0.0027 \text{ km/sec parsec},$$

$$l_0 = 324^\circ.4 \pm 2^\circ.4\,.$$

Mean values of R can be used, the means being computed with the aid of equations (25), (26), or (27).

CARNEGIE INSTITUTION OF WASHINGTON
MOUNT WILSON OBSERVATORY
August 1936

A SPECTROGRAPHIC STUDY OF φ PERSEI[1]

HERBERT F. SCHIEFER

ABSTRACT

The spectral variations of φ Persei were measured on 32 two-prism spectrograms. The radial velocity of the central absorption of hydrogen shows cyclic variations in a period of 126.6, days with a secondary variation on the descending portion of the velocity-curve which increases progressively with decreasing wave-length. Microphotometric studies of the intensities of the hydrogen absorption and of the emission components of hydrogen show similar variations.

At maximum positive velocity of the hydrogen absorption the red edges of the hydrogen emission show a similar displacement to the red, while the violet edges show a violet displacement, resulting in a maximum width for the total emission and in a maximum intensity of the violet emission component relative to the red emission component. At maximum negative velocity of the hydrogen absorption the violet edges of the hydrogen emission show a similar violet displacement, while the red edges show a red displacement, resulting in a second maximum width for the total emission and in a maximum intensity of the red emission component relative to the violet emission component. The widths of the hydrogen emission and the components vary therefore in one-half of the star's velocity period, while the relative intensity of the emission components and of the central absorption of hydrogen relative to the continuous spectrum show periodic and secondary variations similar to the star's velocity of hydrogen absorption.

The truly periodic spectral variation of φ Persei is interpreted satisfactorily by the hypothesis of orbital motion and rapid axial rotation of two stars, each having a very extensive atmosphere. The hydrogen emission is assumed to originate in the projecting atmospheres of the stars at right angles to the line of sight. The hydrogen absorption is assumed to originate mainly in the outer atmosphere between the observer and the fairly well-defined bright photosphere of the primary star. The pronounced secondary spectral variations, which vary progressively with wave-length, appear to be explained most readily by an apparent atmospheric expansion which is produced in the intervening extensive, rarefied, and transparent atmosphere of the companion star due to excitation by radiation from the hot photosphere of the primary star at the time it is partially eclipsed by the extensive atmosphere of the companion star.

INTRODUCTION

The spectrum of φ Persei, class Bope, is of unusual interest because of the great variations of the hydrogen lines. Each line consists of a very broad absorption upon which is superimposed a narrower emission. The emission is divided into two components by a sharp central absorption. The emission is very strong for $H\beta$ but vanishes rapidly for lines below $H\delta$.

The spectral variations of this star have been extensively investi-

[1] A dissertation submitted in partial fulfilment of the requirements for the degree of Doctor of Philosophy in the University of Michigan (1928). The general results were presented at the annual meeting of the Iowa Academy of Science, April, 1929. In preparing this paper for publication several additions have been made, as well as many excisions.

gated by Campbell and Reese,[2] Cannon,[3] Ludendorff,[4] Jordan,[5] Frédette,[6] Lockyer,[7] and Dustheimer.[8] The radial velocity of the central absorption of hydrogen has been found to vary in a period of 126.6 days. The relative intensities of the hydrogen emission components vary in a similar period. The results of Lockyer in 1925 indicate a cyclic variation of intensity in a period of 21 days in addition to the 126-day period. Subsequent data published by him in 1926, however, do not confirm this short period. The widths of the hydrogen emission lines show a cyclic variation in one-half of the star's velocity period. Photoelectric measurements by Guthnick[9] during 1916–17 indicate a cyclic variation of about 0.11 mag. in a period of 18.1 days. This short period corresponds to that determined from his visual observations in 1911–12. The photoelectric measurements by Güssow[10] during 1925–28 indicate variations of about 0.1 mag. which do not satisfy the previously announced periods.

With the attachment of the two-prism spectrograph to the Ann Arbor $37\frac{1}{2}$-inch reflector in the summer of 1927, it seemed worth while to obtain a series of two-prism spectrograms of φ Persei for a more accurate study of its spectral variations. Thirty-two spectrograms were obtained over an interval slightly more than the star's velocity period. On each two-prism plate ten standard intensity spots were photographed by means of a tube-sensitometer.

The results which will be presented in this paper include a study of the intensity variations of the hydrogen lines with the Moll microphotometer, of the widths of the hydrogen emission lines and components, and of the measures for radial velocity of the following features: the central absorption of $H\beta$, $H\gamma$, $H\delta$, $H\epsilon$, and $H\zeta$; the central absorption edges of $H\beta$, $H\gamma$, and $H\delta$; the emission edges of $H\beta$, $H\gamma$, and $H\delta$; K of calcium; helium at λλ 3964, 4026, and 4471; and the central absorption of ionized iron at λλ 4233, 4352, 4584, 4630,

[2] *Lick Obs. Bull.*, **1**, No. 20, 158, 1902.

[3] *J.R.A.S., Can.*, **4**, 195, 1910.

[4] *A.N.*, **186**, 17, 1911.

[5] *Pub. Allegheny Obs.*, **3**, 31, 1913.

[6] *J.R.A.S., Can.*, **19**, 185, 1925.

[7] *M.N.*, **85**, 580, 1925; **86**, 474, 1926.

[8] Dissertation, University of Michigan, 1927, unpublished.

[9] *Veröff. Kgl. St. Babelsberg*, **2**, 89, 1918.

[10] *A.N.*, **237**, 321, 1929.

and 4924. Some results of the intensity variations of the hydrogen emission, obtained from 109 unstandardized single-prism spectrograms, are presented for comparison.

A SPECTROGRAPHIC STUDY OF φ PERSEI

Relative intensities.—The variations with phase in the intensity of the hydrogen lines of φ Persei are shown in Figure 1. The intensity

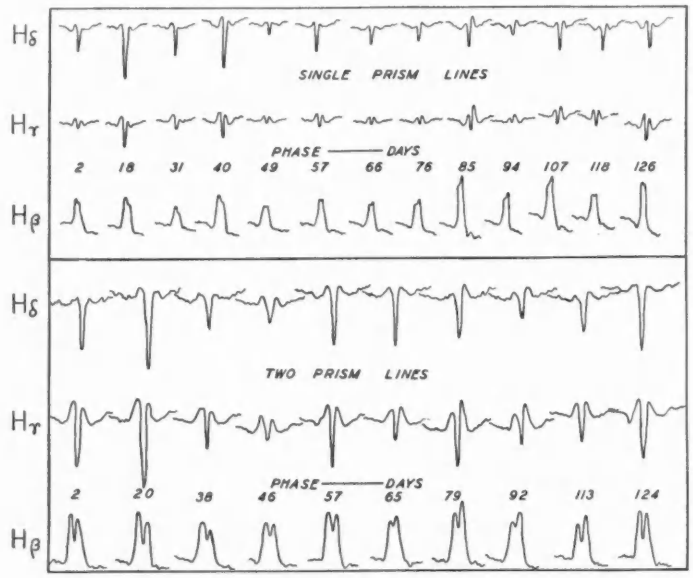

FIG. 1.—Microphotometric tracings showing the periodic variation in the intensity of the hydrogen lines of φ Persei.

variations were determined quantitatively with the aid of the standard spots. The results are expressed in an arbitrary unit which is equal to the logarithm to the base 10 of 1.5, that is, the logarithm of the ratio of the aperture areas of the tube-sensitometer.

The relative intensities based upon the individual two-prism plates are given in Figure 2. The period used in computing the phases and the epoch to which they are referred are those given by Dustheimer, namely, a period of 126.626 days and zero phase at November 18.000, 1925, G.M.T.

The curves for the relative intensities of the emission components

of $H\beta$, $H\gamma$, and $H\delta$, at the bottom of Figure 2, show that at zero phase the violet emission component is slightly more intense than the red emission component. This difference in intensity increases with phase and becomes a maximum at approximately 28 days. On the descending portion of the curves, in the region where the intensity of the red emission component is approximately equal to that of the violet emission component, the curves show a secondary varia-

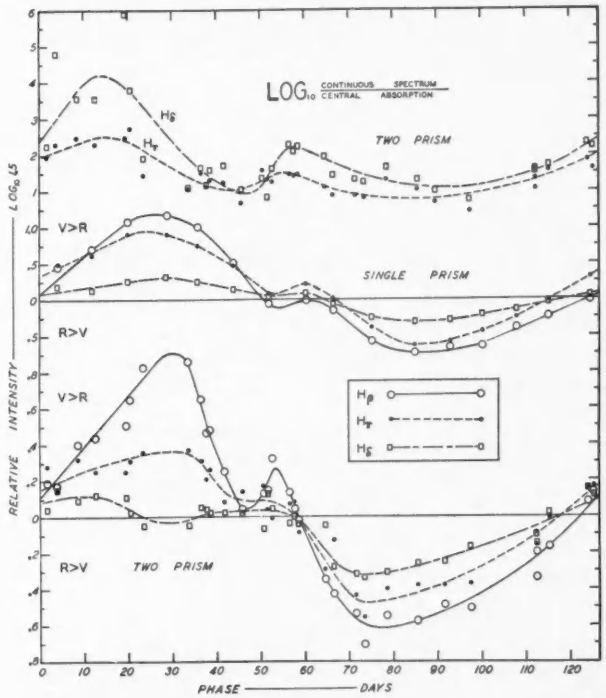

FIG. 2.—Relative intensity of the hydrogen emission components and of the central absorption of hydrogen relative to the continuous spectrum of φ Persei.

tion. Beyond phase 60 days the intensity of the red emission component is greater than that of the violet emission component. The difference is a maximum between phases 70 and 80 days and then decreases again to complete the cycle in 126.6 days.

The range of variation appears to increase with the wave-length. The secondary variation which is pronounced in $H\beta$ is only indicated for $H\gamma$ and is practically absent in $H\delta$. The absence of a dis-

tinct maximum at phase 28 days for $H\delta$ and the shape of the secondary variation for $H\gamma$ suggest that the secondary variation occurs earlier and may be of greater magnitude in lines of shorter wavelength.

TABLE I

RADIAL VELOCITIES OF φ PERSEI IN KM/SEC

DATE (G.M.T.)	PHASE (DAYS)	CENTRAL ABSORPTION*					RED EMISSION EDGE			VIOLET EMISSION EDGE			K OF CA	MEAN HE	MEAN FE
		$H\beta$	$H\gamma$	$H\delta$	He	$H\zeta$	$H\beta$	$H\gamma$	$H\delta$	$H\beta$	$H\gamma$	$H\delta$			
1927															
July 29.780	112.276	−17	−16	−21	− 6	−47	174	152	153	−219	−209	−182	−32	−21	−21
Aug. 1.803	115.299	−18	−17	−18	− 9	−53	174	173	144	245	189	218	+ 5	− 5	−12
10.798	124.294	−12	−11	− 9	− 5	−31	182	143	155	218	176	172	− 4	−28	−16
11.802	125.298	− 8	−10	− 7	− 0	−24	188	164	154	208	161	196	+ 4	+ 3	+ 7
14.847	1.717	− 7	− 2	+ 1	+ 9	....	211	173	....	187	168	.....	+ 3	− 3	− 4
21.797	8.667	+ 4	+ 6	+11	+16	− 4	197	180	167	206	188	149	+ 5	+19	+ 8
25.816	12.686	+ 7	+13	+15	+22	+ 6	181	179	172	199	188	160	+14	+22	+ 2
Sept. 1.728	19.598	+33	+37	+35	+38	+49	203	184	....	215	201	.....	+34	+60	−12
2.753	20.623	+31	+29	+29	+44	+24	212	165	149	200	192	132	+43	+54	−13
5.770	23.640	+26	+26	+30	+35	+ 6	178	196	191	203	181	173	− 6	+30	+ 8
15.782	33.652	+30	+26	+21	+29	− 5	206	195	191	212	191	165	.....	+45	+13
18.775	36.645	+27	+30	+26	....	....	196	182	182	206	202	161	.....	.....	−19
19.792	37.662	+33	+30	+17	+35	−40	197	195	183	193	188	160	−62	+33	+ 4
20.758	38.628	+36	+23	+21	....	....	179	210	....	190	193	.....	.....	+48	− 3
Oct. 2.785	50.655	−11	+ 2	+ 1	....	....	184	179	....	213	174	.....	.....	+34	−11
3.716	51.586	+ 2	− 9	−14	....	....	165	176	....	187	177	.....	.....	.....	−12
4.792	52.662	+ 5	+ 9	+ 4	0	....	183	177	214	195	159	175	+ 7	+13	− 9
8.712	56.582	+ 4	+ 8	+ 5	+11	−18	189	180	161	208	174	146	+ 3	+ 1	+10
9.715	57.585	+ 6	+ 7	+ 5	+11	−25	195	154	162	226	179	176	− 2	+ 1	−12
10.708	58.578	0	+ 6	+10	+14	−16	183	167	152	212	184	147	+ 2	+ 6	−14
16.717	64.587	− 7	− 1	+ 5	+ 9	−26	157	121	130	222	186	141	+ 4	+ 4	− 7
18.679	66.549	− 1	0	+ 1	+ 8	....	149	150	....	206	190	.....	.....	+ 5	− 2
23.763	71.633	−20	− 6	− 2	+ 4	−30	186	121	112	222	178	143	− 2	+ 3	−14
25.732	73.602	− 8	− 7	− 9	− 1	−35	162	139	128	202	212	174	− 9	− 8	−12
30.715	78.585	−13	−10	− 9	+ 3	....	158	136	131	192	145	162	.....	+ 1	−10
Nov. 6.702	85.572	−19	−14	−13	−11	−45	188	152	144	217	216	211	− 4	−19	−16
12.705	91.575	−24	−16	−19	− 3	−54	177	162	176	227	219	186	− 1	+11	−17
18.627	97.497	−18	−34	−34	−19	....	181	173	169	227	222	201	− 6	.....	−38
Dec. 3.640	112.510	− 9	−19	−18	−13	−49	184	139	164	230	185	174	+10	−13	−13
21.613	3.857	+ 1	+ 7	+ 4	+17	+ 8	197	164	155	189	182	134	+11	+15	+ 3
1928															
Jan. 28.513	41.757	+17	+11	+11	+ 8	−32	210	178	180	219	174	206	−11	+ 4	− 7
Feb. 1.562	45.806	+ 1	− 4	− 9	−31	−25	197	166	178	−195	−186	−196	− 6	− 6	+ 6

* The values for $H\beta$, $H\gamma$, and $H\delta$ are weighted means of measures on the central absorption edges and their bisection. This procedure was used because the average of the settings on the edges agreed very well with the settings on the absorption center.

The variations of the relative intensities of the hydrogen emission components shown in Figure 2 for the single-prism spectrograms appear to be in substantial agreement with those of the two-prism plates.

The variations in intensity of the central absorption of $H\gamma$ and $H\delta$ relative to the continuous spectrum at these lines are shown by the curves at the top of Figure 2. The variation is similar for the two

lines. The absorption is a maximum relative to the continuous spectrum at a phase of approximately 18 days. This precedes the phase of maximum positive velocity, shown later in this paper, by about 10 days and confirms the results of Lockyer. The absorption is a minimum at a phase of approximately 90 days. The secondary variation is marked, with a minimum at phase 45 days and a maximum at phase 56 days.

Radial velocities and widths of hydrogen emission.—The radial velocities are given in Table I. The velocity-curves for the hydrogen

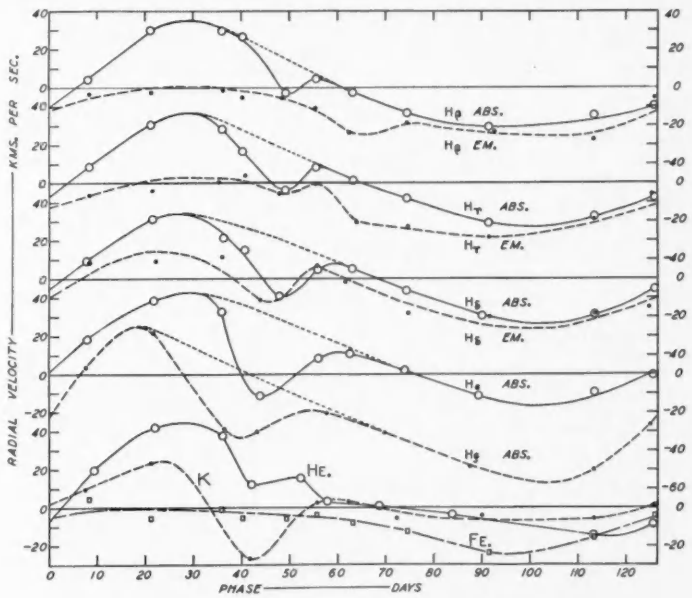

FIG. 3.—Radial velocity of spectral lines of φ Persei

absorption lines, based upon weighted mean places, are given in Figure 3. The curves have, in general, the same form but differ in some respects. A striking difference is the secondary variation, which occurs on the descending branch after maximum positive velocity. It becomes progressively more pronounced with decreasing wave-length. It appears earlier, increases in magnitude, and persists longer for lines of shorter wave-length, which is a strong confirmation of the results noted for the secondary variation of the relative intensities of the hydrogen emission components. These pro-

gressive variations are shown in Figure 4 by curves representing the isolated secondary velocity. They suggest that this variation is caused by a disturbance which affects the lower atmospheric levels of the star more than the higher levels, assuming that the lines of shorter wave-length originate at lower effective levels.

In isolating the secondary variation from the main velocity-curve, smooth curves were drawn in such a manner that the secondary variations were entirely below these curves. This procedure is suggested by the natural trend of the curves and is justified since the smooth

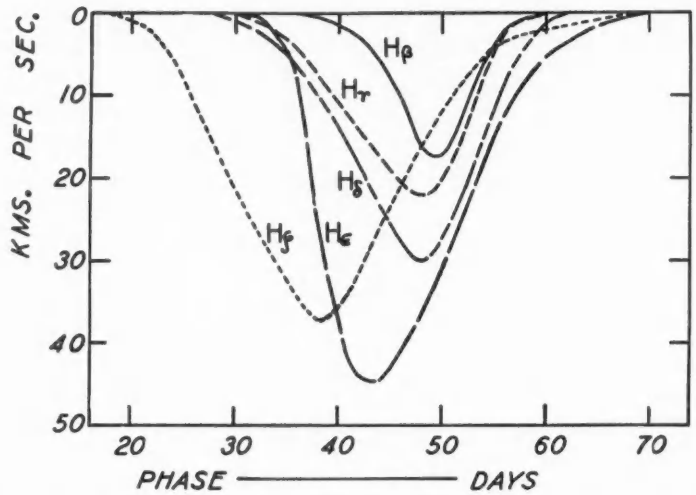

FIG. 4.—Isolated secondary velocity of the hydrogen absorption lines of φ Persei

curves thus formed are essentially the same for $H\beta$, $H\gamma$, $H\delta$, and also for $H\epsilon$, provided a constant correction of -8 kilometers is first applied to this curve. It should be added that the measures of $H\epsilon$ are rendered uncertain by the proximity of the H line of *Ca* II. The curve for $H\zeta$ is doubtless influenced by blending with the line λ 3888.65 of *He* I. Since both the hydrogen and the helium absorptions vary in intensity, the position of the resulting blend is rendered uncertain. The main variation is undoubtedly produced by the same cause. Similar velocity-curves should therefore be expected for the different hydrogen lines. Since such curves are obtained by isolating the secondary velocity variation in this manner, the method appears to be a rational one.

The secondary velocity variation, interpreted as radial motion in the line of sight, indicates a mass of hydrogen gas which begins to have an apparent motion of approach toward the observer immediately after maximum positive velocity (recession) of the main variation. This apparent motion of approach reaches a maximum value and then decreases again to zero at the phase where the main positive velocity has decreased approximately to zero. It should be noted

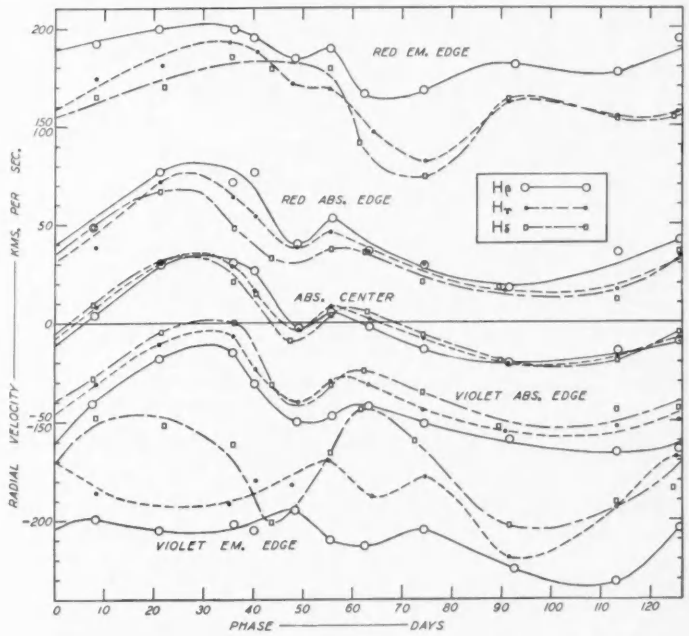

FIG. 5.—Radial velocity of hydrogen emission and absorption edges of φ Persei

that this interpretation of the secondary variation does not require a subsequent recession of this mass of gas relative to the observer.

The velocity-curves for K of calcium, for the mean of the helium lines, and for the mean of the ionized iron lines are given at the bottom of Figure 3. The K line exhibits the maximum positive velocity and the secondary variation. For the remainder of the period the velocity is practically constant. The line appears strong between phases 0 and 16 days. At the maximum and during the secondary variation it appears weak. This and the fact that it shows little variation in

velocity during the greater portion of the star's period, suggest that its origin is chiefly interstellar.

The mean velocity-curve for the helium lines is similar to the velocity-curves for the hydrogen absorption lines. The helium lines differ from the hydrogen lines with respect to intensity, being strong between phases 50 and 86 days and weak during the remainder of the period. A secondary velocity variation is indicated near phase 50 days.

TABLE II

MEAN WIDTHS OF HYDROGEN EMISSION LINES AND COMPONENTS OF φ PERSEI IN ANGSTROMS

PHASE (DAYS)	TOTAL EMISSION			RED COMPONENT			VIOLET COMPONENT		
	$H\beta$	$H\gamma$	$H\delta$	$H\beta$	$H\gamma$	$H\delta$	$H\beta$	$H\gamma$	$H\delta$
8.403	6.32	5.22	4.28	2.32	1.82	1.58	2.56	2.24	1.64
21.284	6.55	5.42	.....	1.96	1.60	.....	3.05	2.62	.....
22.132	.....	.....	4.42	.....	.....	1.47	.....	.....	2.03
35.986	6.54	5.58	4.76	2.08	1.84	1.87	3.05	2.71	2.20
40.192	6.47	5.48	.....	1.91	2.02	.....	2.82	2.35	.....
43.782	.....	.....	5.21	.....	.....	2.00	.....	.....	2.33
49.349	6.16	5.12	.....	2.29	1.99	.....	2.39	2.01	.....
55.610	6.46	4.94	4.72	2.19	1.81	1.94	2.61	2.04	1.83
61.582	.....	.....	3.90	.....	.....	1.42	.....	.....	1.68
63.238	6.10	4.83	.....	2.05	1.60	.....	2.76	2.25	.....
74.607	6.06	4.51	3.88	2.29	1.48	1.39	2.49	1.92	1.68
91.548	6.57	5.53	5.01	2.67	2.15	2.01	2.66	2.35	1.98
113.362	6.61	5.07	4.72	2.28	2.01	1.95	2.68	2.05	1.99
124.796	.....	.....	4.64	.....	.....	1.70	.....	.....	1.94
125.978	6.44	4.77	.....	2.45	1.82	.....	2.26	1.72	.....

The mean curve for the ionized iron lines shows only a negative velocity with respect to the center of mass velocity. The velocity is zero at phase 28 days when the velocity of the hydrogen lines is a maximum. The minimum is similar to that for the hydrogen lines, occurring at phase 96 days with a minimum velocity of -24 km/sec.

The displacements of the emission and absorption edges of the hydrogen lines expressed as radial velocity are shown by the curves in Figure 5. The velocity-curves for the central absorption of hydrogen are also plotted for comparison. The widths of the total emissions, of the emission components, and of the central absorptions

are related to the distances between the respective velocity-curves. The widths in angstroms for the emission lines and components are given in Table II, and the changes are shown by the curves in Figure 6.

The velocity-curves for the red emission edges of $H\beta$, $H\gamma$, and $H\delta$ are similar in form during the last half of the period but differ in the first half. The secondary variation is pronounced in $H\beta$, is only indicated in $H\gamma$, and is absent in $H\delta$, thus showing the same pro-

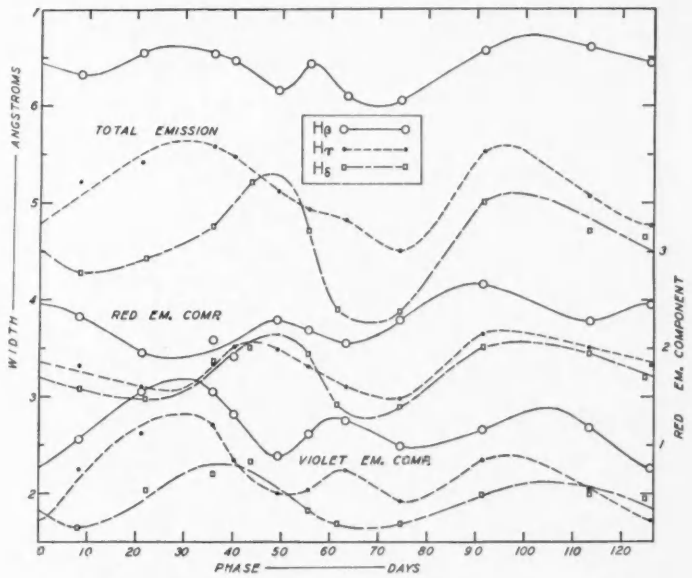

FIG. 6.—Widths of the hydrogen emission lines and components of φ Persei

gressive change found in the relative intensity of the emission components and in the total emission width. The maximum displacement to the red occurs at a later phase than for the absorption. This lag in phase increases for lines of shorter wave-length, a fact also to be noted in the widths of the total emission. The maximum displacement toward the violet, between 70 and 80 days, corresponds to the phase at which the total width of the emission lines is a minimum, and at which the intensity of the red emission component is a maximum relative to the intensity of the violet emission component. Between 90 and 100 days the red emission edges show a displace-

ment toward the red, while the hydrogen absorption lines show a displacement toward the violet. At this phase the widths of the red emission components are a maximum.

The velocity-curves for the violet emission edges of $H\beta$ and $H\gamma$ are similar in form, and during the last half of the period show variations similar to the hydrogen absorption, namely, a displacement toward the violet. During the first half of the period, however, when the hydrogen absorption lines show a displacement toward the red, the violet emission edges of $H\beta$ and $H\gamma$ show a displacement toward the violet. They show a similar secondary variation, but at a later phase than the hydrogen absorption.

The velocity-curve for the violet emission edge of $H\delta$ is different. It resembles the curves for hydrogen absorption at phases of maximum and minimum velocity. The secondary variation between phases 40 and 70 days is exceedingly great. The secondary minimum at 44 days corresponds to the phase of maximum emission width of $H\delta$, while the secondary maximum at 64 days corresponds to the phase of minimum emission width.

The widths of the hydrogen emission (Fig. 6) are greater for lines of longer wave-length. This fact was noted by Curtiss for Be stars[11] and was later verified by Dustheimer for φ Persei. The range of variation in width is greater for lines of shorter wave-length. The curves show two maxima and two minima in the period of 126.6 days, which was also found by Dustheimer from his measures of the one-prism spectrograms. The phase of the first maximum is greater, and of the second maximum is smaller, for lines of shorter wave-length. The phases of the two minima are the same for $H\beta$ and $H\delta$, while for $H\gamma$ the first minimum occurs at an earlier phase and the second minimum occurs at a later phase. The secondary variation is pronounced in $H\beta$, is doubtfully indicated in $H\gamma$, and appears to be absent in $H\delta$. This progressive change of the secondary variation with wave-length confirms the two-prism microphotometric results discussed earlier in this paper (see Fig. 2).

The curves for the widths of the violet emission component of $H\beta$, $H\gamma$, and $H\delta$ are similar in many respects to the curves for the total emission widths. The progressive changes in the phase at the first

[11] *Pub. Obs. U. of Michigan*, 3, 1, 1923.

maximum and in the secondary variation are practically identical with those noted for total widths.

The curves for the widths of the red emission component of $H\beta$, $H\gamma$, and $H\delta$ show in many respects variations just opposite to those observed for the widths of the violet emission components. This is particularly true for $H\beta$. It is apparent, therefore, why the microphotometric results for $H\beta$ show such great changes in the relative intensities of the two emission components. On the other hand, the curves for the widths of the violet and red emission components of $H\delta$ show practically the same variations. These similar variations in the width of the emission components of $H\delta$ explain why the microphotometric results for this line show comparatively small variations in the relative intensity.

At phase 90 days, when the violet emission edges show a violet displacement similar to that of the hydrogen absorption lines, the red emission edges show a red displacement; and at phase 30 days, when the red emission edges show a red displacement similar to that of the hydrogen absorption lines, the violet emission edges show a violet displacement. At these phases the widths of the total emission lines are maxima. It may be said, therefore, that an emission velocity-curve for this star, formed by taking the average of the settings on the outer emission edges, has little meaning. Such a curve can be interpreted readily only when the two edges show identical variations. The values obtained by taking the average of the settings on the outer emission edges are plotted in Figure 3 as broken curves. As expected, the range of the "apparent" emission velocity is small. The emission velocity is roughly zero at the phase where the absorption velocity is a maximum. The minimum occurs at the same phase as the minimum of the absorption and is approximately of the same magnitude. This behavior may be interpreted on the assumption that when the absorption velocity is a maximum, at phase 30 days, the central absorption is greatly displaced toward the red relative to the emission, thus exhibiting a maximum width for the violet emission component, a minimum width for the red emission component, and a maximum intensity of the violet emission component relative to the red emission component. When the absorption velocity is a minimum, at a phase of about 90 days, the emission

velocity is also a minimum and nearly of the same magnitude, thus indicating approximately equal widths for the two emission components, even though the width of the red emission component is then at its maximum. However, at this phase the intensity of the red emission component is greater than the intensity of the violet emission component, instead of being equal to it. Furthermore, the intensity of the red emission component is a maximum relative to the intensity of the violet emission component at an earlier phase, 75 days, corresponding to the phase when the width of the emission is a minimum and when the width of the violet emission component is greater than the width of the red component. It is apparent, therefore, that the intrinsic intensity distribution of the emission lines must vary greatly during the star's period, in addition to variations caused by the relative displacement of the absorption with respect to the emission.

It should be added that the foregoing spectral variations of φ Persei occur without conspicuous variations in the visual brightness of the star.

DISCUSSION

Any system which is proposed for φ Persei must account for the foregoing spectral variations. Simple orbital motion, as suggested by previous investigators, is not capable of explaining the observed spectral variations. If it is assumed, however, that the two stars of a binary system contribute to the emission of hydrogen, then changes in the width and in the intensity of the hydrogen lines would be produced by the relative motions of the superimposed lines from the two stars. These changes may be enhanced somewhat by the photographic effects or shifts discussed by Frédette. Even such a modified binary system cannot account adequately for all of the observed spectral variations of φ Persei.

Curtiss[12] suggested radial pulsation for the spectrum variables of the φ Persei group. Dustheimer[13] adopted the pulsation hypothesis for φ Persei and suggested a secondary pulsation of shorter period and smaller range to explain the secondary velocity variation. This hypothesis must assume that the inconspicuous light variation ob-

[12] *Pub. A.A.S.*, 34th Session, 1925; *Pub. Obs. U. of Michigan*, **4**, 174, 1932.

[13] *Pop. Astr.*, **35**, 484, 1927; dissertation University of Michigan, unpublished.

served by Guthnick and Güssow is explained by periodic changes in the effective temperature of the photosphere. It does not account satisfactorily for the cyclic variations in the widths of the emission lines and components in one-half of the star's velocity period, since the range of velocity variation of the emission edges of hydrogen is of the same magnitude as the range of the central absorption (see Table III). The assumptions of a transparent atmosphere and no appreciable occultation by the photosphere are therefore not sufficient. The chief objection to the pulsation hypothesis is that it requires a change in the radius of the star which is greater than the radii of normal B-type stars.

TABLE III

RANGE OF VELOCITY VARIATION OF THE HYDROGEN LINES OF φ PERSEI

	$H\beta$	$H\gamma$	$H\delta$
	km/sec	km/sec	km/sec
Red emission edge....	34	61	61
Central absorption....	51	52	50
Violet emission edge..	36	51	57

The writer suggested, at the time this work was completed in 1928,[14] a star of very low density, pear-shaped or apioidal in form, with a very extensive atmosphere and a small and ill-defined photosphere, and which is rotating about a line greatly displaced from the effective center of the apparent photospheric area with a period of 126.6 days. It was assumed, further, that the star's atmosphere is pulsating in the same period, that it is contracting while the apparent photosphere is receding, and that it is expanding while the apparent photosphere is approaching; while a secondary pulsation was assumed for the secondary variation. Finally, it was assumed that the hydrogen absorption originates in the atmosphere between the photosphere and the observer, while the hydrogen emission originates in the atmosphere projecting beyond the photosphere at right angles to the line of sight, as suggested by Rosseland.[15] The amplitude of pulsation required in this hypothesis would be much smaller than is required by pulsation alone. The arguments ad-

[14] *Iowa Acad. of Sci. Proc.*, **36**, 281–93, 1929. [15] *Ap. J.*, **63**, 218, 1926.

vanced in favor of the pulsation hypothesis apply equally well; and the effects of rotation, pulsation, and the shape of the star are such as to explain the observed variations of φ Persei more satisfactorily.

The most promising hypothesis for explaining the spectral variations of φ Persei consists in assuming a system of orbital motion in which each star is rotating rapidly about its axis, combined with an apparent atmospheric pulsation of expansion in the companion star at the phase of the secondary variation. Certainly the truly periodic variations of φ Persei with respect to width and intensity of the hydrogen emission and with respect to radial velocity of the hydrogen absorption can be explained satisfactorily by this system. It is only necessary to assume that both of the rotating stars of the binary system have very extensive atmospheres which contribute to the hydrogen emission, the emission originating in the atmospheres of the stars at right angle to the line of sight, and that the hydrogen absorption originates mainly in the outer atmosphere between the observer and the fairly well-defined bright photosphere of the primary star. The great widths of the hydrogen emission lines and the variation in one-half of the star's velocity period are explained readily by the resultant motion produced by rotation and orbital motion in the line of sight. For example, at maximum positive velocity (phase 30 days) the primary star is receding in orbital motion. The red emission component of hydrogen is greatly displaced to the red, owing to rotation, since it originates in the receding atmosphere of the primary star, which itself is receding because of orbital motion. The violet emission component of hydrogen is displaced toward the violet, owing to rotation, since it originates in the approaching atmosphere of the companion star, which itself is approaching because of orbital motion. Since the central absorption of hydrogen is produced mainly in the atmosphere of the receding primary star, it appears to be displaced toward the red with respect to the violet emission component. The violet emission component should therefore show maximum width and greatest intensity relative to the red emission component at this phase. Furthermore, the width of the total emission should be a maximum because of opposite displacements of the two emission edges. It should be noted that these observations are in com-

plete agreement with the results presented in this paper. Obviously, the reverse occurs at the phase of maximum negative velocity; and it is to be noted that at this phase the red emission component shows maximum width and approximately maximum intensity relative to the violet emission component. The width of the total emission shows a maximum for the same reason as at maximum positive velocity. At the intermediate phases of zero velocity for the absorption of hydrogen the widths of the emission components should be minima and the relative intensities of the two emission components should be equal. Also, the widths of the total emission should be minima. Thus, the main and truly periodic variations of φ Persei can be explained satisfactorily by this binary system.

McLaughlin[16] recently suggested a rotating and pulsating mechanism for Be stars. Dodson[17] has successfully applied this hypothesis to explain the irregular cyclic spectral variations of 25 Orionis. There seems to be no reason why a pulsation of this nature could not be operative in a rotating star of a binary system, such as β Lyrae, for example. The spectral variations produced by this type of pulsation could be quite independent from the truly periodic spectral variations caused by orbital motion and axial rotation, and could be merely superimposed upon them. The pronounced secondary variations of φ Persei, which vary progressively with wave-length and probably vary also with time, would appear to be explained by atmospheric pulsation of this type.

It should be noted, however, that immediately after maximum positive velocity resulting from the orbital system suggested above, the primary star, with the well-defined and bright photosphere, may be partially eclipsed by the extensive, rarefied, and transparent atmosphere of the companion star. It is noteworthy that this is the phase at which the pronounced secondary variations occur in φ Persei. This condition of partial eclipse could produce spectral variations which may be termed "secondary variations" and which would probably vary progressively with wave-length. At this phase an apparent atmospheric pulsation of expansion or approach along the

[16] *Proc. Nat. Acad.*, **19**, 44, 1933.

[17] Dissertation, University of Michigan, 1934, *Ap. J.*, **84**, 180, 1936; abstract in *Pub. A.A.S.*, **8**, 109, 1935.

line of sight may be produced in the intervening extensive, rarefied, and transparent atmosphere of the companion star, owing to excitation by radiation from the hot photosphere of the partially eclipsed primary star. Obviously, secondary variations would result also in the relative intensity of hydrogen absorption and emission. This type of excitation would necessarily be continuous, but its effect would be observed only during the partial eclipse. It is probable, however, that, owing to rotation, the excitation would be very much more effective in the receding atmosphere of the companion star at the beginning of the partial eclipse than in the approaching atmosphere of this star toward the end of the eclipse, which is in agreement with the fact that the observed secondary velocity variation of hydrogen absorption appears and practically subsides before the absorption velocity has decreased to zero. This interpretation of the secondary variations of φ Persei appears to be the most promising of any so far suggested.

It is with great pleasure that the writer expresses his thanks to the late Professor Ralph H. Curtiss for making the investigation possible and for his kindly criticism, suggestions, and direction; and to those who have helped in procuring the spectrograms.

National Bureau of Standards
Washington, D.C.

THE SPECTRUM OF H_2 FROM λ 3612 TO λ 4224

NORTON A. KENT

ABSTRACT

The wave-lengths of 512 lines of H_2 have been measured on plates taken with a 21-foot concave grating at the California Institute of Technology. The results have been compared with the measurements by Gale, Monk, and Lee, and by Finkelnburg.

In 1927 Dr. Millikan suggested to the writer that, although several determinations of the wave-lengths of the lines of the secondary spectrum of hydrogen had already been made, further work in this direction would be of value. While plates taken with this end in view were being measured, the extensive papers of Gale, Monk, and Lee,[1] and Finkelnburg[2] appeared. However, since there were present in numerous instances marked wave-length differences between their determinations, it seemed advisable to push to its completion this present set of values.

THE APPARATUS EMPLOYED

The grating used was the 21-foot concave (vertical Rowland mount) of the California Institute of Technology. The tube was of

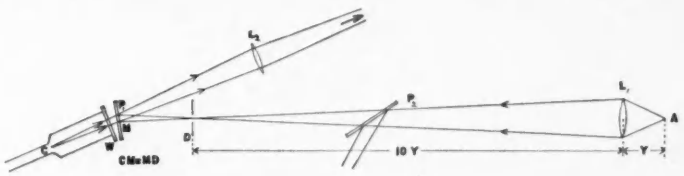

FIG. 1

pyrex glass, the capillary, C (see Fig. 1), being 1 cm in internal diameter and 40 cm long, air-cooled by a fan. A removable quartz window, W, permitted the introduction of molybdenum or tungsten (in the form of numerous small cylinders) to the capillary, resulting in enhancement of the secondary spectrum and partial submergence of

[1] *Ap. J.*, **67**, 89, 1928.

[2] *Zs. f. Phys.*, **52**, 27, 1929. Attention may be called to the excellent bibliography in this article.

the primary. Quartz lenses were used throughout. A constant-flow method was employed, the hydrogen being generated by a Hoffman apparatus and dried by phosphorus pentoxide. The current, given by a 10-kw transformer (ratio of transformation 1:74), was always under 0.6 amp (current density under 0.7 amp per square centimeter), and the pressure was about 0.1 mm.

When the iron spectrum from the Pfund arc, *A* (length 15 mm and current 4–5 amp), alone was desired, a platinum mirror, *M*, was placed as shown. The magnification given by the lens, L_1, being 10, the image of the arc upon the diaphragm, *D*, was 15 cm. Of this the central part was allowed to pass through a rectangular opening 1 cm high. When the tube spectrum alone was desired, *M* was removed. Both spectra could be photographed simultaneously by replacing *M* by a plane quartz plate, P_1, and putting another quartz plate, P_2, between the arc and the lens, L_1. By rotating P_2 about a vertical axis, the amount of transmitted light could be adjusted. The loss of light at P_2 by reflection, together with that at P_1 by transmission, so reduced the intensity of the arc that correct relative intensities of the hydrogen and iron spectra could be obtained, and the arc exposure could be completely simultaneous with that of the tube.

Upon each photographic plate three strips were exposed, obtained by shifting the position of the plate. These contained (*A*) the arc alone, merely for identification, (*B*) the arc and tube taken simultaneously, and (*C*) the tube alone. On (*A*) the exposure time was but a few minutes, on (*B*) some hours, and on (*C*) many hours—up to eleven in some cases. First- and second-order spectra were used. The definition on all the plates measured is excellent. The wave-lengths of the iron lines employed in calculating the hydrogen wave-lengths of strip (*B*) were the recommended wave-lengths of the *Transactions of the International Astronomical Union* (Volume 3, 1928). The wave-lengths of the hydrogen lines on strip (*C*) were calculated by means of interferometer wave-lengths[3] of certain standard hydrogen lines obtained by Reginald G. Lacount and Robert E. Hodgdon in the Rumford Room of the Massachusetts Institute of Technology. These thirty-four wave-lengths are marked *L* in Table II. Their accuracy is attested by the fact that the

[3] Unpublished.

maximum probable error of the mean of the determinations as obtained from three plates is 0.0006 A and the average probable error 0.0003 A.

The plates were measured by a Société Génevoise comparator, mounted in a thermostatically controlled case. The average variation of temperature during the time between settings on standards (generally 1–3 cm apart) was under 0.3° C.

In measuring a plate the following procedure was employed: All the settings (from two to five, or even ten on some standards) of the single-thread cross-hair were made from one side of the spectrum

TABLE I

WEIGHTS GIVEN TO VARIOUS DETERMINATIONS

	Second-Order Plates	First-Order Plates
Intensities 0^3–6 inclusive	4	2
Intensities 0^4 and from 7 to 25 inclusive	2	1

line. Two distinct runs were made with the plate set red left (RL_1 and RL_2), then two with the plate set red right (RR_1 and RR_2). The mean of RL_1 and RR_1 was calculated, then the mean of RL_2 and RR_2. The mean of these two means constituted one determination of the wave-length of a line on that strip of the plate. The means of the determinations made on either part (*B*) of the various plates referred to the iron standards, or part (*C*) of the various plates referred to the Lacount and Hodgdon hydrogen interferometer standards, were then used to obtain the weighted mean value of the wave-length, given in column M_w of Table II.

As the intensities of a given line on different plates were different, the values of the various determinations were weighted as shown in Table I. Double weight was given to second-order plates. 0^4 is the intensity assigned to a line just visible. Few lines on the writer's scale were stronger than intensity 10. The illumination used in measuring was adjusted to fit the intensity of the line being measured.

The intensities *I* recorded in Table II are those given by Gale. With these the writer's are in general agreement; in a few cases, the

TABLE II

λ	F	G	I	L	M_w	N	PE	ν
3612.....	874	897	1	.....	913	1	.....	2767063
20.....	038	052	1	.....	048	1	.....	2761610
22.....	.....	161	1	.....	163	1	.....	2759997
22.....	958	.....	0	.....	034*	1	.....	2559333
27.....	281	.....	1	.....	249	1	.....	2756127
32.....	660	681	1	.....	689	1	.....	2752000
33.....	316	328	1	.....	322	2	001	2751521
35.....	096	094	1	.....	112	1	.....	2750166
36.....	961	017	1	.....	040†	1	.....	2748708
46.....	830	830	0	.....	849	2	001	2741315
48.....	339	.....	0	.....	389	1	.....	2740158
50.....	084	.....	1	.....	149	3	003	2738837
52.....	456	460	2	.....	472	3	001	2737095
54.....	912	.....	0	.....	845	2	001	2735318
55.....	649	673	0	.....	680	2	001	2734693
57.....	940	.....	1	.....	966	1	.....	2732984
58.....	651	664	0	.....	674	2	002	2732655
62.....	.....	480	0	.....	495	1	.....	2729605
62.....	731	698	0	.....	722	1	.....	2729435
63.....	046	055	1	.....	070	3	001	2729176
64.....	115	132	3	.....	142	6	001	2728379
64.....	890	911	0	.....	905	3	002	2727810
65.....	238	242	1	.....	256	3	001	2727548
65.....	887	907	3	.....	907	4	001	2727064
67.....	.....	524	∞	.....	533	1	.....	2725855
68.....	862	840	0	.....	868	1	.....	2724863
69.....	018	000	0	.....	026	1	.....	2724746
72.....	.....	342	0	.....	362	1	.....	2722271
73.....	637	621	3	.....	650	5	001	2721316
73.....	.....	773	1	.....	815	2	001	2721194
74.....	378	398	7	.....	400	6	000	2720761
76.....	777	800	0	.....	801	2	000	2718984
77.....	977	985	∞	.....	005‡	1	.....	27 '94
80.....	537	526	1	.....	547	1	.....	271 '7
81.....	355	343	1	.....	356	1	.....	2715020
81.....	951	963	2	.....	975	6	001	2715164
82.....	274	291	1	.....	298	2	001	2714925
84.....	305	313	5	.....	317	4	002	2713438
84.....	481	463	1	.....	457	3	000	2713335
87.....	290	304	0	.....	303	1	.....	2711240
88.....	551	590	0	.....	597	1	.....	2710289
90.....	142	143	1	.....	151	3	001	2709148
94.....	316	295	∞	.....	348	1	.....	2706070
95.....	.....	146	1	.....	164	1	.....	2705473
97.....	824	855	1	.....	861	1	.....	2703500
99.....	779	783	1	.....	792	3	002	2702088
3700.....	067	048	1	.....	059	4	001	2701894
01.....	861	883	1	.....	884	2	004	2690562
02.....	118	112	3	.....	118	5	002	2690391
04.....	564	567	0	.....	586	1	.....	2698592
14.....	370	.....	∞	.....	470	1	.....	2691411
14.....	644	686	0	.....	704	1	.....	2691242

* 3623.034. † 3637.040. ‡ 3678.005.

TABLE II—*Continued*

λ	*F*	*G*	*I*	*L*	M_w	*N*	*PE*	ν
3715	975	990	1	.....	001§	1	.....	2690303
17	243	317	0	.....	315	2	003	2689351
19	176	178	0	.....	195	1	.....	2687992
21	252	.....	00	.....	221	1	.....	2686529
22	106	093	2	.....	109	3	001	2685888
24	795	843	0	.....	850	2	002	2683911
32	108	108	2	.....	116	4	001	2678686
34	541	.....	$H\lambda$	.....	373	3	004	2677067
39	.....	623	00	.....	649	1	.....	2673290
40	262	268	0	.....	278	1	.....	2672841
41	207	209	1	.....	206	3	003	2672178
48	028	.....	00	.....	036	1	.....	2667309
50	134	.....	$H\kappa$	.....	148	3	002	2665807
51	871	879	2	.....	884	3	004	2664573
52	593	629	0	.....	628	1	.....	2664045
55	084	.....	00	.....	119	1	.....	2662278
55	869	.....	00	.....	886	1	.....	2661734
56	632	590	1	.....	605	1	.....	2661226
57	581	590	0	.....	601	1	.....	2660519
59	666	598	0	.....	583	1	.....	2659117
60	764	.....	0	.....	752	1	.....	2658290
62	992	982	1	.....	003‖	1	.....	2656700
64	.....	434	00	.....	467	1	.....	2655667
68	.....	280	00	.....	289	1	.....	2652973
68	423	.....	00	.....	462	1	.....	2652851
68	734	726	0	.....	744	1	.....	2652653
70	229	230	1	.....	252	1	.....	2651592
70	621	.....	Hi	.....	632	3	002	2651325
71	486	500	3	505	(506	2	001)	2650711
74	317	301	1	.....	316	4	001	2648738
75	554	576	1	.....	587	4	001	2647845
76	671	.....	00	.....	673	1	.....	2647084
76	972	980	1	.....	985	2	008	2646865
77		104	1	.....	137	1	.....	2646759
77	,	500	00	.....	511	1	.....	2646497
80	329	.....	00	.....	330	1	.....	2644523
82	007	.....	0	.....	026	1	.....	2643337
82	490	522	0	.....	527	2	005	2642987
82	794	756	0	.....	782	2	002	2642809
83	040	966	00	.....	990¶	1	.....	2642664
84	168	156	1	.....	176	3	001	2641836
87	282	.....	0	.....	295	1	.....	2639660
87	.....	419	1	.....	425	1	.....	2639569
90	955	962	0	.....	968	3	002	2637103
91	397	403	2	.....	409	6	001	2636796
94	457	464	1	.....	467	3	002	2634671
96	.....	062	1	.....	075	2	004	2633555
96	585	595	6	596	(597	6	001)	2633193
96	876	.....	00	.....	913	1	.....	2632974
97	148	128	2	.....	135	3	003	2632820
97	509	518	5	.....	526	4	001	2632549
97	905	908	$H\theta$	.....	904	6	002	2632277

§ 3716.001. ‖ 3763.003. ¶ 3782.990.

TABLE II—*Continued*

λ	*F*	*G*	*I*	*L*	M_w	*N*	*PE*	ν
3798.....	853	816	1	.....	837	3	004	2631640
99.....	029	032	3	.....	038	5	001	2631501
3800.....	004	045	1	.....	045	3	004	2630804
00.....	857	.....	∞	.....	872	1	.....	2630162
01.....	605	616	0	.....	623	1	.....	2629712
02.....	091	076	1	.....	086	1	.....	2629392
03.....	023	031	5	033	(031	4	001)	2628737
03.....	323	269	0	.....	284	1	.....	2628563
06.....	.....	733	1	.....	740	1	.....	2626177
07.....	.....	971	1	.....	976	1	.....	2625325
09.....	021	021	1	.....	034	3	004	2624595
11.....	254	.....	∞	.....	187	1	.....	2623113
12.....	172	174	1	.....	181	3	002	2622429
12.....	737	744	2	.....	752	4	001	2622036
13.....	424	497	1	.....	514	1	.....	2621512
14.....	.....	568	∞	.....	593	1	.....	2620770
15.....	316	333	1	.....	334	2	001	2620261
16.....	.....	343	1	.....	362	1	.....	2619556
16.....	.....	482	∞	.....	490	1	.....	2619473
16.....	794	789	1	.....	800	2	001	2619255
18.....	176	184	1	.....	199	3	002	2618296
18.....	.....	895	1	.....	875	1	.....	2617818
19.....	319	257	1	.....	284	3	003	2617551
19.....	.....	464	1	.....	477	3	005	2617419
21.....	713	.....	∞	.....	719	1	.....	2615884
21.....	.....	872	1	.....	879	1	.....	2615765
23.....	035	086	1	.....	093	1	.....	2614943
24.....	921	940	2	.....	942	4	000	2613680
25.....	.....	622	0	.....	633	1	.....	2613208
28.....	872	.....	∞	.....	890	1	.....	2610085
29.....	167	.....	0	.....	168	1	.....	2610796
31.....	093	101	1	.....	116	3	001	2609468
32.....	423	415	0	.....	431	1	.....	2608572
33.....	607	489	0	.....	496	1	.....	2607848
35.....	345	381	*Hη*	.....	385	4	002	2606563
36.....	457	443	2	.....	461	6	005	2605832
37.....	629	609	0	.....	632	2	000	2605037
39.....	.....	296	0	.....	287	1	.....	2603914
40.....	.....	167	∞	.....	115	2	003	2603353
			0	.....	201	1	.....	2603295
40.....	.....	548	1	.....	553	2	001	2603056
42.....	435	453	∞	.....	454	1	.....	2601768
43.....	042	.....	0	.....	987**	1	.....	2601407
44.....	051	.....	∞	.....	023	1	.....	2600706
44.....	284	.....	0	.....	231	1	.....	2600565
44.....	997	.....	0	.....	022††	1	.....	2600031
45.....	.....	395	0	.....	414	1	.....	2599766
45.....	832	834	0	.....	837	2	001	2599479
46.....	219	226	1	.....	231	3	001	2599213
46.....	710	.....	0	.....	650	1	.....	2598930
47.....	905	.....	1	.....	888	1	.....	2598094
48.....	791	784	1	.....	810	3	005	2597472

** 3842.987. †† 3845.022.

TABLE II—*Continued*

λ	*F*	*G*	*I*	*L*	M_w	*N*	*PE*	ν
3849.....	066	.....	oo	.....	020	1	.....	2597330
49.....	320	304	2	.....	325	5	001	2597124
49.....	714	700	o	.....	717	2	005	2596860
49.....	.....	988	o	.....	004‡‡	3	001	2596666
50.....	648	.....	oo	.....	641	1	.....	2596237
51.....	269	266	3	.....	270	4	003	2595813
51.....	567	.....	oo	.....	518	1	.....	2595646
52.....	446	.....	o	.....	396	1	.....	2595054
53.....	265	.....	o	.....	217	1	.....	2594501
53.....	547	.....	1	.....	486	1	.....	2594320
54.....	138	.....	o	.....	048	1	.....	2593942
54.....	525	489	1	.....	512	2	007	2593629
55.....	432	480	o	.....	404	1	.....	2593029
55.....	692	.....	1	.....	617	1	.....	2592886
56.....	.....	332	o	.....	365	1	.....	2592383
56.....	718	549	oo	.....	642	1	.....	2592197
57.....	763	782	2	.....	796	3	003	2591422
58.....	668	662	2	.....	675	5	002	2590831
58.....	975	008	1	.....	009§§	2	002	2590607
59.....	877	.....	3	.....	888	3	002	2590017
60.....	.....	060	1	.....	068	2	001	2589896
60.....	313	365	oo	.....	404	1	.....	2589671
60.....	.....	552	oo	.....	611	1	.....	2589532
60.....	697	711	4	.....	721	4	001	2589458
61.....	494	496	4	508	(506	5	001)	2588931
62.....	549	.....	1	.....	483	2	000	2588277
63.....	198	202	4	210	(210	5	001)	2587790
63.....	445	.....	1	.....	375	2	002	2587679
64.....	096	074	1	.....	091	4	002	2587204
64.....	313	272	1	.....	289	4	001	2587067
65.....	204	.....	1	.....	144	1	.....	2586495
65.....	.....	477	2	.....	490	2	000	2586264
66.....	018	990	oo	.....	984|| ||	1	.....	2585933
67.....	063	076	2	.....	081	4	001	2585199
67.....	672	.....	o	.....	620	2	002	2584839
			o	.....	750	2	002	2584736
68.....	022	991	o	.....	005	1	.....	2584582
68.....	472	.....	1	.....	406	2	001	2584314
68.....	836	.....	oo	.....	808	1	.....	2584046
3869.....	156	155	2	.....	163	5	001	2583808
69.....	477	.....	1	.....	405	1	.....	2583647
69.....	938	931	3	940	(940	3	002)	2583290
70.....	180	158	o	.....	147	1	.....	2583152
70.....	638	630	2	.....	647	5	002	2582818
70.....	923	910	2	.....	917	5	001	2582638
71.....	284	.....	1	.....	369	1	.....	2582269
71.....	585	594	5	598	(600	4	001)	2582183
72.....	357	354	4	.....	363	4	001	2581673
72.....	991	.....	o	.....	084¶¶	1	.....	2581193
73.....	472	.....	o	.....	371	1	.....	2581001
74.....	100	120	2	.....	118	3	005	2580504
79.....	.....	526	4	533	(529	3	002)	2576902

‡‡ 3850.004. §§ 3859.009. \|\|\| 3865.984. ¶¶ 3873.084.

TABLE II—*Continued*

λ	*F*	*G*	*I*	*L*	M_w	*N*	*PE*	ν
3882.....	044	045	1	.....	057	1	.....	2575227
84.....	148	144	3	.....	151	4	001	2573839
86.....	217	218	1	.....	224	3	001	2572466
87.....	416	388	1	.....	405	1	.....	2571684
87.....	838	836	2	.....	847	4	002	2571392
88.....	990	988	*Hζ*	.....	004***	6	003	2570627
89.....	292	299	1	.....	309	4	001	2570425
90.....	699	700	1	.....	709	1	.....	2569500
98.....	118	120	1	.....	135	1	.....	2564605
3902.....	614	620	3	.....	640	3	004	2561645
07.....	489	476	2	.....	491	2	005	2558464
10.....	023	040	1	.....	045	1	.....	2556794
16.....	936	958	1	.....	980	1	.....	2552267
17.....	943	953	1	.....	969	1	.....	2551623
24.....	383	409	6	414	(414	2	003)	2547432
28.....	359	388	1	.....	399	1	.....	2544848
30.....	661	676	0	.....	704	1	.....	2543356
33.....	586	598	2	.....	613	1	.....	2541475
44.....	277	272	4	.....	280	6	001	2534602
44.....	830	818	1	.....	847	2	008	2534238
46.....	048	108	0	.....	110	2	003	2533427
47.....	101	091	1	.....	097	1	.....	2532793
47.....	362	.....	0	.....	297	2	003	2532665
			1	.....	502	1	.....	2532533
47.....	627	.....	2	.....	590	1	.....	2532477
49.....	406	400	0	.....	407	1	.....	2531312
50.....	583	573	2	.....	580	4	001	2530560
51.....	493	484	1	.....	497	3	002	2529973
52.....	765	819	0	.....	826	1	.....	2529122
55.....	195	177	1	.....	191	4	003	2527610
57.....	041	020	0	.....	027	2	001	2526437
59.....	568	603	0	.....	624	2	006	2524781
59.....	961	955	1	.....	963	4	002	2524564
60.....	203	188	1	.....	191	3	002	2524419
61.....	175	.....	00	.....	141	1	.....	2523814
62.....	340	328	3	336	(339	5	001)	2523052
63.....	152	144	4	.....	150	4	001	2522534
63.....	552	525	1	.....	542	2	005	2522285
63.....	732	730	1	.....	739	2	003	2522159
65.....	082	090	1	.....	110	2	002	2521287
66.....	.....	800	1	.....	818	2	001	2520202
68.....	947	912	1	.....	920	2	002	2518867
70.....	073	.....	*Hε*	.....	070	7	001	2518138
71.....	454	448	1	.....	462	3	001	2517255
74.....	214	210	1	.....	223	4	002	2515506
74.....	760	772	1	.....	782	4	002	2515152
75.....	689	666	2	.....	681	6	001	2514584
76.....	827	835	2	.....	834	2	003	2513855
77.....	113	091	1	.....	098	3	001	2513688
78.....	141	147	1	.....	156	4	003	2513019
78.....	444	.....	0	.....	461	3	001	2512827
78.....	708	666	2	.....	660	3	000	2512701

*** 3889.004.

TABLE II—*Continued*

λ	*F*	*G*	*I*	*L*	M_w	*N*	*PE*	ν
3979.....	353	322	1	.....	337	3	001	2512275
79.....	760	740	1	.....	757	3	001	2512008
80.....	994	.....	0	.....	997	1	.....	2511226
81.....	231	.....	0	.....	175	1	.....	2511114
81.....	556	.....	0	.....	543	1	.....	2510881
82.....	096	.....	0	.....	080	1	.....	2510543
82.....	562	557	1	567	(567	5	001)	2510236
82.....	780	.....	0	.....	740	2	005	2510127
83.....	662	.....	0	.....	669	2	001	2509541
83.....	814	.....	0	.....	824	1	.....	2509444
83.....	936	971	1	.....	979	4	000	2509346
84.....	868	.....	0	.....	710	1	.....	2508886
85.....	476	.....	0	.....	431	2	000	2508432
85.....	692	702	3	.....	731	1	.....	2508243
86.....	921	921	0	931	(928	6	001)	2507488
90.....	036	031	0	039	(041	7	001)	2505535
90.....	712	.....	0	.....	765	1	.....	2505080
90.....	956	.....	0	.....	967	1	.....	2504952
91.....	179	145	1	.....	155	4	002	2504834
91.....	832	833	5	.....	845	8	001	2504402
92.....	012	.....	3	.....	016	6	001	2504294
92.....	340	.....	3	.....	337	5	001	2504093
93.....	261	255	5	.....	257	5	001	2503516
93.....	850	848	3	.....	857	4	001	2503140
94.....	063	.....	00	.....	001	1	.....	2503050
94.....	430	.....	3	.....	426	2	001	2502783
94.....	941	.....	0	.....	857	2	004	2502513
96.....	641	657	2	.....	672	2	003	2501377
96.....	939	.....	0	.....	016†††	1	.....	2501162
97.....	145	143	2	.....	155	6	002	2501075
97.....	336	.....	0	.....	387	1	.....	2500930
98.....	243	254	1	.....	267	3	002	2500379
99.....	254	260	1	.....	274	3	001	2499750
4000.....	212	210	2	.....	217	4	001	2499160
00.....	838	840	3	.....	845	6	001	2498768
01.....	762	.....	0	.....	665	1	.....	2498256
02.....	124	074	0	.....	064	2	002	2498007
02.....	502	496	4	.....	506	7	001	2497731
02.....	985	983	3	.....	992	4	001	2497428
03.....	774	781	0	.....	766	2	002	2496945
04.....	616	630	0	.....	646	2	002	2496396
05.....	.....	398	1	.....	417	2	001	2495916
05.....	499	492	5	.....	504	4	001	2495862
05.....	949	943	4	.....	956	5	001	2495580
06.....	120	110	1	.....	118	3	002	2495479
08.....	741	715	2	.....	729	3	000	2493854
09.....	291	258	0	.....	261	2	003	2493517
09.....	567	561	2	.....	575	3	001	2493328
09.....	943	012	0	.....	037‡‡‡	2	000	2493040
10.....	741	738	0	.....	748	3	001	2492598
11.....	225	238	0	.....	232	2	004	2492298
11.....	798	778	0	.....	780	2	002	2491957

††† 3997.016. ‡‡‡ 4010.037.

TABLE II—*Continued*

λ	*F*	*G*	*I*	*L*	M_w	*N*	*PE*	ν
4012.....	753	770	0	.....	763	1	.....	2491347
13.....	154	146	1	.....	155	3	002	2491103
14.....	188	175	0	.....	186	2	007	2490464
15.....	.....	833	1	.....	841	3	001	2489437
16.....	360	310	1	.....	325	2	003	2489137
16.....	553	547	2	.....	561	3	002	2488991
17.....	777	757	00	.....	782	3	002	2488235
18.....	890	899	3	.....	912	3	002	2487535
20.....	932	926	1	.....	939	3	002	2486279
21.....	341	339	2	.....	359	5	002	2486021
21.....	651	568	0	.....	588	2	006	2485880
21.....	.....	792	2	.....	796	2	001	2485751
23.....	328	340	0	.....	338	2	004	2484799
24.....	761	734	4	.....	748	4	001	2483928
26.....	227	218	2	.....	237	3	002	2483010
26.....	608	605	3	.....	610	4	001	2482780
27.....	377	377	3	.....	388	7	001	2482300
28.....	328	333	8	341	(342	6	002)	2481713
28.....	964	975	0	.....	007§§§	1	.....	2481303
30.....	078	030	00	.....	195‖ ‖ ‖	1	.....	2480571
31.....	371	370	2	.....	380	6	001	2479842
31.....	756	757	3	.....	762	2	002	2479607
32.....	715	671	0	.....	672	1	.....	2479048
33.....	782	777	0	.....	772	2	000	2478372
34.....	085	074	0	.....	081	3	002	2478182
35.....	553	567	4	.....	567	3	001	2477269
35.....	837	.....	2	.....	719	1	.....	2477176
36.....	307	334	1	.....	345	2	003	2476792
36.....	.....	708	0	.....	654	2	001	2476602
38.....	321	.....	00	.....	312	1	.....	2475585
38.....	537	527	2	.....	524	2	001	2475455
39.....	130	156	1	.....	142	2	000	2475077
39.....	639	.....	0	.....	629	1	.....	2474778
40.....	354	.....	0	.....	400	1	.....	2474306
42.....	676	.....	0	.....	664	2	001	2472920
43.....	107	110	0	.....	105	2	000	2472651
43.....	231	.....	0	.....	204	2	002	2472590
43.....	563	567	5	568	(567	4	001)	2472367
44.....	450	465	1	.....	470¶¶¶	2	002	2471816
45.....	.....	487	0	.....	480	1	.....	2471199
46.....	161	.....	00	.....	208	1	.....	2470754
46.....	553	.....	0	.....	555	3	002	2470542
47.....	522	581	2	.....	567	1	.....	2469925
47.....	952	950	1	.....	968	3	002	2469680
48.....	.....	296	1	.....	320	3	001	2469465
48.....	449	451	4	.....	454	4	001	2469384
49.....	342	.....	0	.....	351	2	002	2468836
51.....	225	221	2	.....	222	4	003	2467697
53.....	537	511	1	.....	526	3	000	2466294
54.....	015	990	2	.....	002	3	001	2466004
54.....	372	383	0	.....	379	2	002	2465775

§§§ 4029.007. ‖ ‖ ‖ This may be a different line from that measured by G. and F.
¶¶¶ Two unresolved lines.

TABLE II—*Continued*

λ	*F*	*G*	*I*	*L*	M_w	*N*	*PE*	ν
4055.....	281	278	2	.....	284	5	002	2465225
56.....	410	409	2	.....	413	4	003	2464539
57.....	162	152	0	.....	158	2	004	2464086
57.....	545	551	1	.....	556	3	001	2463844
59.....	272	254	3	.....	261	3	000	2462809
61.....	.....	085	1	.....	101	3	001	2461694
61.....	280	300	0	.....	298	1	.....	2461574
62.....	462	457	8	.....	456****	4	001	2460873
62.....	760	.....	0	.....	620	4	003	2460773
62.....	912	910	0	.....	922	4	004	2460590
63.....	230	258	1	.....	258	2	003	2460387
63.....	365	.....	0	.....	310	1	.....	2460355
63.....	.....	631	4	.....	628	4	000	2460163
65.....	619	617	3	.....	618	6	001	2458959
66.....	137	133	1	.....	143	4	001	2458641
66.....	860	877	1	.....	823††††	1	.....	2458230
			9	.....	886††††	3	001	2458192
67.....	160	162	1	.....	166	3	002	2458023
69.....	018	968	00	.....	999‡‡‡‡	2	005	2456916
69.....	.....	358	0	.....	354	1	.....	2456701
69.....	633	631	10	632	(635	9	001)	2456533
69.....	893	884	2	.....	897	7	001	2456373
70.....	853	.....	2	.....	781	1	.....	2455840
71.....	242	235	4	.....	246	6	001	245556c
71.....	419	395	0	.....	408	2	001	2455462
71.....	.....	656	1	.....	662	2	002	2455309
72.....	958	961	3	963	(962	6	001)	2454525
73.....	864	.....	0	.....	894	1	.....	2453964
74.....	096	100	4	.....	103	10	001	2453838
76.....	919	960	0	.....	945	1	.....	2452127
77.....	884	.....	0	.....	835	2	003	2451592
78.....	149	165	1	.....	173	2	001	2451389
78.....	852	843	7	838	(842	7	001)	245099c
78.....	.....	963	1	.....	969	1	.....	2450910
79.....	926	.....	0	.....	854	2	003	2450379
80.....	101	092	0	.....	087	1	.....	2450239
80.....	.....	655	0	.....	667	1	.....	2449891
81.....	478	478	2	.....	483	2	002	2449401
82.....	383	383	5	383	(379	4	001)	2448861
83.....	323	341	0	.....	334	1	.....	2448290
83.....	832	838	1	.....	844	2	003	2447985
84.....	021	010	0	.....	982§§§§§	1	.....	2447902
84.....	357	.....	0	.....	498	2	.....	2447593
85.....	034	008	2	.....	002	2	002	2447291
85.....	281	243	3	.....	244	4	001	2447146
87.....	745	755	9	749	(750	8	002)	2445646
88.....	666	685	1	.....	680	2	001	2445089
88.....	871	905	1	.....	884	1	.....	2444967
89.....	272	293	00	.....	263	1	.....	2444741
90.....	.....	710	0	.....	711	1	.....	2443875

**** A doublet, resolved on one plate.

†††† Two lines, not well resolved on even second-order plates. First-order plates give .865.

‡‡‡‡ 4068.999.

§§§§ 4083.982.

TABLE II—*Continued*

λ	*F*	*G*	*I*	*L*	M_w	*N*	*PE*	*p*
4090.....	999	068	00	.....	038|| || || ||	1	.....	2443680
91.....	638	624	0	.....	625	1	.....	2443330
92.....	808	812	0	.....	815	1	.....	2442619
93.....	.....	803	0	.....	798	1	.....	2442033
94.....	188	208	1	.....	211	3	003	2441786
95.....	531	533	2	.....	536	3	002	2440996
95.....	939	946	1	.....	964	2	001	2440741
96.....	066	068	1	.....	075	1	.....	2440675
97.....	437	433	3	.....	447	3	002	2439858
97.....	.....	547	0	.....	563	2	001	2439789
4101.....	729	737	*Hδ*	.....	736	8	001	2437307
02.....	402	.....	0	.....	359	1	.....	2436937
04.....	202	.....	00	.....	258	1	.....	2435809
06.....	233	231	3	.....	233	4	002	2434637
07.....	272	.....	0	.....	209	1	.....	2434059
07.....	793	788	2	.....	794	4	001	2433712
09.....	292	297	2	.....	305	2	002	2432817
09.....	527	494	0	.....	503	1	.....	2432700
10.....	130	116	2	.....	124	3	002	2432333
10.....	591	.....	0	.....	598	1	.....	2432052
11.....	035	055	1	.....	049	2	001	2431785
13.....	515	515	2	.....	524	4	001	2430322
15.....	933	937	0	.....	939	1	.....	2428896
16.....	308	306	1	.....	313	1	.....	2428676
23.....	277	266	0	.....	274	1	.....	2424576
23.....	455	.....	0	.....	605	3	002	2424381
23.....	753	750	1	.....	759	2	001	2424290
29.....	545	535	2	.....	551	3	001	2420890
30.....	.....	025	2	.....	034	3	001	2420607
31.....	498	453	2	.....	462	3	001	2419771
31.....	989	953	1	.....	971	2	001	2419472
33.....	407	381	0	.....	416	1	.....	2418627
33.....	998	995	3	998	(992	1	.....)	2418286
39.....	492	519	0	.....	497	2	005	2415074
40.....	805	817	0	.....	826	3	002	2414299
42.....	801	801	0	.....	815	3	002	2413139
43.....	.....	286	0	.....	297	1	.....	2412859
43.....	.....	858	0	.....	870	2	001	2412525
45.....	564	546	2	.....	565	2	003	2411539
46.....	240	241	2	.....	250	2	002	2411140
46.....	.....	912	0	.....	924	1	.....	2410748
51.....	334	.....	0	.....	487	3	001	2408099
51.....	604	573	2	.....	582	3	002	2408044
52.....	652	637	2	.....	649	3	002	2407425
55.....	806	804	2	.....	816	3	001	2405590
56.....	633	623	4	.....	637	5	003	2405115
56.....	873	861	4	.....	866	4	001	2404983
57.....	183	173	1	.....	173	2	002	2404805
58.....	744	.....	0	.....	793	1	.....	2403868
59.....	320	302	5	313	(310	5	002)	2403568
61.....	486	490	1	.....	487	1	.....	2402312
61.....	745	718	1	.....	730	6	001	2402172

\|\|\|\| 4091.038.

TABLE II—*Continued*

λ	*F*	*G*	*I*	*L*	M_w	*N*	*PE*	ν
4161.....	949	941	5	.....	942	6	002	2402050
63.....	015	012	1	.....	025	2	003	2401425
63.....	406	393	2	.....	401	4	003	2401208
63.....	608	605	3	.....	605	6	001	2401091
65.....	188	195	3	.....	193	5	002	2400175
66.....	.....	727	00	.....	726	1	.....	2399292
67.....	573	567	2	.....	571	2	001	2398805
68.....	581	571	2	.....	575	2	002	2398228
71.....	309	308*	10	307	(305	5	001)	2396657
73.....	749	846	00	.....	797	1	.....	2395227
74.....	011	050	00	.....	995¶¶¶¶	1	.....	2395119
75.....	001	957	0	.....	971*****	1	.....	2394554
75.....	163	165	6	161	(161	7	001)	2394445
77.....	113	125	10	112	(111	7	001)	2393326
77.....	718	720	5	.....	716	5	002	2392980
79.....	591	598	4	588	(593	4	001)	2391909
80.....	105	111	5	107	108	8	001	2391612
80.....	705	692	1	.....	687	3	004	2391280
82.....	166	170	8	169	(165	7	001)	2390432
84.....	376	400	0	.....	391	1	.....	2389163
85.....	041	.....	0	.....	055	1	.....	2388784
88.....	206	229	1	.....	213	3	002	2386983
89.....	456	462	2	.....	462	2	000	2386271
92.....	105	107	1	.....	109	3	000	2384764
94.....	019	016	1	.....	026	3	001	2383674
94.....	368	305	1	.....	309	3	002	2383514
95.....	668	674*	6	670	(670	7	001)	2382741
98.....	221	210	3	.....	214	2	000	2381297
98.....	710	717	1	.....	728	1	.....	2381005
99.....	787	793	5	790	(789	7	001)	2380403
4200.....	044	099	1	.....	101	3	001	2380226
00.....	959	971	1	.....	955	3	002	2379743
02.....	305	279	1	.....	286	2	000	2378989
02.....	427	439	1	.....	438	1	.....	2378903
04.....	904	887	1	.....	898	3	002	2377512
05.....	102	098	9	.....	098	7	001	2377398
05.....	301	279	1	.....	270	1	.....	2377301
06.....	091	085	2	.....	085	4	001	2376841
07.....	530	541	1	.....	545	2	002	2376016
08.....	238	225	0	.....	236	1	.....	2375626
08.....	490	430	1	.....	443	1	.....	2375509
09.....	175	169	4	169	(172	5	001)	2375099
10.....	129	131	5	.....	129	6	002	2374558
11.....	824	821	1	.....	828	3	001	2373600
12.....	047	036	1	.....	041	4	001	2373480
12.....	507	498*	10	500	(499	7	001)	2373221
14.....	288	279	0	.....	287	2	003	2372217
16.....	078	063	0	.....	080	1	.....	2371206
16.....	.....	210	0	.....	217	1	.....	2371129
16.....	683	669	1	.....	684	2	004	2370867
19.....	479	495	2	.....	503	2	000	2369282
22.....	160	158	5	.....	161	4	001	2367791
22.....	514	518	5	522	(521	4	003)	2367588
23.....	941	935	3	942	(948	2	007)	2366792
24.....	512	503	5	.....	512	5	001	2366473

¶¶¶¶ 4173.995.

***** 4174.971.

writer's intensity is substituted, and where the line was not measured by Gale, a value is assigned which agrees with that scale. Further, in Table II, λ is the integer value of the wave-length in angstroms; *F*, Finkelnburg's fractional value; *G*, that obtained by Gale, Monk, and Lee; *L*, the Lacount interferometer value; M_w, the writer's weighted mean determination; *N*, the number of "sets" of measurements entering into the calculation of M_w; *PE*,[4] the probable error of the weighted mean, M_w; and ν, the "vacuum" wave-number[5] obtained from M_w or from *L*, where the latter is present.

With the interferometrically determined wave-lengths, *L*, the grating determinations, M_w (shown in parentheses and based on the iron standards), are listed for comparison. The maximum deviation of M_w from *L* is 0.006, the average 0.002 A.

The average probable error of the mean for the values of M_w for the 512 lines listed is less than 0.002 A.

In three cases Lacount and Hodgdon measured lines determined interferometrically by Gale, Monk and Lee. These are λ 4171.308, $L = .307$; λ 4195.674, $L = .670$; λ 4212.498, $L = .500$. They are marked by an asterisk in column *G* of Table II.

DISCUSSION OF RESULTS

The writer's values agree, in general, more closely with those of Gale. The average difference between *G* and M_w without regard to sign is 0.011 A; that between *F* and M_w, 0.022 A.

A comparison of the 34 interferometer values, *L*, with the mean M_w, reveals that the sum of the positive values of $L - M_w$ is .034 A and the sum of the negative is also .034, showing an average deviation of .001 in each case, which indicates a random distribution of differences and attests the accuracy of the entire set of measurements. For $L - G$ the sums are $+ .127$ and $- .051$; for $L - F$, $+ .176$ and $- .047$.

It is the writer's purpose to publish the wave-lengths of lines in other regions as soon as possible.

[4] It should be borne in mind that the probable error of a mean is of small significance in cases where few determinations are involved.

[5] Calculated from Kayser's table.

Grateful acknowledgment is made to Dr. Millikan for the use of the facilities of the California Institute of Technology; to the Rumford Committee of the American Academy of Arts and Sciences for its generous financial assistance; and to the Elizabeth Thompson Science Fund for the loan of a calculating machine.

CALIFORNIA INSTITUTE OF TECHNOLOGY, 1927
BOSTON UNIVERSITY, March 1936

PHOTOMETRY OF THE DIFFUSE NEBULA NGC 7023

PHILIP C. KEENAN

ABSTRACT

The reflection nebula NGC 7023 was photographed in red and in blue light with the Perkins reflector. The photographic surface brightness is inversely proportional to the distance from the central star for radii of the order of 1′, but the curve is steeper for smaller radii. The observations do not fit any of the predicted curves computed on the assumption of uniform density, but indicate that there is a concentration of matter about the star, which probably lies a relatively short distance inside the nebula.

The color of some of the brighter parts of the nebula was compared with that of the star. For the larger part of the nebula the reflecting power is only slightly greater in red light than in blue, as would be expected if the particles are fairly large; but there is a well-defined portion in which a red excess of the order of 0.3 mag. was found.

NGC 7023 in Cepheus is one of the brightest of those diffuse nebulae which are known to have a predominantly continuous spectrum,[1] presumably due to light from the central star reflected by the nebular matter. Because of its comparative symmetry, in contrast to several other objects of its class, as well as its brightness, it was selected for a reconnaissance of the intensity gradient and the color of the nebulosity.

METHOD OF OBSERVATION AND REDUCTION

The observations were carried out at the 25-foot Newtonian focus of the Perkins reflector, which was diaphragmed down to an aperture of 60 inches in order to eliminate vignetting arising from the smallness of the secondary mirror. Exposures were made on Eclipse 850 Soft plates to give photographic magnitudes and on Eastman 1 C plates through a ciné-red filter as used by C. Payne Gaposchkin and S. Gaposchkin[2] to give red magnitudes with an effective wavelength of 6300 A. All plates were backed and were provided with intensity-calibration exposures made through a tube sensitometer.

Measurements of image density were made for the most part with a Kipp registering microphotometer in the Mendenhall Laboratory, but some of the supplementary plates were measured on a Stetson photometer at the Perkins Observatory.

[1] In NGC 7023 the hydrogen lines have been observed to be bright in both nebula and star. Cf. V. M. Slipher, *Pub. A.S.P.*, **30**, 63, 1918.

[2] *Harvard Ann.*, **89** (No. 5), 93, 1935.

UNIV. OF WICH.

PLATE XVIII

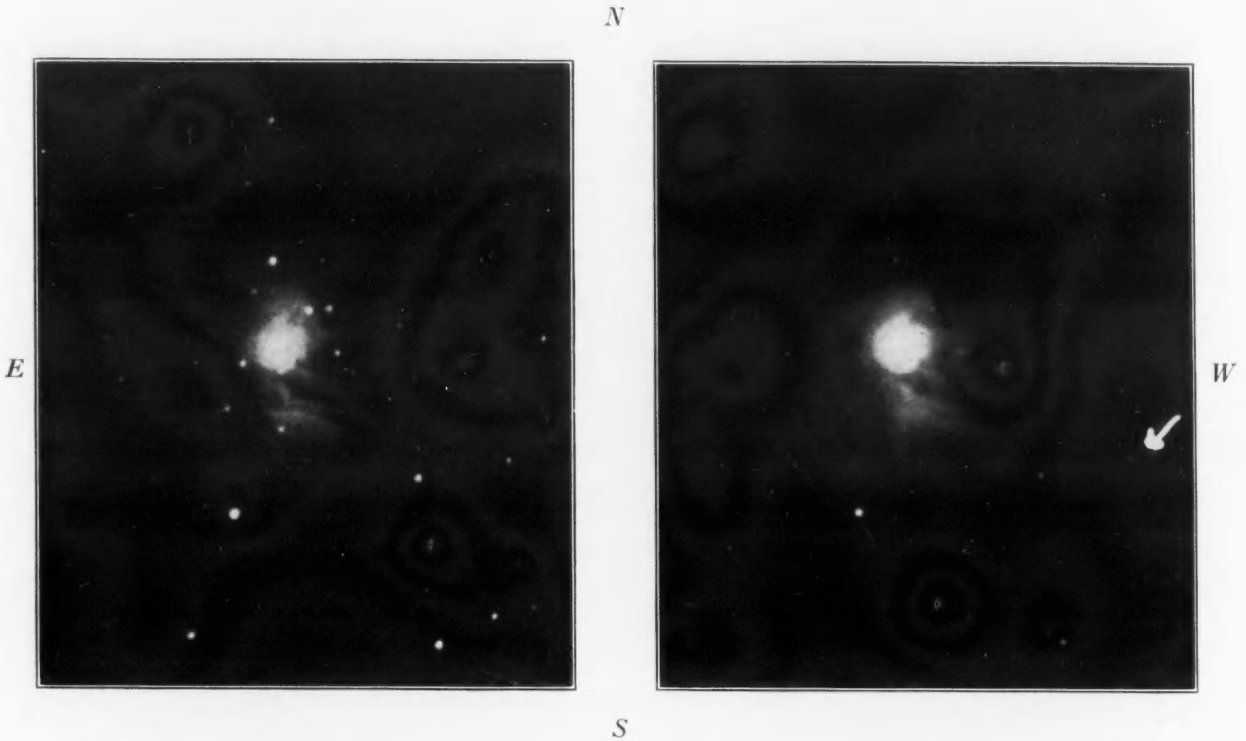

RED
(191 min.)

BLUE
(16 min.)

NGC 7023
Scale: 8″.7 = 1 mm

The central star of the nebula, BD+67° 1283, of photographic magnitude 7.51 and spectrum B2p, was chosen as the standard for photographic brightness and relative color. On each plate to be used for color determination the star was photographed 12 mm out of focus both before and after the exposure on the nebula. Between exposures the plate was shifted so as to place the annular star image outside the measurable limits of the nebula but on the same background of sky fog, in order to eliminate, as far as possible, any effect of the sky background on the measures.

By using an exposure ratio, nebula to star, of 30:1, the density of the inner nebula was matched satisfactorily with that of the stellar image. This procedure required that the value of Schwarzschild's constant be known for both types of emulsion and for the given exposure times. On the basis of a laboratory determination checked by exposures on several Selected Areas, the values of p adopted were 0.83 for the Eclipse plates and 0.74 for the 1 C plates with the red filter, but the uncertainty amounts to several per cent.

Comparison of the densities of the nebular and stellar images in each color gave directly the relative reflecting power of the nebulosity in red and blue light. The color determined in this way is expressed in terms of that of the central star. The absolute photographic surface brightness of the nebula was then found by measuring the area of the annular image of the star, which was always photographed on the optical axis of the telescope in order to secure a circular ring of sufficiently uniform density.

The observations were greatly facilitated by a rack-and-pinion focusing device and a removable filter-holder, which were constructed in the Observatory shops by Mr. Decker and mounted on the double-slide plate-carrier.

OBSERVATIONAL RESULTS

Although NGC 7023 possesses so many irregularities of structure (Pl. XVIII) that measures along any one radius have little significance, it was found that the means from several diameters followed a comparatively smooth curve which gave a fair representation of the gradient of photographic brightness in passing outward from the central star. The values obtained by combining data from eight radii on

each of three of the best plates taken here are plotted in Figure 1. The abscissae in the diagram give the $\log_{10}$ of the distance from the

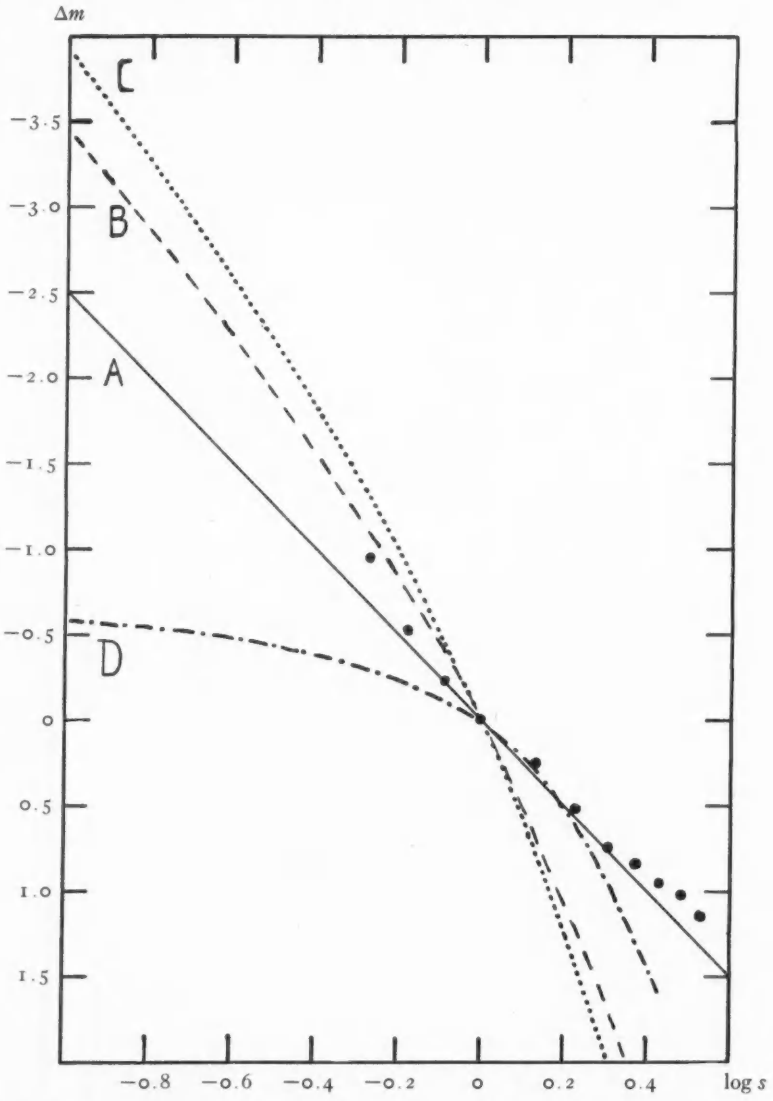

FIG. 1.—Relative intensity gradients in reflection nebulae. The photographic observations on NGC 7023 are represented by the black dots.

central star in minutes of arc. The ordinates represent relative brightness in magnitudes, the zero-point being placed arbitrarily at

a distance of 1 minute. The significance of the curves in the figure will be discussed in the next section.

From comparison with the central star on three additional plates the actual surface brightness at eleven points in the inner nebula was determined. These data led to a value of 11.61 ± 0.03 mag. as the factor to be added to the relative magnitudes of Figure 1 to obtain photographic surface brightness in magnitudes per square minute of arc. Thus the luminosity of the nebula decreases from 10.6 mag./□′ at a radius of 0′.5 to 12.8 mag./□′ at a radius of 3′.2. A few rough comparisons with stars of Selected Area 18 confirmed the absence of any large systematic error in these values.

TABLE I

+0.19 mag.	+0.23 mag.
− .19	+ .26
+ .24	+ .06
+0.02	−0.23

With the inclusion of data from three red-sensitive plates it was possible to derive colors for the brighter parts of the nebula along three radii. Expressed as the difference between the brightness of the nebula relative to the central star in red light and in blue light, the color differences for eight points of measurement are given in Table I, where positive values indicate red excess.

The large scatter is due in part to uncertainties in the measures and in part to variations of color within the nebula. The average of the measures is +0.09 mag. The nebula is thus nearly white, but appears to have a slight increase in reflecting power toward the red end of the spectrum. The general similarity in the structural details visible in the two colors is apparent in Plate XVIII, but it may be noticed that there is a wedge-shaped dark region about 40″ northwest of the center that is crossed by a curved bright filament which is much more conspicuous on the red plate than in blue light. Three additional points measured within this region show a strong red excess, the values being +0.30, +0.39, and +0.55 mag. It is evident that either there is selective absorption amounting to about 0.3 mag. in this region or there is an excess of emission in red wave-lengths, possibly the result of local excitation giving rise to emission lines. The

former explanation appears the more plausible, but observations with a fast spectrograph are desirable to settle the point.

By increasing the red exposures to more than three hours with the fastest 1 C Special plates, made available through the co-operation of Dr. C. J. Staud of the Eastman Kodak Company, it was possible to extend the measures far enough from the center to indicate that the mean intensity gradient in red light is similar to that found for the blue; but an accurate color chart of the whole nebula cannot be made until plates of still greater sensitivity in the red are developed.

Nebulae such as NGC 7023, which are nearly as blue as the early-type stars which they surround, are particularly difficult to photograph through a red filter. On the other hand, the emission-line nebulae have a greater proportion of their light in the visual region.

A good example is the Swan nebula NGC 6618 (M17), which is reproduced in Plate XIX from a one-hour exposure through the red filter. If this picture is compared with that taken by J. C. Duncan[3] on an ordinary blue-sensitive plate with the 60-inch reflector at Mount Wilson, it will be seen that practically every detail is reproduced with the same relative contrast on the two plates, from which it seems reasonable to conclude that there are no very great differences in excitation within the nebula. The conspicuous rectangular dark marking near the center is as black in reality as it appears to be in contrast to the brilliant surrounding regions, for measures on our plate showed that it had the same density as the sky background near the edge of the field.

The star indicated by the white arrow in the right-hand image of Plate XVIII is of interest as having an unusually low color index for an object of its luminosity. From our plates its color can be estimated as somewhere between those of an A5 and a G2 star. Since it lies within the area of the dark nebula which covers the whole field of the plate and is classified as very opaque by Struve and Miss Story,[4] it is almost certainly situated between the sun and the nebula. The distance of the nebula is uncertain; but if, for the moment, we accept Lundmark's estimate of about 200 parsecs,[5] the apparent photographic magnitude of 15.5 for the star leads to a value of +8 or +9

[3] *Ap. J.*, **51**, 4, 1920, Pl. IV.

[4] *Ibid.*, **84**, 203, 1936.

[5] *Pub. A.S.P.*, **34**, 40, 1922.

PLATE XIX

THE SWAN NEBULA, M. 17 (NGC 6618)
Exposure one hour through red filter

as its maximum absolute magnitude. It would thus appear to be intermediate between the main-sequence stars and the white dwarfs, and it deserves further attention.

THEORETICAL INTENSITY GRADIENTS

The theory of the illumination of small particles by a star was developed by Seeliger[6] and elaborated by Schoenberg[7] and by Struve.[8] Its adaptation to the conditions of our present problem is simple. We assume that the density throughout the nebula is constant.

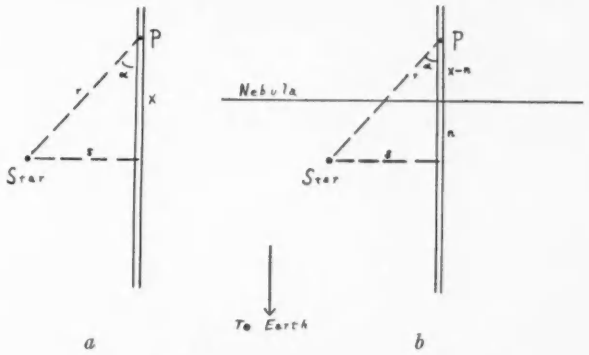

FIG. 2.—Position of star with respect to nebula

Consider first the case of a star imbedded in a very large nebula (Fig. 2*a*). Then, in comparing the brightness of the nebula with that of the star, we can neglect the absorption of the light after reflection, for, on the average, this will be very nearly the same as the absorption of the direct beam from the star to the earth. At any point P the illumination of a particle will be

$$E_r = \frac{E_o\, e^{-kr}}{r^2}, \qquad (1)$$

where E_o is the flux over the same cross-sectional area at unit distance from the star and k is the linear absorption coefficient.

The radiation scattered in the direction of the earth is given by

[6] *Sitz. d. Akad. d. Wiss.* (München), Heft III, p. 272, 1901.

[7] *Handb. d. Astroph.*, **2**, Part I, 163, 1928; *Mitt. Universitätssternwarte Breslau*, **3**, 53, 1932.

[8] Struve and Elvey, *Ap. J.*, **83**, 162, 1936; Struve and Story, *op. cit.*

$K\Theta(\alpha)E_r$, where K is a constant proportional to the albedo of the particle and $\Theta(\alpha)$ is the factor giving the distribution of the scattered light as a function of the phase angle α. For a line of sight passing through the nebula at apparent distance s from the star, the total intensity of the scattered light is then given by

$$I_s = KnE_o \int_{-\infty}^{\infty} \frac{e^{-kr}}{r^2}\,\Theta(\alpha)dx \qquad (r = \sqrt{s^2 + x^2}), \tag{2}$$

n being the number of particles per cm^3.

Since the factors outside the integral are constant throughout the nebula by our assumptions, the apparent intensity gradient can be found by evaluating the integral as a function of s.

An alternative form of equation (2) is

$$I_s = KnE_o \int_0^{\eta} \frac{e^{-ks\csc\alpha}}{s}\,\Theta(\alpha)d\alpha, \tag{3}$$

from which it may be seen that, if there is no appreciable absorption and the phase-angle factor can be neglected, the brightness of the nebula is inversely proportional to the apparent distance from the star. This case is represented by the straight line A in Figure 1.

For the more general case equation (2) was integrated graphically for

$$\Theta(\alpha) \sim \frac{\sin\alpha + (\pi - \alpha)\cos\alpha}{\pi}$$

(large particles subject to Lambert's law[9]) and for $\Theta(\alpha) \sim 1 + \cos^2\alpha$ (Rayleigh or Thomson scattering) as well as for $\Theta(\alpha) = 1$. As expected, the phase function was found to affect the curves so slightly that it can be neglected in comparison with other sources of error. Consequently, only the curve for $\Theta(\alpha) = 1$ has been reproduced (curve B). For small radii the slope of the curve approaches that of the line A.

If the star is at the near edge of the nebula, equation (2) becomes

$$I_s = KnE_o \int_0^{\infty} \frac{e^{-k(r+x)}}{r^2}\,\Theta(\alpha)dx\,, \tag{4}$$

[9] Schoenberg, *Handb. d. Astroph.*, **2**, Part I, 64, 1928.

since it is now necessary to take account of absorption after reflection. This is essentially Seeliger's expression.[10] As shown by curve C, the gradient is now somewhat steeper at any given radius. There will be a gradual transition from C to B as the star is taken inside the nebula.

If the star lies in front of the nebula, we have (Fig. 2*b*):

$$I_s = KnE \int \frac{e^{-k(r'+x-n)}}{r^2} \cdot \Theta(\alpha) dx \,, \tag{5}$$

where

$$r' = \frac{r(x-n)}{x} \,.$$

As shown by the curve D, computed for $n = 1$, the gradient flattens out very rapidly near the star if there is any considerable distance between star and nebula.

In all of the plotted curves the zero-point for the ordinates was chosen to make the curves pass through the point (0, 0). As a matter of convenience, k was chosen as 0.6. Actually the abscissae are fixed by the opacity ks; and when the actual distance of any nebula is known, the absorption coefficient may be determined approximately by sliding the curves along the log s-axis until one of them fits the slope of the observed curve at corresponding abscissae.

In the case of NGC 7023 the observations cannot be fitted well to any of the theoretical curves. The observed gradient is nearly proportional to the inverse radius over most of the curve but becomes steeper near the star. This increase in slope is probably real, for the observations have been corrected for atmospheric and photographic scattering of light from the central star. Probably the discrepancy is due to the fact that our assumption of uniform density fails to hold for this nebula; the appearance of the photographs suggests strongly that there is an abrupt condensation of matter in the immediate vicinity of the star. Whether this is accidental or is due to gravitational influence of the star can best be settled by similar observations on other reflection nebulae. Visual examination of plates taken here suggests that NGC 2023 and NGC 2071 do not show a

[10] *Ibid.*, p. 165, eq. 77.

correspondingly rapid increase in brightness toward the star, but NGC 2247 appears quite similar to NGC 7023.

From the observations presented here, it can be concluded tentatively that NGC 7023 consists of particles having diameters too great to scatter according to Rayleigh's λ^{-4} law, the concentration being so low as to cause very little absorption in the light from the star at distances of the order of 10,000 to 30,000 astronomical units but increasing rapidly at smaller distances. The star probably lies within the nebula but not far from the nearer edge.

I am greatly indebted to Dr. Struve, director of the Yerkes Observatory, for his suggestion of the importance of this observational problem and for valuable discussions in the course of the work. I should like also to acknowledge the help of Mrs. J. A. Hynek in carrying out the computations.

PERKINS OBSERVATORY
September 1936

ON THE POLARIZATION OF LIGHT IN REFLECTION NEBULAE

L. G. HENYEY

ABSTRACT

Observations for the purpose of detecting the presence of polarization in the light of the reflection nebula NGC 7023, the nebulae in the Pleiades and the nebulous patches associated with γ Cygni have been made through a Polaroid screen used as an analyzer. Each set of observations consisted of two plates having the principal plane of the Polaroid of one plate perpendicular to that of the other. The relative weakening or strengthening of the image along radii drawn from the star parallel to the positions of the principal plane of the Polaroid would indicate polarization.

Measurements on the plates of NGC 7023 indicate the presence of polarization up to 12 per cent. The plates of the Pleiades and of γ Cygni indicate little or no polarization.

These results are shown to be compatible with the reflection theory of diffuse nebulae, provided the reflecting particles are fairly large. In the case of the nebulae around γ Cygni, the lack of evidence of polarization does not favor the hypothesis of the presence of Rayleigh scattering in these objects. This hypothesis was suggested by the blue color of these nebulosities.

1. The investigation of polarization in reflection nebulae which is reported in the following article was undertaken to provide information concerning the nature of the nebular particles which scatter the light of the associated stars. Certain definite deductions are possible from a knowledge of the state of polarization, while certain other facts can be elucidated by combining the results of observations of polarization with results of other methods of attack.

The existence of polarization in any amount indicates that the scattering particles are not free atoms, for processes of emission all give rise to unpolarized light, except in the case of the scattering of light in a resonance line. But the observations of Meyer[1] on emission nebulae show that these objects exhibit no appreciable polarization.

If we know beforehand that a nebula is not of the emission type, observations of its polarization enable us to go a step farther. In general, if a particle scatters light in such a way that it does not hold the energy for any length of time but simply deflects it without change of wave-length, then the polarization of the deflected light has the following characteristics: (*a*) its plane of polarization is usually perpendicular to or, more rarely, parallel to the plane formed

[1] *Lick Obs. Bull.*, **10**, 68, 1920.

by the incident and the scattered rays; and (*b*) the amount of polarization is inversely correlated with the size of the particles. When the scattering particles are of the order of size of a few hundred molecules or smaller we have what is usually known as Rayleigh scattering. Here the polarization reaches very large values, as is evidenced by our own blue atmosphere, which gives values up to 70 per cent. For larger particles the polarization is much smaller and is quite negligible, except for the case of specular reflection near the polarizing angle on the surfaces of very large bodies.

The orientation of the plane of polarization should give an independent confirmation of the fact that reflection nebulae are illuminated by stars. For if the nebula is sufficiently spread out, the plane of polarization will have different orientations at different points, depending on the direction of the line joining the star and the point in question. Consequently, if we observe polarization in a nebula such that its plane is symmetrical with respect to a star, we can safely say that this star is the source of illumination. It must be remembered that these relationships, strictly speaking, hold true only if we consider light which has suffered but one deflection after leaving the star; for light which has been deflected more than once the case is more complicated. However, in almost any case the planes of polarization of multiply scattered light will be so thoroughly mixed that all trace of polarization is lost. It therefore seems that radial polarization should be present.

The distribution of polarization over the apparent disk of a nebula could, under favorable circumstances, give additional information concerning the structure of the nebula. Here, unfortunately, the situation is much more difficult to analyze, since irregularities in the space density of the particles in the nebula can influence the result tremendously. But it may be well to keep this source of attack in mind, since undoubtedly in the future it will provide valuable information.

While several attempts have previously been made to detect traces of radial polarization in nebulae, no quantitative measures have been published. Most nebulae are faint and visual observations are therefore out of the question. Previous attempts to make observations, together with the difficulties encountered in the con-

struction of suitable analyzers, have been described by Dr. W. F. Meyer.[2] He found that the best results were obtained with a Nicol prism. The nebula was photographed in two perpendicular positions of the Nicol and the photographic densities of the two images were measured with a microphotometer. A comparison of the two sets of measures was then made to detect traces of polarization. Owing to the large optical thickness of the Nicol, it was necessary to collimate the light of the nebula before it passed through the prism. A camera lens on the other side of the Nicol focused the light on the photographic plate. With this arrangement Meyer obtained a series of observations of emission nebulae, of a number of spirals, and of one true reflection nebula, NGC 2261 (Hubble's Variable Nebula), in which we are here primarily interested. He found that in this object the polarization is small, probably less than 10 per cent. More recently Struve, Elvey, and Roach[3] found that the nebula near ρ Ophiuchi exhibits a definite but rather small amount of polarization, and they pointed out that this is compatible with the reflection theory. Since the effect is radial with respect to ρ Ophiuchi (unless the principal plane of the Polaroid was taken by chance in just the right direction), we have a confirmation of the association of the star and the nebula.

2. The detection of a state of radially symmetrical polarization can be very simply accomplished by the use of the Polaroid screen. Since the Polaroid is thin, it is unnecessary to collimate light which passes through it. The Polaroid is primarily a film of some celluloid-like material into which are imbedded numerous minute crystals of a double-refracting material. The optic axes of these crystals have been oriented into parallel directions, so that the film will polarize light which passes through it. This polarizing property is not complete and depends on the wave-length.[4] It is sufficient to state here that the region of transmission is toward the longer wave-lengths from 4200 A, and that the region of good polarization (better than 80 per cent) is between this limit and about 7200 A. The average polarization between these limits will depend on the color character-

[2] *Ibid.* [3] *Ap. J.*, **84**, 219, 1936.

[4] A description of the transmission and polarization of the Polaroid can be found in a paper by Ingersoll, Winans, and Krause, *J. Opt. Soc. Amer.*, **26**, 233, 1936.

istics of the source and of the photographic plate, but it will usually be over 90 per cent. In the discussion which follows it will be assumed that the polarization of the Polaroid is 100 per cent.

On long exposures of bright stars, peculiar streaks were noticed passing through the images. Each streak is along a line parallel to the principal plane of the Polaroid, and decreases in intensity with increasing distance from the star, the total intensity depending on the density of the stellar image. The source of the effect is undoubtedly in the Polaroid and may be due to the scattering of the light in the polarized component removed from the principal beam. It was only on the plates of the Pleiades that the effect was noticeable, but even here little difficulty was experienced. It should be remarked that the effect is one which is in the opposite sense from the effect resulting from radial polarization.

The use of the Polaroid in detecting radial polarization is illustrated in Plate XX*a*. This plate shows two photographs, each taken through a Polaroid film, of a rectangular glass tank full of a colloidal dispersion of rosin in water which is illuminated by a light placed in the center. The center is greatly overexposed, so that the lamp is not visible. The lines represent the directions of the principal planes of the Polaroid in the two cases. Now the light scattered by such a medium is polarized in a plane perpendicular to the radius vector, so that the Polaroid will weaken the light to the greatest extent along the radii parallel to the principal planes. This is readily seen by comparing the two cases. A pair of such photographs of a nebula will then provide the means of detecting the presence of polarization.

3. In Figure 1 let O be a star illuminating a nebula surrounding it, and choose two points, P_1 and P_2, lying on radii which are perpendicular to each other. Let the surface brightness at the two points be J_1 and J_2, respectively, and the fraction of the light polarized be p_1 and p_2 in a plane perpendicular to the radius. Then the light intensity at each point can be resolved into two components, one along the radius and one along the tangent. The two components have intensities for P_1

$$J_{1\mathrm{Rad}} = \frac{1 - p_1}{2} J_1 , \qquad J_{1\mathrm{Tan}} = \frac{1 + p_1}{2} J_1 ,$$

PLATE XX

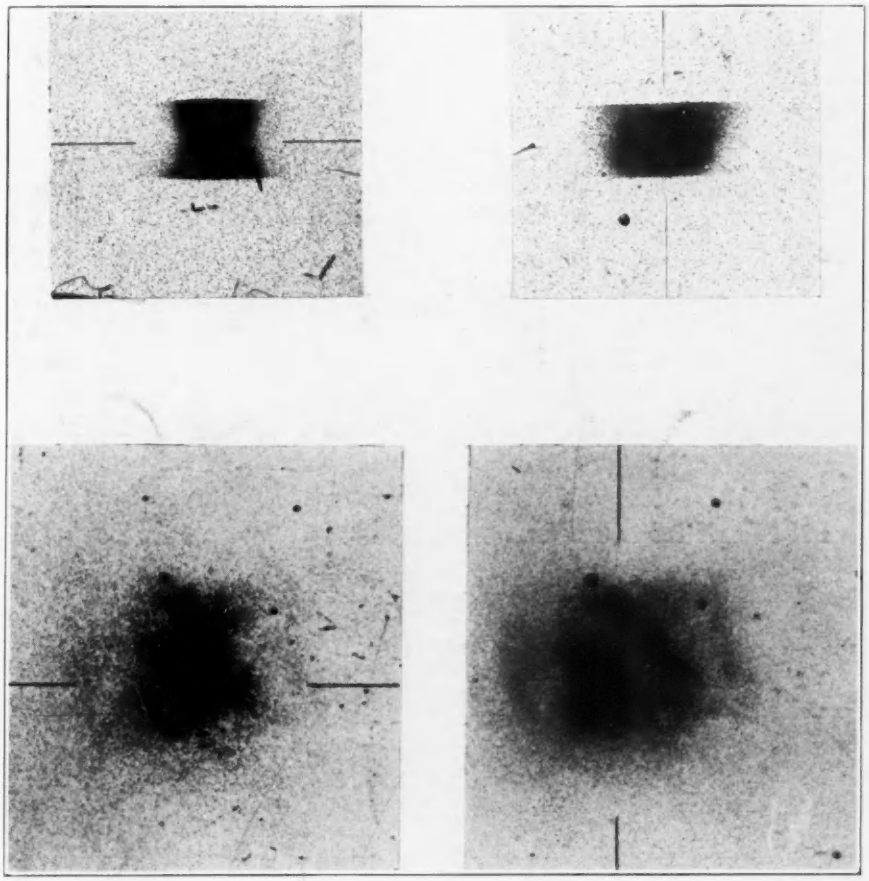

a) Polarization in a Colloidal Dispersion of Rosin in Water
b) Polarization in NGC 7023

UNIV OF MICH.

and for P_2 corresponding values. Now if we take two photographs of such a nebula through a Polaroid disk such that the principal plane in one is along OP_1 and in the other along OP_2, we will have

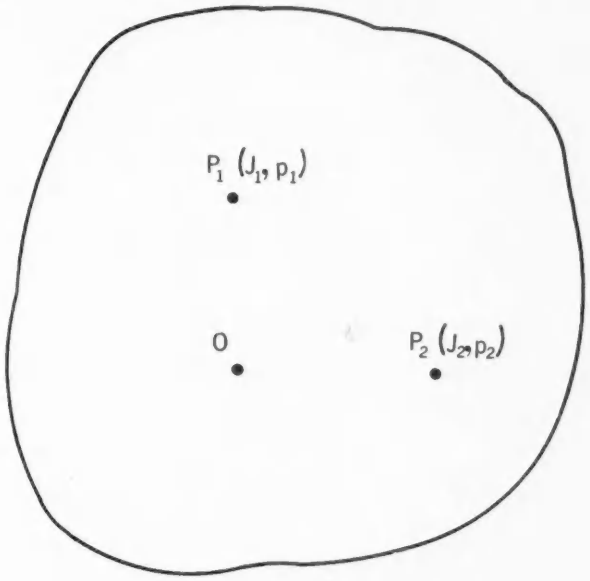

FIG. 1

but one of the components passing through. The transmitted light in each case is given below:

Case A.—Principal plane of Polaroid along OP_1:

$$J_{1A} = \frac{1 - p_1}{2} J_1 , \qquad J_{2A} = \frac{1 + p_2}{2} J_2 .$$

Case B.—Principal plane of Polaroid along OP_2:

$$J_{1B} = \frac{1 + p_1}{2} J_1 , \qquad J_{2B} = \frac{1 - p_2}{2} J_2 .$$

It is convenient to express surface brightnesses in terms of the sky as a unit. Now on different plates the sky will be somewhat different, so the intensities on different plates are not directly com-

parable. However, if we take the ratios of intensities on the two plates for both points, we have

$$\frac{\dfrac{J_{1A}}{J_{A,\mathrm{sky}}}}{\dfrac{J_{1B}}{J_{B,\mathrm{sky}}}} = \frac{1-p_1}{1+p_1}\cdot\frac{J_{B,\mathrm{sky}}}{J_{A,\mathrm{sky}}}, \quad \frac{\dfrac{J_{2A}}{J_{A,\mathrm{sky}}}}{\dfrac{J_{2B}}{J_{B,\mathrm{sky}}}} = \frac{1+p_2}{1-p_2}\cdot\frac{J_{B,\mathrm{sky}}}{J_{A,\mathrm{sky}}}. \tag{1}$$

Taking the ratio of these two quantities, we have

$$\frac{\dfrac{J_{1A}}{J_{A,\mathrm{sky}}}}{\dfrac{J_{1B}}{J_{B,\mathrm{sky}}}} \div \frac{\dfrac{J_{2A}}{J_{A,\mathrm{sky}}}}{\dfrac{J_{2B}}{J_{B,\mathrm{sky}}}} = \frac{(1-p_1)(1-p_2)}{(1+p_1)(1+p_2)}. \tag{2}$$

The left-hand side consists of known quantities, so we can compute the right-hand side. If we assume that the polarization is the same at the two points, we determine the quantity

$$\left(\frac{1-p}{1+p}\right)^2,$$

from which p can be computed. In any case, although p_1 and p_2 are different, p represents an average value.

4. The objects which have been examined for polarization are NGC 7023, the nebulae in the Pleiades and the nebulae around γ Cygni.

The plates of NGC 7023 have been obtained with the 24-inch reflector of the Yerkes Observatory, on Eastman Hyper-press plates. Each plate has been standardized with a tube sensitometer. The Polaroid used was a piece mounted in a bakelite rim having a clear aperture of 4 cm. It was mounted on the plateholder carrier of the reflector, a few millimeters in front of the plate, with the principal plane always parallel to the short dimension of the plate. Since the carrier may be rotated about the optical axis, the adjustment of the orientation could be made by rotating the carrier any amount desired, according to the divided circle on it. However, only two positions were used: the principal plane parallel and perpendicular to the hour circle through the nebula.

Two photographs are reproduced in Plate XX*b*. The straight

lines give the direction of the principal plane of the Polaroid. It is seen that an effect is present which is somewhat similar to the effect shown by the colloidal solution. The relative weakening of points along the two radii is, for points which show maximum effects, about 0.3 mag.

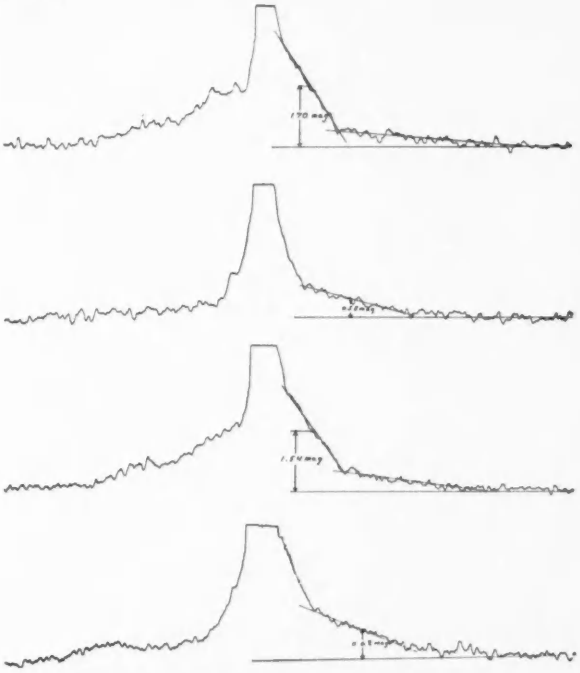

FIG. 2.—Microphotometer tracings of NGC 7023

The plates have been measured in two independent ways which give the same results. Microphotometer tracings have been made along the two radii. These are reproduced in Figure 2, where the process of reduction is indicated. The average density along two regions on the perpendicular radii was determined by drawing a straight line through the region and taking the density of the middle point on the line. The difference in magnitude between this point and the sky is shown in the figure. Measurements were also made at selected points along these radii by means of a Hartmann microphotometer. These measures are collected in Table I. The upper part of the table gives the results for one plate, the lower those for

a second plate. The principal plane of the Polaroid is indicated in the first column. The measures on the left are along the north–south radii, while those on the right are along the east–west radii. The table gives the measured difference in magnitude between the points on the nebula and on the sky, the corresponding intensity (plus that of the sky) in terms of the intensity of the sky, and the intensities corrected for the sky. The next to the bottom row gives the quantity involved in equation (1)—namely, the ratio of intensities of points on plate A to those on plate B. In the bottom row is the mean for the three sets of measures along each radius. Taking

TABLE I

Plate		North–South Radii			East–West Radii		
A. Polaroid NS	$-m$	1.54	1.41	1.62	0.68	0.58	0.79
	I+I	4.13	3.66	4.45	1.87	1.71	2.07
	I	3.13	2.66	3.45	0.87	0.71	1.07
B. Polaroid EW	$-m$	1.70	1.47	1.80	0.55	0.42	0.65
	I+I	4.79	3.87	5.25	1.66	1.47	1.82
	I	3.79	2.87	4.25	0.66	0.47	0.82
A/B		0.85	0.93	0.81	1.32	1.51	1.30
Mean				0.86			1.38

the ratio of these values, we obtain for these points the mean of the quantity

$$\left(\frac{1+p}{1-p}\right)^2,$$

from which we find

$$p = 12 \text{ per cent}.$$

It should be repeated that this result is an average for those points which show large amounts of differences from plate to plate. Consequently, the average for the whole nebula is probably somewhat smaller.

The plates of the Pleiades were taken in the same manner as those of NGC 7023, except that Eastman Ortho-press plates were used. The exposures were approximately $3\frac{1}{2}$ hours. The length of the ex-

posures and the brightness of some of the stars caused the appearance of the anomalous streaks already mentioned. However, the principal features of several nebulae were well marked, and comparisons could be made satisfactorily. The reader is referred to Plate 4 of Barnard's *Atlas of Selected Regions of the Milky Way*, on which the features described in the following discussion can be easily identified.

Surrounding Maia, there are a number of faint wisps of nebulosity and one very well-marked tonguelike patch curving from west of the star around the northwest and gradually fading away toward the north. Considerable weight can be given to an examination of this feature because of its large spread in position angle. No effect of polarization was found in it.

The results for Merope are, similarly, negative. Here too, there is a well-defined curved patch, running from the east to the north. No effect was noticed along the points of this nebulosity. A comparison of its eastern portion and of other patches nearer the star with the extended cloud south of the star also failed to reveal a relative change.

A small trace of polarization was found in the approximately straight filament running eastward from Electra. This filament was compared with another narrow and straight filament southeast of Electra and apparently running through a faint star (BD$+23^{\circ}510$) from east to west. It was found that, when the Polaroid is parallel to the first filament, it is weakened with respect to the second. A comparison with the plate as a whole showed the same effect. It seems, therefore, that Electra provides the illumination for this nebula. The magnitude of the effect, even in this nebulous filament, is definitely less than that found in NGC 7023.

The plates of γ Cygni were taken with a Schmidt camera having a focal ratio of one to two. The camera has been described in the paper by Struve, Elvey, and Roach already referred to. The observing procedure is the same as that used by these observers. A visual examination of these plates reveals that the polarization, if present, is exceedingly weak. Owing to the small scale of the plates and the closeness of the star images, it did not seem advisable to measure these plates.

5. The results given in the foregoing section indicate that the polarization in these nebulae is quite weak. It is considerably weaker than the polarization of the corona,[5] for which the maximum is about 27 per cent. The polarization in NGC 7023 is about of the same order of magnitude as that found in the zodiacal light, namely, 15 per cent.[6] This small amount is in accordance with the reflection theory. Scattering by very small particles, such as Rayleigh scattering, would, for a probable distribution of the particles of the nebula in space, give values of the polarization much larger than this—perhaps between 30 and 70 per cent. The small amount of polarization in NGC 7023, in the nebulae of the Pleiades and around ρ Ophiuchi justifies the conclusion that the scattering particles are not of molecular size, or of a size comparable with, or smaller than, the wave-length of light. Since color observations of these nebulae have already shown[7] that they are not appreciably bluer than the illuminating stars, it is permissible to assume that the nebular particles are fairly large in size and that they scatter the light of the neighboring stars in accordance with the theory of Seeliger. A discussion of this theory will be given in another paper.

If Rayleigh scattering is indeed ruled out for the nebulosity associated with γ Cygni, then we should not expect selective scattering to take place. This point seems to be at variance with the color index for this object.[8] An explanation of this discrepancy may be found in the spectrum of the nebulosity. If there are any emission lines, they may give rise to such a spurious result. On the other hand, the presence of emission lines would not be expected from the spectrum of the exciting star, which is F8p, unless there are peculiar conditions of excitation. Further observations are needed before this point can be cleared up.

YERKES OBSERVATORY
October 1936

[5] Dufay and Grouiller (*C.R.*, **196**, 1574, 1933) find 26 per cent 10′ from the solar limb, while Johnson (*Pub. A.S.P.*, **46**, 226, 1934) finds 28 per cent 8′.5 from the limb.

[6] Dufay, *C.R.*, **181**, 399, 1925.

[7] Struve, Elvey, and Keenan, *Ap. J.*, **77**, 274, 1933; Struve, Elvey, and Roach, *ibid.*, **84**, 219, 1936; and Keenan, *ibid.*, **84**, 600, 1936.

[8] Struve, Elvey, and Roach, *op. cit.*, p. 226.

INDEX TO VOLUME 84

SUBJECTS

PAGE

Absolute-Magnitude Distributions, with Application to the Early K Stars, An Improved Method of Determining. *Gustaf Strömberg* 412
Absorption Lines, Intensities of Blended. *A. D. Thackeray* 433
Absorption Lines, Note on Equivalent Breadths of. *J. G. Baker* . . . 474
Absorption Lines, The Theoretical Interpretation of Equivalent Breadths of. *Donald H. Menzel* 462
Atomic Synthesis and Stellar Energy. III. *R. d'E. Atkinson* 73
Binary of Large Parallax, A New. *G. P. Kuiper* 478
Capella H, Confirmation of the Duplicity of. *G. P. Kuiper* 359
Carbon in the Spectra of Novae, Lines of Neutral Oxygen and. *Dean B. McLaughlin* 104
γ Cassiopeiae, Recent Changes in the Spectrum of. *Dean B. McLaughlin* 235
Colors of Globular Clusters, Absorption and Space Reddening in the Galaxy from the. *Joel Stebbins and A. E. Whitford* 132
P Cygni, Variations in the Spectrum of. *O. C. Wilson* 296
Globular Clusters, Absorption and Space Reddening in the Galaxy from the Colors of. *Joel Stebbins and A. E. Whitford* 132
H_2 from λ 3612 to λ 4224, Wave-Lengths of the Spectrum of. *Norton A. Kent* 585
Mean Parallaxes, Mean Absolute Magnitudes, and Mean Distances for Groups of Stars from Components of the Proper Motions, Computation of. *Gustaf Strömberg* 555
Meteorites, A Spectroscopic Examination of. *Arthur S. King* . . . 507
Milky Way, The Age of the. *Henri Mineur* 113
Multiplet Strengths for Transitions Involving Equivalent Electrons. *Donald H. Menzel and Leo Goldberg* 1
Multiplet Strengths, Note on Absolute. *Leo Goldberg* 11
Nebula NGC 7023, Photometry of the Diffuse. *Philip C. Keenan* . . 600
Nebulae, Effects of Red Shifts on the Distribution of. *Edwin Hubble* . 517
Nebulae. I. The Luminosity Function of Resolved Nebulae as Indicated by Their Brightest Stars, The Luminosity Function of. *Edwin Hubble* 158
Nebulae. II. The Luminosity Function as Indicated by Residuals in Velocity-Magnitude Relations, The Luminosity Function of. *Edwin Hubble* 270
Nebulae, On the Polarization of Light in Reflection. *L. G. Heyney* . . 609
Nebulae, Reflection. *Otto Struve, C. T. Elvey, and F. E. Roach* . . . 219

PAGE

Nebulae, Scattering of Light in Diffuse. *Otto Struve and Helen Story* . 203
Nova Herculis 1934, April–November, 1935, Spectrum of. *Walter S. Adams and Alfred H. Joy* 14
25 Orionis, A Study of the Spectrum of. *Helen W. Dodson* 180
Oxygen and Carbon in the Spectra of Novae, Lines of Neutral. *Dean B. McLaughlin* 104
Parallaxes with the 60- and 100-Inch Reflectors. Fifteenth Series. The Photographic Determination of Stellar. *Adriaan van Maanen* . . 409
φ Persei, A Spectrographic Study of. *Herbert F. Schiefer* 568
Photoelectric Photometry at the Sproul Observatory. *John S. Hall* . . 369
Photographic Photometry. *Frank E. Ross* 241
Polaris, The System of. *B. P. Gerasimovič* 229
Polarization of Light in Reflection Nebulae, On the. *L. G. Heyney* . . 609
Prominences of the Eruptive and Sun-Spot Types, The Motions of. *Edison Pettit* 319
Reviews:
Eberhard, G.; A. Kohlschütter; and H. Ludendorff (eds.). *Handbuch der Astrophysik*, Vol. VII (Otto Struve) 111
Heitler, W. *The Quantum Theory of Radiation* (Carl Eckhart) . . 239
Labérenne, Paul. *L'origine des mondes* (Otto Struve) 367
Moulton, F. R. *Consider the Heavens* (Philip Fox) 363
Sarton, George (ed.). *Osiris*, Vol. I (Otto Struve) 112
Sponer, H. *Molekülspectren* (David M. Dennison) 362
Stokley, James. *Stars and Telescopes* (O. C. Collins) 366
Samarium, Analysis of the Spectrum of Singly Ionized. *Walter Albertson* 26
Solar Velocity with Increasing Distances of the Stars from the Galactic Plane, The Change of the. *Emma T. R. Williams* 346
Spectra of Red Stars, Low-Dispersion. *Rupert Wildt* 303
Spectroscopic Binaries, A Rediscussion of the Orbits of Seventy-seven. *W. J. Luyten* 85
Temperature Scale, The Stellar. *A Pannekoek* 481
Visual Binaries of Large Parallax, Notes on. *G. P. Kuiper* 359
Wave-Length of a Spectral Line, Constancy of. *Guy C. Omer, Jr., and James L. Lawson* 477

INDEX TO VOLUME 84

AUTHORS

PAGE

ADAMS, WALTER S., and ALFRED H. JOY. Spectrum of Nova Herculis 1934, April–November, 1935 14

ALBERTSON, WALTER. Analysis of the Spectrum of Singly Ionized Samarium 26

ATKINSON, R. d'E. Atomic Synthesis and Stellar Energy. III . . . 73

BAKER, J. G. Note on Equivalent Breadths of Absorption Lines . . 474

COLLINS, O. C. Review of: *Stars and Telescopes*, James Stokley . . 366

DENNISON, DAVID M. Review of: *Molekülspektren*, H. Sponer . . . 362

DODSON, HELEN W. A Study of the Spectrum of 25 Orionis . . . 180

ECKHART, CARL. Review of: *The Quantum Theory of Radiation*, W. Heitler 239

ELVEY, C. T., F. E. ROACH, and OTTO STRUVE. Reflection Nebulae . 219

FOX, PHILIP. Review of: *Consider the Heavens*, F. R. Moulton. . . . 363

GERASIMOVIČ, B. P. The System of Polaris 229

GOLDBERG, LEO. Note on Absolute Multiplet Strengths 11

GOLDBERG, LEO, and DONALD H. MENZEL. Multiplet Strengths for Transitions Involving Equivalent Electrons 1

HALL, JOHN S. Photoelectric Photometry at the Sproul Observatory . 369

HENYEY, L. G. On the Polarization of Light in Reflection Nebulae . . 609

HUBBLE, EDWIN. Effects of Red Shifts on the Distribution of Nebulae . 517

HUBBLE, EDWIN. The Luminosity Function of Nebulae. I. The Luminosity Function of Resolved Nebulae as Indicated by Their Brightest Stars 158

HUBBLE, EDWIN. The Luminosity Function of Nebulae. II. The Luminosity Function as Indicated by Residuals in Velocity-Magnitude Relations 270

JOY, ALFRED H., and WALTER S. ADAMS. Spectrum of Nova Herculis 1934, April–November, 1935 14

KEENAN, PHILIP C. Photometry of the Diffuse Nebula NGC 7023 . . 600

KENT, NORTON A. Wave-Lengths of the Spectrum of H_2 from λ 3612 to λ 4224 585

KING, ARTHUR S. A Spectroscopic Examination of Meteorites . . . 507

KUIPER, G. P. Confirmation of the Duplicity of Capella H 359

KUIPER, G. P. A New Binary of Large Parallax 478

KUIPER, G. P. Notes on Visual Binaries of Large Parallax 359

LAWSON, JAMES L., and GUY C. OMER, JR. Constancy of Wave-Length of a Spectral Line 477

PAGE

LUYTEN, W. J. A Rediscussion of the Orbits of Seventy-seven Spectroscopic Binaries 85
McLAUGHLIN, DEAN B. Lines of Neutral Oxygen and Carbon in the Spectra of Novae 104
McLAUGHLIN, DEAN B. Recent Changes in the Spectrum of γ Cassiopeiae 235
MENZEL, DONALD H. The Theoretical Interpretation of Equivalent Breadths of Absorption Lines 462
MENZEL, DONALD H., and LEO GOLDBERG. Multiplet Strengths for Transitions Involving Equivalent Electrons 1
MINEUR, HENRI. The Age of the Milky Way 113
OMAR, GUY C., JR., and JAMES L. LAWSON. Constancy of Wave-Length of a Spectral Line 477
PANNEKOEK, A. The Stellar Temperature Scale 481
PETTIT, EDISON. The Motions of Prominences of the Eruptive and Sun-Spot Types 319
ROACH, F. E.; OTTO STRUVE; and C. T. ELVEY. Reflection Nebulae . . 219
ROSS, FRANK E. Photographic Photometry 241
SCHIEFER, HERBERT F. A Spectrographic Study of φ Persei 568
STEBBINS, JOEL, and A. E. WHITFORD. Absorption and Space Reddening in the Galaxy from the Colors of Globular Clusters 132
STORY, HELEN, and OTTO STRUVE. Scattering of Light in Diffuse Nebulae 203
STRÖMBERG, GUSTAF. Computation of Mean Parallaxes, Mean Absolute Magnitudes, and Mean Distances for Groups of Stars from Components of the Proper Motions 555
STRÖMBERG, GUSTAF. An Improved Method of Determining Absolute-Magnitude Distributions, with Application to the Early K Stars . . 412
STRUVE, OTTO. Review of: *Handbuch der Astrophysik*, Vol. VII, G. Eberhard, A. Kohlschütter, and H. Ludendorff (eds.) 111
STRUVE, OTTO. Review of: *L'origine des mondes*, Paul Labérenne . . . 367
STRUVE, OTTO. Review of: *Osiris*, Vol. I, George Sarton (ed.) . . . 112
STRUVE, OTTO, and HELEN STORY. Scattering of Light in Diffuse Nebulae 203
STRUVE, OTTO; C. T. ELVEY; and F. E. ROACH. Reflection Nebulae . 219
THACKERAY, A. D. Intensities of Blended Absorption Lines 433
VAN MAANEN, ADRIAAN, The Photographic Determination of Stellar Parallaxes with the 60- and 100-Inch Reflectors. Fifteenth Series . 409
WHITFORD, A. E., and JOEL STEBBINS. Absorption and Space Reddening in the Galaxy from the Colors of Globular Clusters 132
WILDT, RUPERT. Low-Dispersion Spectra of Red Stars 303
WILLIAMS, EMMA T. R. The Change of the Solar Velocity with Increasing Distances of the Stars from the Galactic Plane 346
WILSON, O. C. Variations in the Spectrum of P Cygni 296

A Wealth of Illustrative Material
for Teachers, Lecturers, and Students of ASTRONOMY

800 LANTERN SLIDES, prints, and transparencies are now available from Yerkes Observatory (29 slides are new this year). This valuable material is the work of such men as Ross, Ellerman, Barrett, Slocum, Frost, Adams, Pettit, Fox, Lee, Barnard, Hale, Ritchey, and others. A complete, 40-page illustrated catalogue will be sent on request.

A "100 LIST" of these slides has been assembled especially for schools wishing a representative presentation of astronomical material. This excellent set is $62.50, a saving of $12.50 since individual slides are 75 cents. Card descriptions are $2.50 a set.

4 MOTION PICTURES from McMath-Hulbert

(1 Reel, 16 mm., silent)

A Motion Picture Journey to the Moon

Sunrise and sunset phenomena in Lunar Craters are shown and an occultation of Delta Capricorni by the Moon.

The Solar Eclipse of August 31, 1932

Shows the actual progress of the Moon across the Sun.

Jupiter

Shows the rotation of Jupiter on its axis . . . . nebulae . . . . star clusters . . . . and star fields.

Solar Phenomena

Analyzes the light of the sun by means of the sun spectrum motion writer and the phenomena are pictured in the light of ionized calcium only.

Sales price for film . $30.00 each

Rental for 1 day . . . . . .
. . . . . $2.00 each plus carriage

SOLAR ECLIPSE OF AUG. 31, 1932

4 NEW TALKING MOTION PICTURES

Produced under the supervision of Walter Bartky. *Ready fall, 1936.* A distinctive contribution to educational methods, the films are designed for use in the University's Physical Science Division.

THE EARTH IN MOTION **THE SOLAR FAMILY** **THE MOON** **THE GALAXY**

For complete information and descriptive catalogues write:

THE UNIVERSITY OF CHICAGO PRESS

5750 Ellis Avenue Chicago, Illinois

THE OBSERVATORY

A Monthly Review of Astronomy, Founded 1877

Contains full Reports (including the speakers' accounts of their work and the discussions which follow) of the Meetings of the Royal Astronomical Society and of the Meetings for Geophysical Discussion: Articles: Reviews of important astronomical books: Correspondence on topics of interest: Notes on current discoveries and research, etc.

Annual Subscription: 20/– for 12 Numbers.

The Observatory, founded in 1877 by Sir Wm. Christie, Astronomer Royal, has been edited in the past by W. H. M. Christie, E. W. Maunder, A. M. W. Downing, T. Lewis, H. H. Turner, A. A. Common, H. P. Hollis, S. Chapman, A. S. Eddington, H. Spencer Jones, F. J. M. Stratton, J. Jackson, W. M. H. Greaves, J. A. Carroll, W. H. Steavenson and R. O. Redman.

Address of Editors: Royal Observatory, Greenwich, England.

Annual Tables of Constants A.T.C. and Numerical Data

A NEW VOLUME

of numerical documentation of SPECTROSCOPY

To the Readers of the Astrophysical Journal.—

This new Volume is a reprint of Volume X (1930) of the A.T.C. All explanations of the Tables are given both in English and in French. It contains, as do the preceding ones, all the numerical documentation on the *Emission-Spectra* (Dr. Bruninghaus)—*Electromagnetooptics* (Prof. Wolfers)—*Zeeman Effect* (Dr. P. Auger) and *Absorption Spectra* (Prof. V. Henri).

This latter part is an original work of considerable value.

310 pp. Bound Copy $10.

Orders ought to be sent directly to the Secretary of the International Committee of A.T.C.

M. C. MARIE

11, Rue Pierre-Curie, Institut de Chimie, Lab. d' Electrochimie, Paris 5°

accompanied by the amount in a check on a Paris bank, or a money-order in the name of M. C. Marie.

Reprints of Spectroscopy from previous Volumes will be sent to you at a 50 per cent reduction.